Western University
Scholarship@Western

Digitized Theses | Digitized Special Collections

2009

CHARACTERIZATION OF HALOPHILIC MICROORGANISMS AND SULFATE SALTS FROM THE HYPERSALINE LAKES OF BRITISH COLUMBIA, CANADA; AN ASTROBIOLOGICAL PERSPECTIVE

Ian S. Foster

Follow this and additional works at: https://ir.lib.uwo.ca/digitizedtheses

Recommended Citation
Foster, Ian S., "CHARACTERIZATION OF HALOPHILIC MICROORGANISMS AND SULFATE SALTS FROM THE HYPERSALINE LAKES OF BRITISH COLUMBIA, CANADA; AN ASTROBIOLOGICAL PERSPECTIVE" (2009). *Digitized Theses*. 3818.
https://ir.lib.uwo.ca/digitizedtheses/3818

This Thesis is brought to you for free and open access by the Digitized Special Collections at Scholarship@Western. It has been accepted for inclusion in Digitized Theses by an authorized administrator of Scholarship@Western. For more information, please contact wlswadmin@uwo.ca.

CHARACTERIZATION OF HALOPHILIC MICROORGANISMS AND SULFATE SALTS FROM THE HYPERSALINE LAKES OF BRITISH COLUMBIA, CANADA; AN ASTROBIOLOGICAL PERSPECTIVE

(Spine title: Sulfate Salts and Halophiles; An Astrobiological Perspective)

(Thesis Format: Integrated-Article)

By:

Ian S. Foster

Department of Earth Sciences
Graduate Program in Earth Science

A Thesis Submitted in Partial Fulfillment of the Requirements for the Degree of Master of Science

School of Graduate and Postdoctoral Studies
The University of Western Ontario
London, Ontario, Canada

© Ian S. Foster 2009

ABSTRACT

Based on geological evidence at Meridiani Planum, the loss of liquid water on Mars would have produced magnesium sulfate rich brines. The Basque Lakes of British Columbia, Canada, are an excellent terrestrial analogue for this site, as they possess highly concentrated brines fed by ground water springs, abundant sulfate salts, and are inhabited by halophilic organisms. All Basque Lake salt samples analyzed with a modified protein assay were found to contain biomass, while confocal/light microscopy revealed both cells and diffuse organic material within fluid inclusions, and in void spaces between intergrown crystals. It is here shown that reflectance IR is capable of detecting biosignatures within a sulfate matrix, the most sensitive of which are the 1550 ± 20 cm^{-1}, C-N, N-H, -COOH absorptions and the 1040 ± 10 cm^{-1} C-OH, C-N, PO_4^{3-} bond features. Due to its sensitivity and non-destructive nature reflectance IR can be regarded as a valuable tool for astrobiological exploration, especially when paired with visualization techniques such as confocal and light microscopy.

KEY WORDS: Mars, Basque Lake, Terrestrial Analogue, Halophile, Magnesium Sulfate, Reflectance IR, Biosignature, Confocal Microscopy, Protein/Biomass Assay.

ACKKNOWLEGMENTS

First and foremost I would like to thank my supervisor Gordon Southam for his incredible insight, advice and guidance. I have learned more in the past two years than I ever thought possible and it is in no small part due to his patient efforts. You have shown me that science is first and foremost about passion, and that it's always worth taking that next step into the unknown. Penny King also deserves a considerable thank you, you have always shown me new ways to progress and improve, and for that I'm grateful. I owe a tremendous debt of thanks to Matt Izawa, Jeremiah Shuster and Brendt Hyde who have always been there for me, whether to lend a hand, bounce ideas off of, be a sympathetic ear, or share a laugh with, thank you so very much. A great deal of thanks also goes out to the entire Southam Lab: Ian Power, Laura, Chris, Dusa, Kebbi, Greg, and Ryan, thank you all for your advice, ideas, and company over the last three years! Special thanks also to Lachlan, Charlie Wu, Richard Harris and Todd Simpson for their time and technical expertise.

Finally, I would like to thank my family for their unwavering support, love and encouragement; I could not be here without you.

TABLE OF CONTENTS

Title Page		i
Certificate of Examination		ii
Abstract		iii
Acknowledgements		iv
Table of Contents		v
List of Figures		vi
List of Tables		ix
List of Appendices		x
List of Abbreviations		xi
1.	Literature Review	1
2.	Characterization of Halophilic Microorganisms in Natural Magnesium Sulfate Salts and Laboratory Enrichment Samples: Astrobiological Implications	
	2.1 Introduction	41
	2.2 Methods	48
	2.3 Results	56
	2.4 Discussion	75
3.	General Discussion of Sulfate Salts and Halophilic Microorganisms in the Basque Lakes System: An Astrobiological Perspective	89
Appendix A		117
Appendix B		121
Appendix C		127
Curriculum Vitae		133

LIST OF FIGURES

CHAPTER 1

1.1 - Global mosaic of Mars, centered over Valles Marinaris..... 3
1.2 - Mars orbital obliquity history. (A) Mars obliquity illustration..... 4
(B) Calculated changes in Mars obliquity, eccentricity and
planetary insulation over the last million years.
1.3 - Current Mars global crustal magnetism; high values are recorded..... 5
for materials located in the southern hemisphere while low values are
recorded for the northern plains, Tharsis region and Hellas basin.
1.4 - Mars global elevation map exemplifying the Martian hemisphereic.....7
dichotomy.
1.5 - Proposed shorelines of Oceanus Borealis and late-stage interior..... 8
lakes that may have occupied the deepest parts of the basin once
water levels receded.
1.6 - MGS MOC images of Hesperian age outflow channels and deltas.....10
(A) Cerberus Rupes outflows. (B) Jezero Crater delta.
1.7 - Comparison of Mars in the Noachian and at Present. (A) Mars as it.....12
may have appeared in the Noachian. (B) Mars as it is observed from
orbit today.
1.8 - MGS MOC image of Mars northern ice cap as seen in March 1999.....14
1.9 - Proposed long-term cold, and short-term warm Martian climate cycles. 17
driven by periodic catastrophic volcanic episodes.
1.10 - Location of the Mars Exploration rover landing sites..... 18
1.11 - Location of the Phoenix lander site..... 19
1.12 - Representative historical summary of major events that have..... 21
occurred in Earths geologic and evolutionary past.
1.13 - Color DIC image of the mobile eukaryotic algae Dunaliella found..... 23
in brine samples from Basque Lake No. 2.
1.14 - Canadian analogue sites funded by the Canadian Space Agency.....26
1.15 - The Cariboo Plateau, located in south-central British Columbia,.....27
Canada. This region is home to a variety of hypersaline
environments, a number of which are considered to be
Mars and analogue sites for the Jovian satellites.
1.16 - Satellite images of the six major Basque Lakes sampled in this study..29

CHAPTER 2

2.1 - Satellite image of the Basque Lakes field site..... 45
2.2 - Basque Lake mud flats and brine pools..... 46
2.3 - Laboratory epsomite and Basque Lake No.1 and 2 control salts..... 52
2.4 - Laboratory enrichments dominated by green-photosynthetic bacteria... 59
2.5 - Laboratory enrichments dominated by red-photosynthetic Archaea..... 59

2.6 - Laboratory enrichments dominated by sulfate reducing bacteria..... 59
2.7 - Diffuse Interference Contrast (DIC) imagery of salt crystals..... 60
growing outward from a microcolony of pink-colored Archaea
in a Basque Lake No. 4 laboratory enrichment culture.
2.8 - Basque Lake No. 1 green microbial mat, ≥ 1 cm thick, containing..... 60
air pockets trapped within the biofilm, and mm size white salt
crystals on the surface.
2.9 - Confocal microscopy images of halophiles and extracellular..... 64
organics trapped within magnesium sulfate crystals.
2.10 - Reflectance IR spectra of dried laboratory grade $MgSO_4 \cdot x H_2O$..... 65
(labeled Laboratory Epsomite), and dried salt crystals formed
from the crystallization of filtered Basque Lake No. 1
(labeled FBS-B1) and No. 2 brine (labeled FBS-B2).
2.11 - Reflectance IR spectra of laboratory enrichments dominated..... 68
by green-photosynthetic autotrophs.
2.12 - Reflectance IR spectra of laboratory enrichments dominated by..... 69
red-photosynthetic Archaea autotrophs.
2.13 - Reflectance IR spectra of laboratory enrichments dominated..... 70
by dissimilatory sulfate reducing bacteria (SRB)
2.14 - Reflectance IR spectra of natural microbial mats obtained..... 71
form Basque Lake No. 2 and No. 2W.
2.15 - Reflectance IR spectra between 1650 and 550 cm^{-1} of natural.....73
salts and crystallized, filtered, field brines obtained form the
Basque Lakes.

CHAPTER 3

3.1 - Distribution of MGS MOC images showing clear evidence of gullies....92
3.2 - MGS MOC images of recent gully formation.....92
3.3 - Meridiani Planum as viewed from the Opportunity rover.....93
3.4 - Basque Lake No. 2 brine pools as seen in August of 2006.....94
3.5 - A multilayered mottled green, red and white microbial mat.....97
found along the shore of Basque Lake No. 2W in August of 2007.
3.6 - Mud ridges and salt coatings separating irregularly shaped.....98
pools at Basque Lake No. 1 in August of 2006.
3.7 - Basque Lake No. 1 as observed from the roadside in August of.....99
2007. The entire lakeshore was coated in a thick algal mat
that was continuous out to the middle of the lake.
3.8 - Salt crystals observed in laboratory enrichment samples.....99
from the Basque Lakes.
3.9 - Large salt crystal 'iceberg' growing under a brine pool's.....102
surface and down into the mud.

3.10 - Confocal microscopy image of cells and organic matter.....105
trapped in a large fluid inclusion from a Basque Lake
No. 1 natural salt crystal.
3.11 - Confocal microscopy image of several planar void space.....107
regions between intergrown Basque Lake No. 2 crystals.

LIST OF TABLES

CHAPTER 2

2.1 - Basque Lake physical conditions and chemical compositions.....57
2.2 - Modified SHAND media for culturing and enrichment of halophiles....50
2.3 - Laboratory enrichments selected for reflectance IR analysis.....61
2.4 - Field sample salts selected for reflectance IR analysis..... 62
2.5 - DRIFTS spectral assignments for dried laboratory brine and.....66
Basque Lake field brine samples.
2.6 - DRIFTS spectral assignments for model laboratory..... 72
enrichment samples
2.7 - DRIFTS spectral assignments for natural biomass containing salt.....74

CHAPTER 3

3.1 - Biomass content of salt samples obtained from a variety of settings.....101
in and around the Basque Lakes.

LIST OF APPENDICES

Appendix A

A.1 - Widefield vs. Confocal microscope light paths..... 119

Appendix B

B.1 - Precipitated salt in a laboratory enrichment dominated by..... 122
red Archaea, sampled from Last Chance Lake. Note the
banding indicating 4 separate crystal growth events.
B.2 - Characteristic growth banding of precipitated salt crystals.....123
in an enrichment sample from Last Chance Lake.
B.3 - Two green enrichment samples with one salt precipitation.....124
layer at the bottom of the tube (left), compared with a
series of sterile media evaporation experiments.
B.4 - Enrichment culture salt precipitation experiments over time....125

Appendix C

FIGURES

C.1 - Sample B4-Brown-Sediment..... 129
C.2 - Sample B2-Black Sediment.....129
C.3 - GADDS images of sample B4-Brown-Sediment.....129
C.4 - GADDS images of sample B2-Black-Sediment.....129
C.5 - (A) Eva diffraction pattern for sample B4-Brown-Sediment....130
(B) Eva diffraction pattern for sample B4-Black-Sediment.
C.6 - Filtered B4-Brown-Sediment.....131
C.7 - Filtered B2-Black-Sediment..... 131
C.8 - GADDS images of sample B4-Brown-Filtered-Sediment.....131
C.9 - GADDS images of sample B2-Black-Filtered-Sediment..... 131
C.10 - (A) Eva diffraction pattern for sample B4-Brown- 132
Filtered-Sediment. (B) Eva diffraction pattern for sample
B4-Black-Filtered-Sediment.

TABLES

C.1 - Mineralogy of dried salt crystal samples from Basque Lake....128
No. 2 and No. 4

LIST OF ABBREVIATIONS

ATP	Adenosine triphosphate
BBM	Brine Basal Medium
CRISM	Compact Reconnaissance Imaging Spectrometer for Mars
cfu	colony forming units
DIC	Differential Interference Contrast
DNA	Deoxyribose Nucleic acid
DRIFTS	Diffuse Reflectance Infrared Fourier Transform Spectroscopy
g	Earth's gravity
Ga	Billion years
IC	Ion Chromatography
ICP	Ion Coupled Plasma
IR	Infrared
MGS	Mars Global Surveyor
Micro-IR	Microscopic Infrared Detector
MOC	Mars Orbital Camera
Ma	Million years
OMEGA	Visible and Infrared Mineralogical Mapping Spectrometer
RT	Room Temperature
SEM	Scanning Electron Microscope
SRB	Sulfate Reducing Bacteria
UV	Ultraviolet

CHAPTER 1

INTRODUCTION AND LITERATURE REVIEW

INTRODUCTION

MARS OVERVIEW

Of the eight planets, one hundred and seventy moons, and countless asteroids and comets in our solar system, only one of these bodies, the Earth, is known to harbor life. Of all the rest, only three others, Mars, Jupiter's moon Europa, and Saturn's moon Titan, are thought to have conditions chemically suitable/stable enough for life to have a chance at survival (Hiscox 2001; Landis 2001; Raulin and Owen 2002; Irwin and Schulze-Makuch 2003; Marion et al., 2003; Mancinelli 2004; Fairen et al., 2005; Pavlov et al., 2006). Of these three potential abodes for life, Mars (Figure 1.1) is the only one (in the inner solar system) with a rocky composition similar to that of the Earth. At a distance of 230 million kilometers from the sun, Mars' orbit is roughly 1.5 times farther out from the sun than the Earth's, resulting in a year that is 687 days long; and yet its rotation rate of 24.6 hours results in a day length that is remarkably similar to our own. With a mass of 6.41×10^{23} kg, only 15.1% that of the Earth, Mars has insufficient gravity to hold on to light molecules (i.e., H_2 and He), resulting in an unstable atmosphere that is slowly degraded by solar winds, and continually lost to space (Lammer et al., 1996; Jakosky and Phillips 2001; Lammer et al., 2003; Terada et al., 2009).

Today, Mars atmospheric pressure is 0.7-0.9 kPa, only 1% that of Earth's, and is composed of 95.72% carbon dioxide, 2.7% nitrogen, 1.6% argon, 0.2% oxygen, 0.07% carbon monoxide, 0.03% water, and trace amounts of other gases. With a current axial tilt of 25.19° Mars experiences seasons that are very similar to those on Earth; however, unlike the Earth, Mars obliquity varies considerably more over time, ranging from 15° to

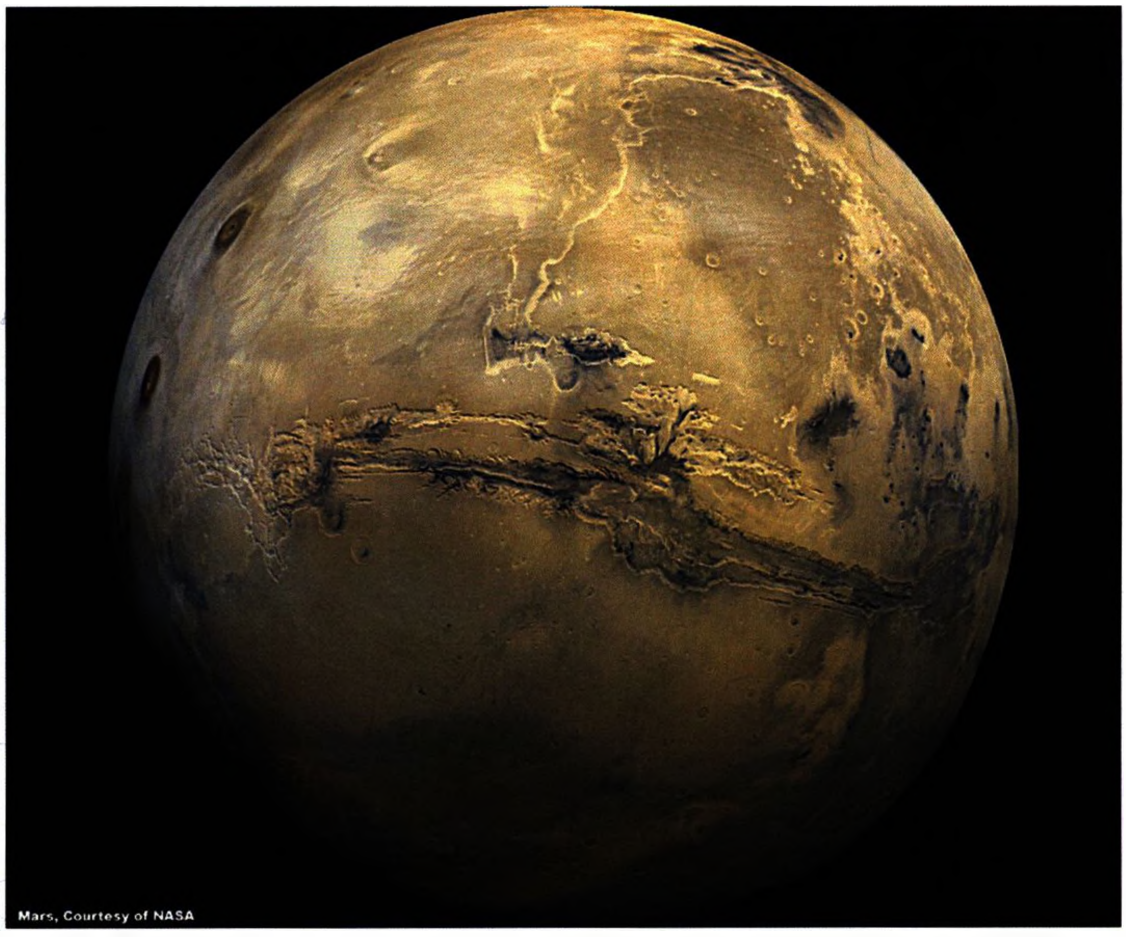

Figure 1.1 – Global mosaic of Mars centered over Valles Marinaris (Courtesy NASA).

35°, progressing over a 124,000-year cycle (Figure 1.2) (Ward 1974; Laskar et al., 2002; Catling 2009). This results in major changes to the distribution of water and carbon dioxide ice on the planet's surface, as these deposits continually sublimate and re-accumulate in colder areas with minimum sun exposure. At inclinations of 15° these ices accumulate at the poles as we observe today, while at high obliquity ~ 35° they are redistributed to regions near the equator (Ward 1974; Laskar et al., 2002; Catling 2009). This effect is suspected to cause large scale climatic variations that redistribute water ice around the planet, providing potential recharge sources that feed both local and regional groundwater systems (Jakosky 1985; Jakosky et al., 1995; Baker et al., 1999; Baker 2001).

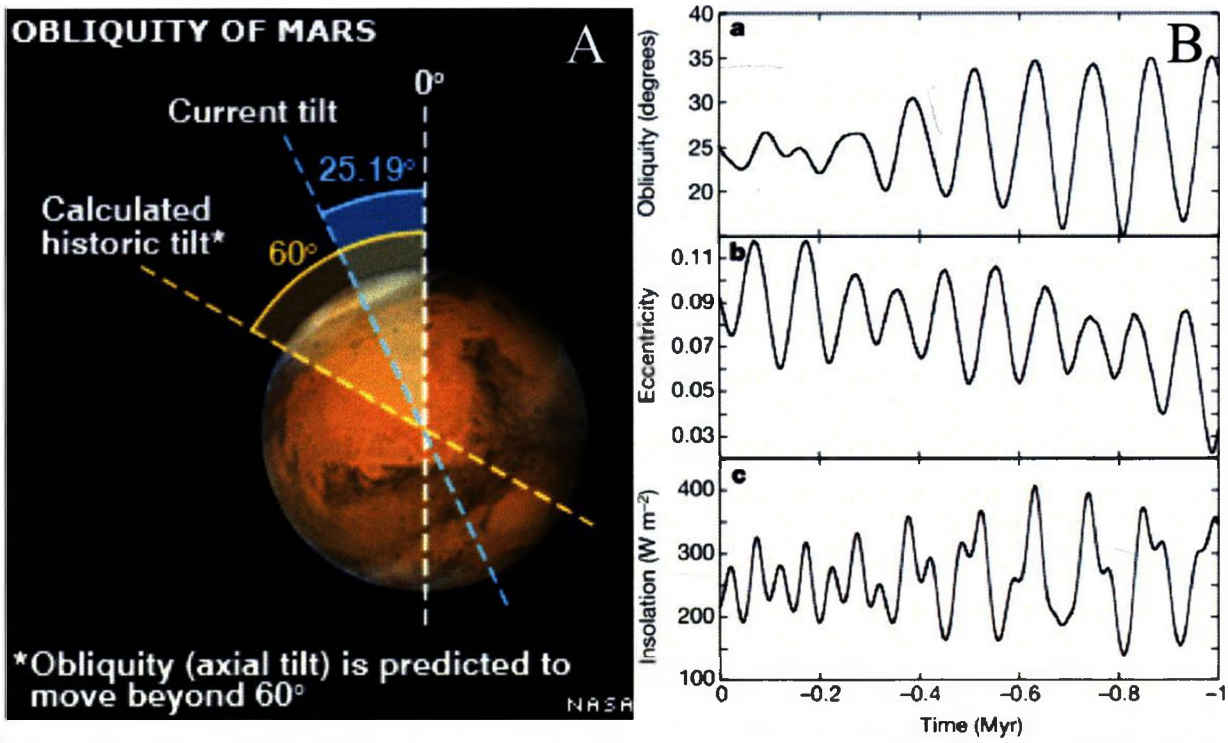

Figure 1.2 – Mars Orbital Obliquity History. (A) Illustration of Mars rotational axis variability due to changes in obliquity (Courtesy NASA). (B) Calculated changes in Mars Obliquity, Eccentricity and the resultant planetary insolation over the last million years. [a] Obliquity [b] Eccentricity and [c] Insolation (Laskar et al., 2002).

MARTIAN GEOLOGIC AND HYDROLOGIC HISTORY

Noachian Epoch 4.6 – 3.5 Ga.

Beginning at the time of Mars formation, 4.6 Ga, and continuing until 3.5 Ga, the Noachian epoch, named after Noachis Terra, is the first of three major periods in Martian history. During this time Mars possessed a short-lived magnetic field, as indicated by the alignment of magnetic minerals in the southern highlands (Figure 1.3). The magnetic field began to wane sometime in the mid to late Noachian (Acuna et al., 1999; Connerney et al., 1999; Connerney et al., 2001; Connerney et al., 2005). The lack of magnetically aligned minerals reported in younger Martian surface materials demonstrates that by the beginning of the Hesperian epoch the magnetic field was no longer active (Acuna et al., 1999; Connerney et al., 2001; Connerney et al., 2005). The loss of the magnetic field by

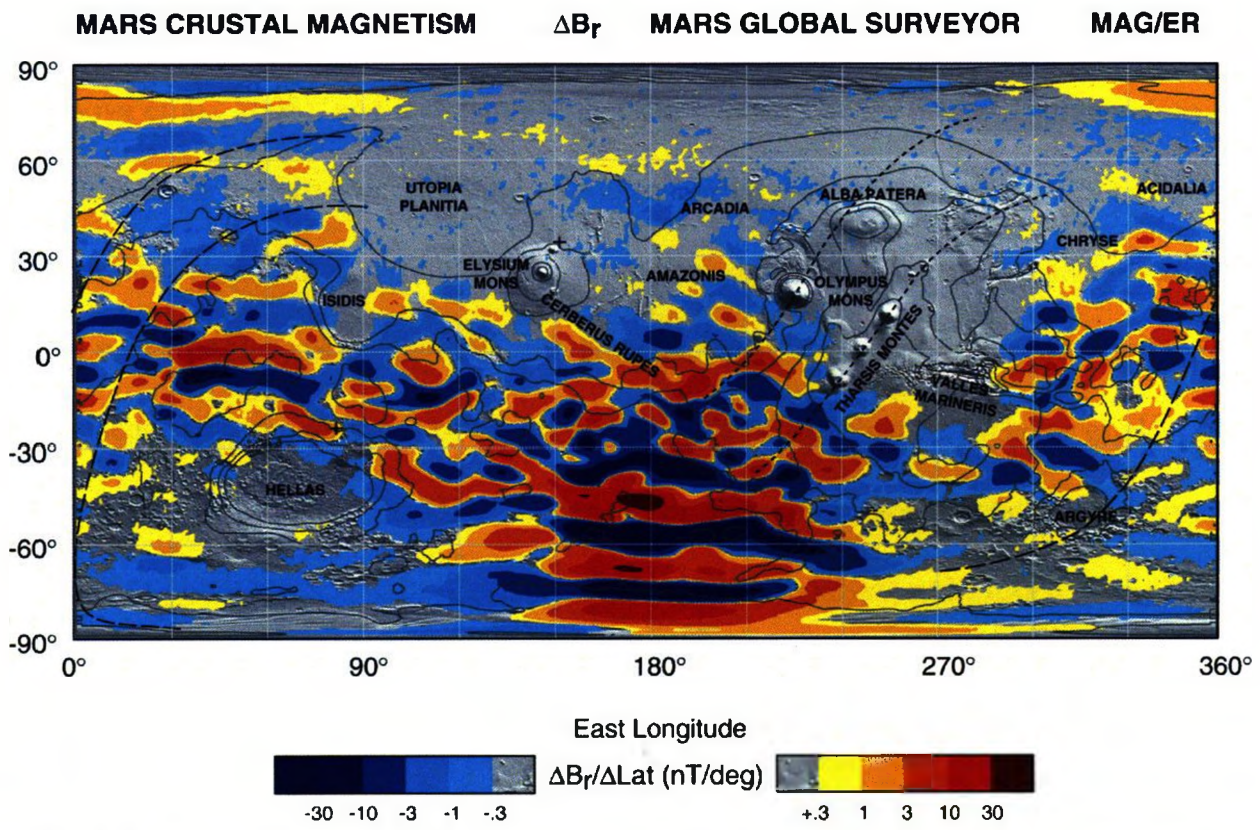

Figure 1.3 – Current crustal magnetism of Mars, note the highest readings are found in the Noachian age southern highlands, while there is a lack of magnetically aligned minerals in the northern plains (top center of image), Tharsis region (middle right of image), and Hellas basin (bottom left of image). These features suggest they have either formed after, or had extant magnetic minerals reset since Mars magnetic field disappeared. (Connerney et al., 2005).

---

the end of this epoch played a major role in subsequent global climate change throughout the rest of the Hesperian and Amazonian.

The oldest Martian surfaces, found in the southern hemisphere, and dated at approximately 4.5 Ga by crater counts and meteorite fragments (Hartmann and Neukum 2001; Nyquist et al., 2001 Hartmann 2005), were formed during this period and have experienced extensive post-formation cratering, substantial alteration from early fluvial processes, and continued eolian weathering and during the last 3.5 Ga of Martian history. Overall, surface and subsurface geologic/hydrologic process experienced peak activity during this time (Sleep 1994; Baker et al., 1999; Baker 2001; Mege et al., 2003; Ansan

and Mangold 2006; Fassett et al., 2008; Langlais and Amit 2008; Lillis et al., 2008; Marinova et al., 2008), and it is thought that the majority of the Tharsis bulge volcanism and associated catastrophic flooding events occurred during this period (Dohm et al., 2001; Dohm et al., 2003). Although the formation, duration, volume, and surface area of extant water bodies are contentious, the Noachian period is at least partially defined by the presence of large volumes of liquid water at the Martian surface (Baker et al., 1999; Baker 2001; Fairen et al., 2003). Evidence for water, and water-related landforms is found throughout the southern highlands (Baker 2001; Jakosky and Philips 2001; Fairen et al., 2005), and can be directly tied to regional phyllosilicate deposits that are typical of Noachian sediments (Poulet et al., 2005).

When observing Mars from orbit it is easy to see that there is a stark difference between surfaces in the northern and southern hemispheres. This phenomenon, known as the Martian surface dichotomy (Figure 1.4), has been attributed to the presence of an early Martian ocean in the northern hemisphere, known as Oceanus Borealis (Baker et al., 1991; Tanaka et al., 2003). The presence of this body of water is thought to have been the cause of the extensive weathering and resurfacing that has occurred in the northern hemisphere, while fluvial and eolian weathering seem to have dominated in the southern hemisphere (Jakosky and Philips 2001; Forsberg-Taylor and Howard 2004).

Several attempts have been made to trace the boundaries of the early ocean by using large-scale 'benches' and strand-lines which rim the dichotomy boundary, and may represent paleo-shorelines and/or subaqueous continental-shelf like deposits (Fairen et al., 2003). Two separate shorelines (Figure 1.5) are highlighted by Fairen et al., (2003), the

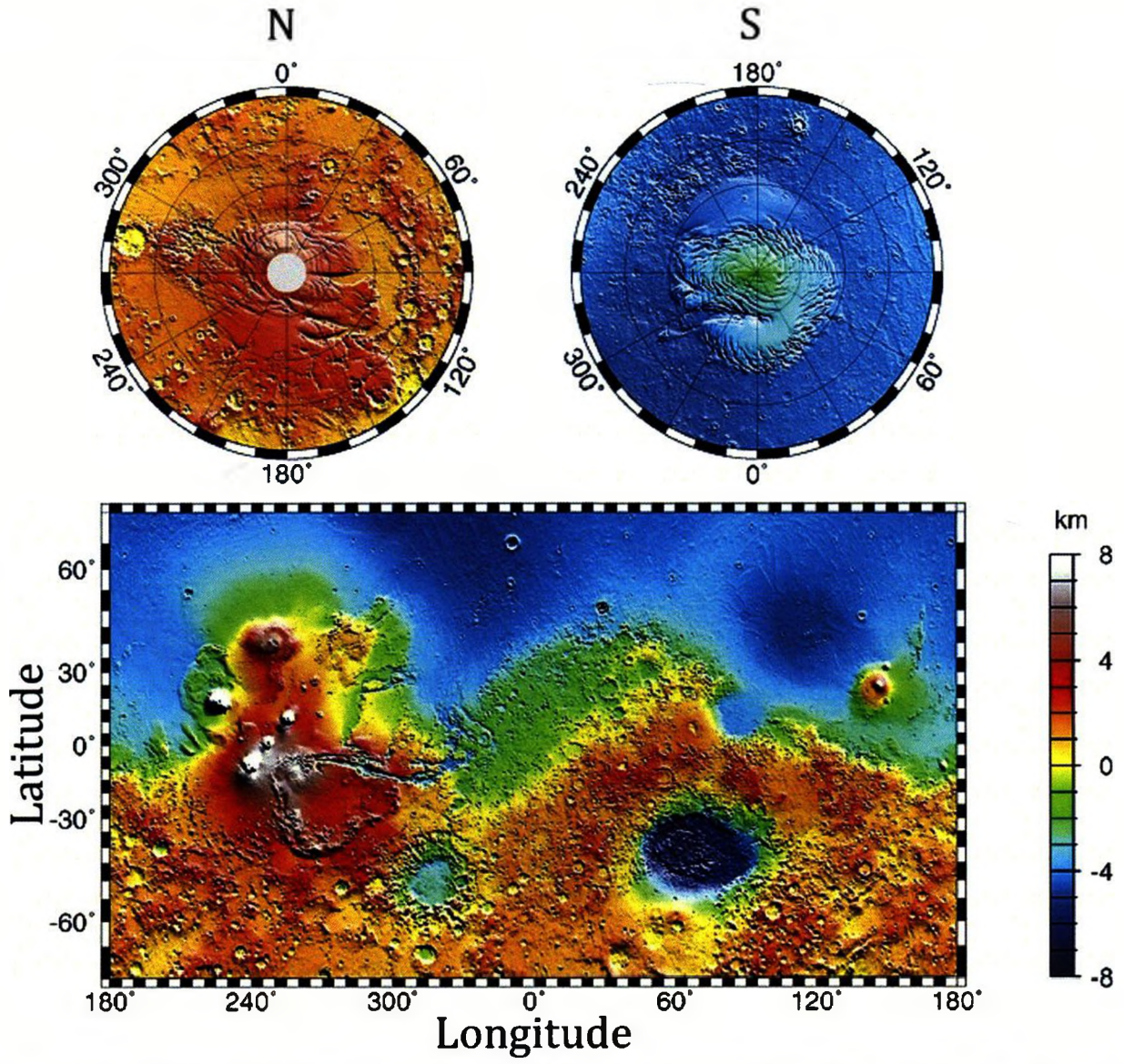

Figure 1.4 – Mars global elevation map exemplifying the Martian hemispheric dichotomy. Note the contrast of the southern highlands with the northern lowland plains, and the presence of the Tharsis Region edging into the plains at the mid-to-top left (Courtesy NASA).

---

larger of which can be found at the contact between Arabia Terra and Noachis Terra, while a less extensive one runs along the boundary between Arabia Terra and Acidalia Terra. These shorelines represent paleo-evidence for a gradually diminishing ocean in the northern plains, which was eventually reduced to a series of large lakes/seas in Amazonis Planitia, Chryse/Acidialia Planitia, and the Borealis, Utopia and Isidis basins.

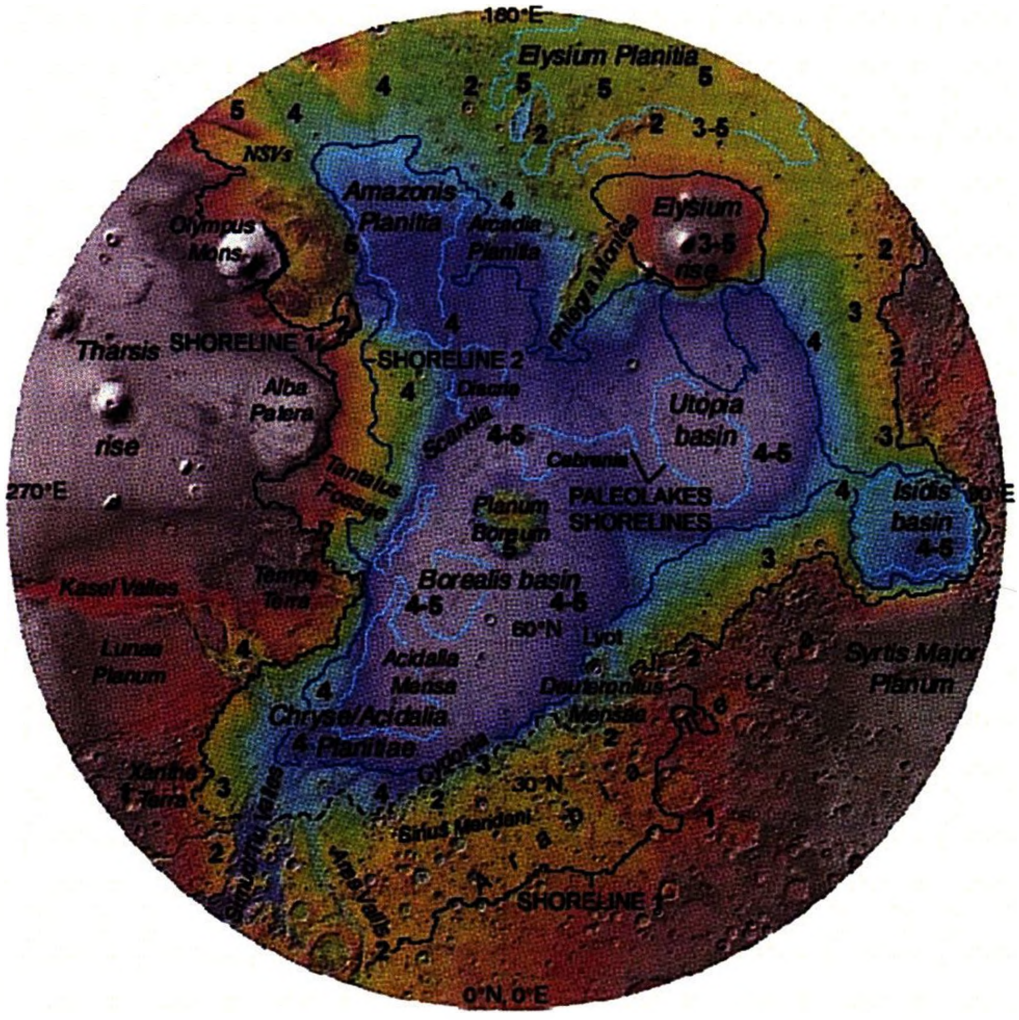

Figure 1.5 – Proposed shorelines of the Oceanus Borealis and the small late-stage interior lakes that may have occupied the deepest parts of the Borealis basin as water levels receded (Fairen et al., 2005). The image is the centered vertically on the Martian North Pole.

Hesperian Epoch 3.5 – 1.8 Ga.

The Hesperian epoch, which began at 3.5 Ga and ended at 1.8 Ga, is named after Hesperia Planum, and is typified by the formation of extensive lava plains on the Martian surface (Dohm et al., 2001; Dohm et al., 2003; Werner 2009). Additionally, an overall global cooling, loss of water to ice deposits, onset of atmospheric erosion, and the formation of surficial iron oxide deposits are all characteristic of this period (Lammer et al., 2003; Fairen et al. 2005). Despite the cooling climate, and loss of most freestanding bodies of liquid water, there is ample evidence which suggests that the surface was being

reshaped periodically by both large and small volumes of water, as suggested by outflow-plains, deltaic formations, and river valleys (Figure 1.6) (Baker et al., 1991; Baker 2001; Dohm et al., 2001; Fairen et al., 2003; Fairen et al., 2005; Ansan and Mangold 2006; Harrison and Chapman 2008). By the mid to late-Hesperian, mantle cooling and resultant crustal thickening signaled the end of large-scale global volcanism, and with it, began the permanent decline of the Martian atmosphere (Baker et al., 1991; Fairen et al., 2003; Connerney et al., 2005).

Amazonian Epoch 1.8 Ga - Present

The Amazonian epoch, which began at 1.8 Ga ago and continues to present day, has been typified by periodic pulses of Tharsis magmatism, and the formation of Martian surface features with very low crater counts (Hartmann 1999; Baker 2001; Fairen et al., 2003; Tanaka et al., 2003; Dohm et al., 2008). Temporary warm periods in which liquid water was stable at the surface appear to be associated with these events, as suggested by local water outflow activity, and the formation of small lacustrine and fluvial environments in Amazonian deposits (Baker et al., 1991; Baker 2001; Fairen et al., 2003; Wood 2006; Schon et al., 2008). Physical weathering processes since the onset of the Amazonian are dominantly eolian, while surficial chemical weathering has been dominated by the presence of a persistently oxidizing atmosphere. Together, these factors are responsible for the development for the red-orange iron oxide deposits that we typically associate with Mars today. With insufficient gravity to hold onto light molecules, and the lack of a magnetic field, the Amazonian atmosphere is continually lost to space. Due to the overall decline in volcanic activity as the Martian interior cooled, there have been no global

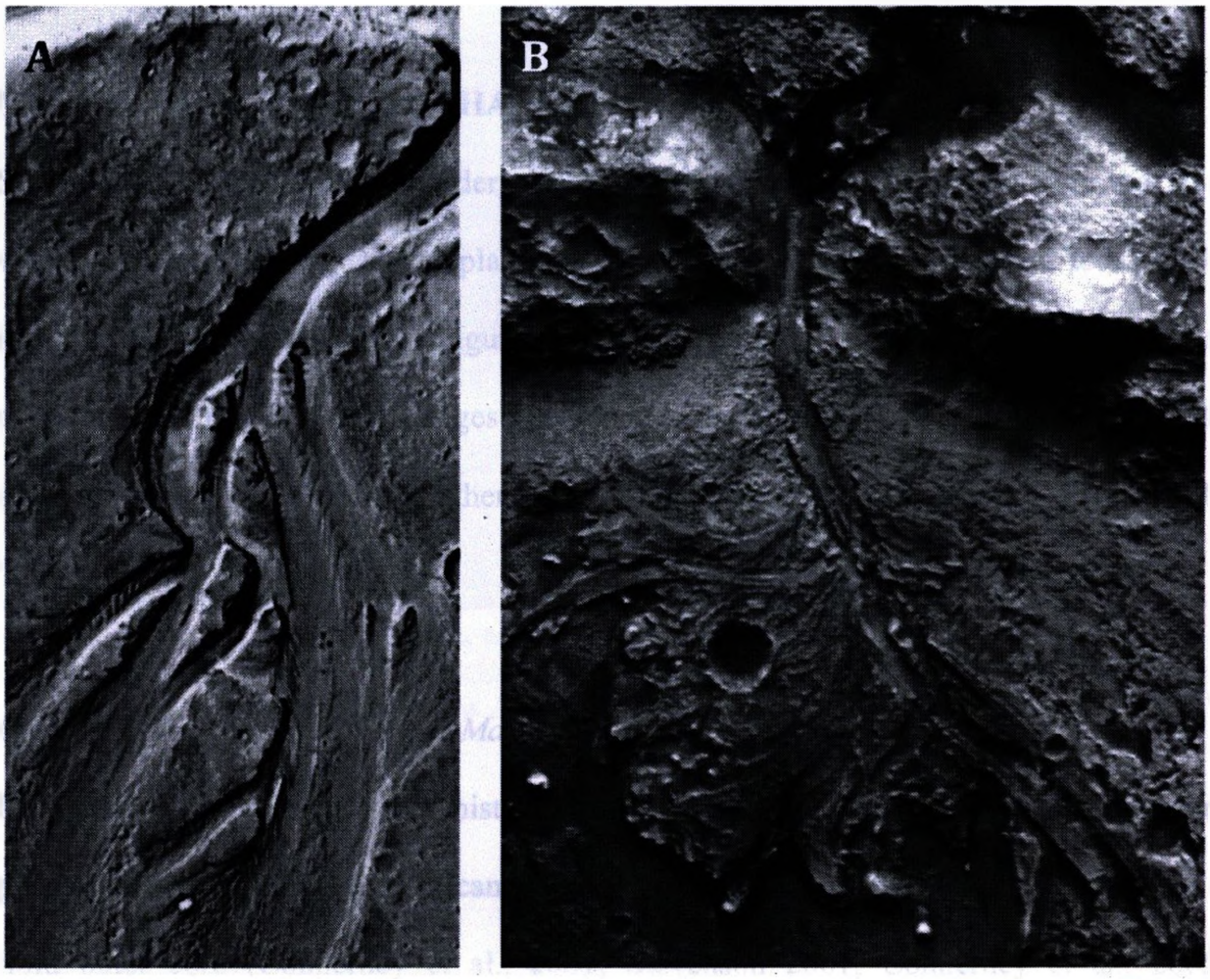

Figure 1.6 – MGS MOC images of Hesperian age outflow channels and deltas. (A) Kilometer scale outflow channels south of Cerberus Rupes, note the terraced terrain suggesting this region has experienced several episodes of flooding, while the lack of craters indicates that as least one of these episodes was geologically recent (Image from Baker 2001). (B) A lobed delta found in Jezero Crater, near Nili Fossae, the presence of this feature indicates several episodes of prolonged river sedimentation have occurred in a paleo crater lake.

processes operating during this period that are capable of permanently replacing/renewing the atmospheric molecules lost to space (Baker et al., 1999; Baker 2001). The net loss of the atmosphere eventually resulted in a destabilization of liquid water at the Martian surface due to both the low temperature and low pressure conditions, resulting in its transfer into polar and subsurface ice deposits (Baker 2001). Additionally, due to the lack of both a magnetic field and ozone layer, materials exposed at the surface have been subjected to direct radiation from space, resulting in a photochemical sterilization of the Martian surface (Cockell et al., 2000; Pavlov et al., 2002).

MARS GLOBAL CLIMATE CHANGE

Since its formation Mars has undergone an enormous change in climate from that of a warm, wet, geologically active planet in the Noachian, to the cold, dry, tectonically inactive planet we see today (Figure 1.7). There is however mounting evidence from contemporary research that suggests Mars may in fact be a "Dormant Planet" with sporadic subsurface activity, rather than an entirely geologically and hydrologically "Dead Planet".

Cooling of the Martian Core and Mantle

In the earliest portion of Mars history, mostly confined to the Noachian epoch, Mars possessed both highly active volcanic processes, and a magnetic field generated from a fluid outer core (Connerney et al., 2001; Stevenson 2001; Connerney et al., 2005; Langlais and Amit 2008; Werner 2009). However, as a result of its small size (15% the mass of the Earth) Mars did not possess enough energy to maintain internal mantle convection throughout its history, which led to a thickening of the Martian crust, and a gradual reduction in volcanic activity throughout the Noachian and Hesperian (Sleep 1994). Currently, the only evidence for active volcanism on Mars since the onset of the Amazonian is found in the Tharsis region, and is thought to be related to mantle plume/hotspot activity (Hartmann 1999). A side effect of reduced mantle activity has been the loss of the planet's magnetic field, and the primary source of volatiles found in the atmosphere (Baker et al., 1999; Baker 2001; Fairen et al., 2003). The result is a slow and permanent depletion of the atmosphere, the consequences of which were the primary driver for climatic change throughout the rest of Mars' history.

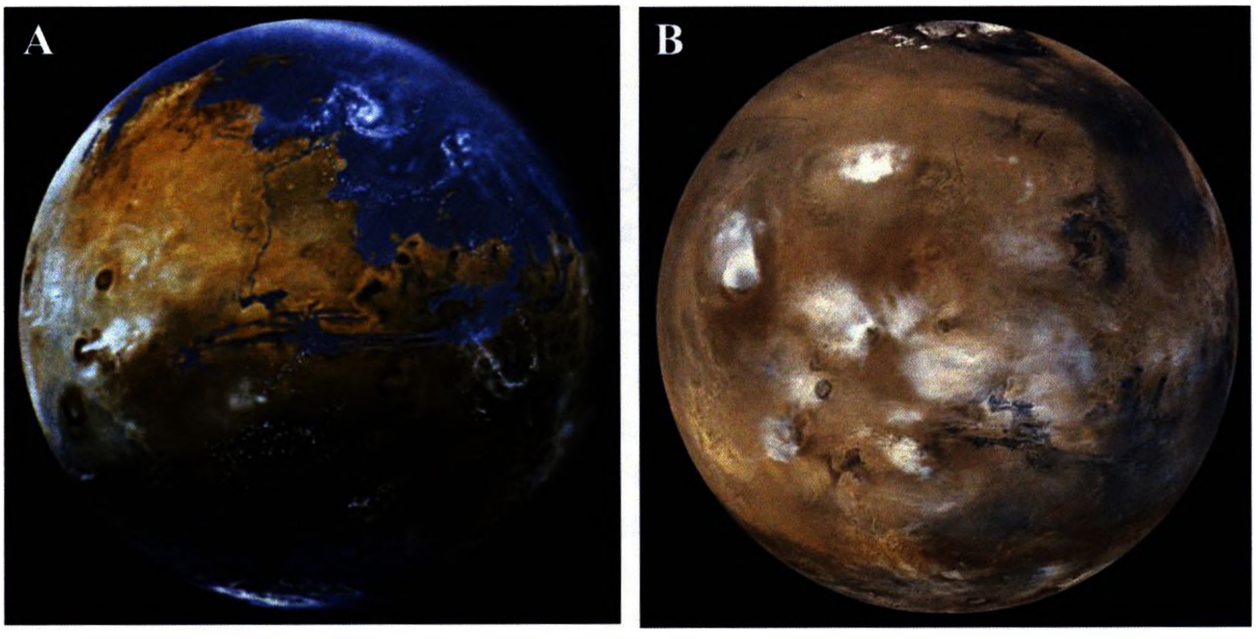

Figure 1.7 – Comparison of Mars in the Noachian and at present. The Tharsis region is visible at the left side of each image. (A) Artist Michael Carroll's interpretation of a terraformed Mars with liquid water at the surface, similar to the Noachian epoch. (B) Present day Mars as observed from orbit (Courtesy NASA).

Atmospheric Erosion

Although Mars must have started out with an appreciable atmosphere (this is required for water stability at the surface, and the creation of globally distributed water related landforms and deposits), this was only a ~1.1 billion year long transient state, maintained by the continual addition of volcanic gasses, and the protective aspects of the magnetic field (Baker et al., 1999; Jakosky and Philips 2001; Stevenson 2001). With the loss of the magnetic field due to internal cooling, Mars became vulnerable to ionizing solar radiation capable of breaking down volatile molecules held in the atmosphere (Lammer et al., 2003; Terada et al., 2009). Two important atmospheric gases that were probably affected by this process are water (which would have been broken down into hydrogen [H^+] and hydroxide [OH^-] ions; Equations 1-4), and carbon dioxide (which could have been broken down into carbon monoxide [CO^+] and oxygen [O^-] radicals; Equation 5-6). Notably, it has been observed that very little carbon dioxide is actually lost by this process, as the positively charged carbon monoxide radical undergoes a secondary reaction with water to

REACTANTS	PRODUCTS	
$H_2O + h\nu$	$\rightarrow H_2O^*$	(1)
H_2O^*	$\rightarrow H^* + OH^*$	(2)
$H^* + OH^*$	$\rightarrow H^*$ lost to space + OH^*	(3)
$OH^* + OH^*$	$\rightarrow H_2O_2$ oxidizes soil minerals	(4)
$CO_2 + h\nu$	$\rightarrow CO^* + O^*$	(5)
$CO^* + O^*$	$\rightarrow O^*$ lost to space	(6)
$CO^* + H_2O$	$\rightarrow CO^+ + O^- + 2\ H^+$ lost to space	(7)
$CO^+ + O^-$	$\rightarrow CO_2$ returns to atmosphere	(8)

regenerate carbon dioxide at the expense of water molecules (Equation 7-8). After the H^+ radicals have been formed, the solar radiation also provides the energy required for these atoms, and other light elements such as Helium (He), to escape Mars' gravity and become permanently lost to space (Kass and Yung 1995; Lammer et al., 1996; Jakosky and Phillips 2001; Lammer et al., 2003; Greenwood et al., 2008; Kumar et al., 2008; Terada et al., 2009).

Since water vapor is a strong greenhouse gas, and large water bodies aid in the thermal regulation of climate, a consequence of its continued loss was an overall global cooling. As this process continued over hundreds of millions of years, it eventually crossed a threshold where the atmosphere was no longer thick enough to allow liquid water to exist either in the atmosphere or on the surface (Baker et al., 1991; Jakosky and Philips 2001). It was at this point that all water remaining at the surface began sublimation and transference to colder areas such as the poles, where it 'froze out' of the atmosphere as a water-rich frost (Baker et al., 1991; Jakosky and Philips 2001). In addition to water,

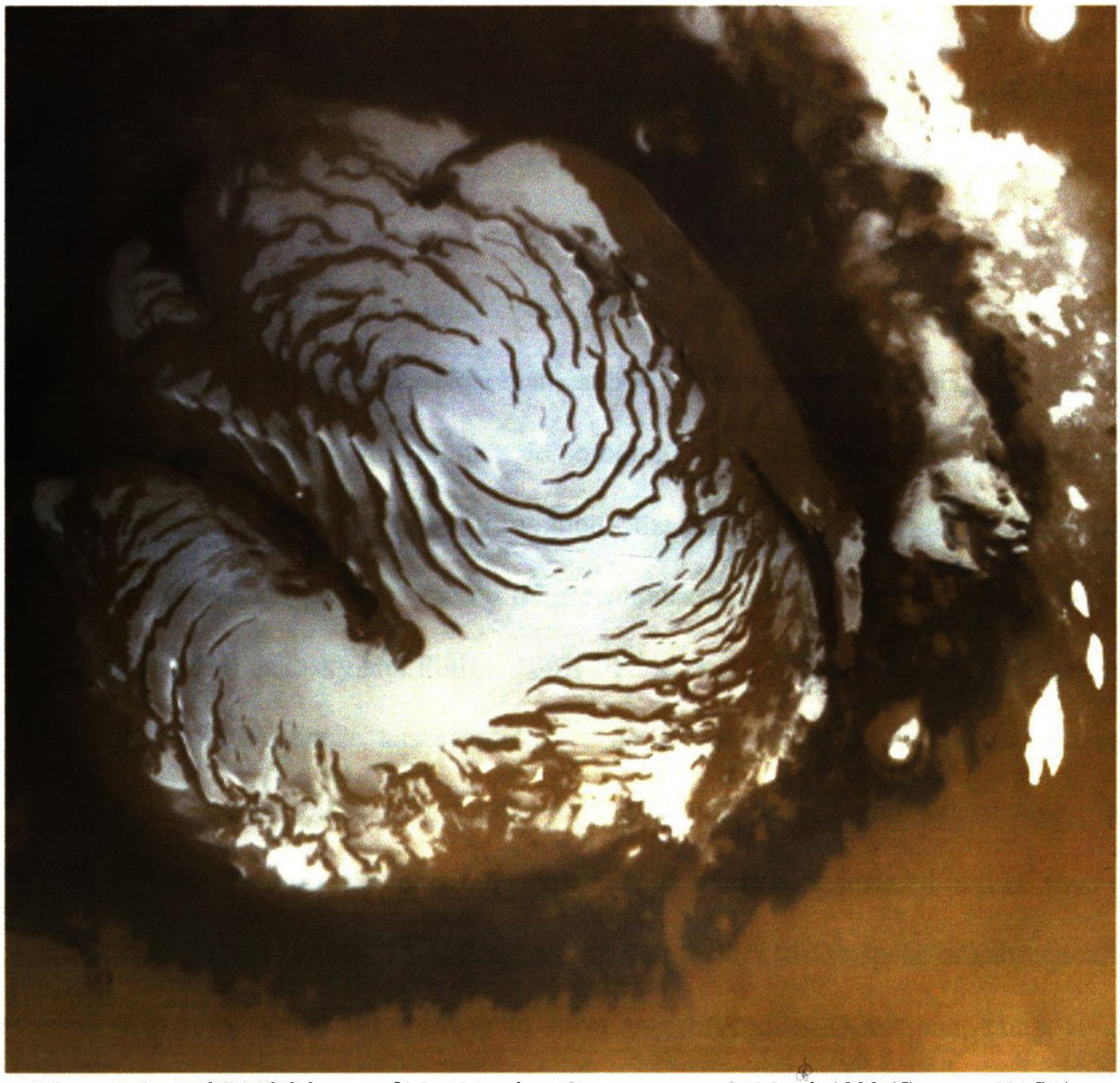

Figure 1.8 – MGS MOC image of Mars' northern ice cap as seen in March 1999 (Courtesy NASA).

atmospheric carbon dioxide also became unstable at high latitudes, and froze out as secondary ice deposits, which capped the extant water ice (Figure 1.8) intensifying the atmospheric cooling effect (Baker et al., 1999; Baker 2001). As a result, Mars now possesses only a thin atmosphere, dominated by carbon dioxide, that cannot support liquid water anywhere on the surface, despite some areas, such as the equatorial regions, reaching temperatures above 0°C in the Martian summer (Baker 2001).

Loss of the Primordial Martian Oceans

The atmospheric instability that resulted from by the loss of the Martian magnetic field, meant that the only way to maintain an atmosphere dense enough to allow liquid water to remain stable at the surface, is to have some other net input of greenhouse gases occurring (Baker et al., 1999; Baker 2001; Jakosky and Philips 2001; Fairen 2005). As the magnetic field waned in the mid to late-Noachian, active volcanic processes occurring at the Martian surface became a requirement for retaining a dense atmosphere. However, as cooling of the mantle continued throughout the Hesperian, widespread volcanism diminished, and Mars primary source of greenhouse gasses disappeared (Baker et al., 1999; Baker 2001; Jakosky and Philips 2001; Fairen et al., 2003; Fairen 2005). Once the net addition of greenhouse gases, derived from volcanic activity, fell below the net volume of gas lost to space, an inevitable atmospheric thinning began. Water vapor, fed into the atmosphere from the oceans, was continually being disassociated into H^+ (lost to space) and OH^- or secondary O^{2-} radicals, which were either lost to space or subsequently reacted with minerals at the surface to form mineral-oxides (Kass and Yung 1995; Lammer et al., 1996; Jakosky and Phillips 2001; Lammer et al., 2003; Greenwood et al., 2008; Kumar et al., 2008; Terada et al., 2009).

Despite the freeze-out of the atmosphere and loss of liquid water at the surface, geologic processes requiring liquid water (i.e. the formation of the vast mid-latitude flood plains) continued to occur throughout the Hesperian and Amazonian, indicating that there must be some intermittent, if not continual, process that can provide both heat and volatiles to the Martian surface (Baker et al., 1999; Baker 2001; Jakosky and Philips 2001; Fairen et al., 2003; Fairen 2005). One mechanism proposed by Baker (2001), suggests that

episodes of catastrophic volcanic activity can explain how the normally cold Martian climate can be temporarily warmed enough to allow liquid water to be stable at the surface (Figure 1.9).

The theory proposes that the long-term, 100 Ma to 1 Ga, stable Martian climate is characterized by frozen deposits of carbon dioxide and water ice at the poles, as well as clathrates and water ice in the subsurface. This state is periodically interrupted by times of intense volcanic activity, lasting ~10 – 1000 yrs, which melt the subsurface ices and release both volatiles into the atmosphere, and liquids as groundwater outflows. This results in a very brief, warm, hydrologically active period (10^{-2} yrs), where liquid water is stable enough to form lakes and seas, which in turn supply atmospheric water resulting in regional precipitation (Baker et al., 1999; Baker 2001). It is during these brief warm periods that it may be possible for extant, dormant, Martian organisms to become active again, proliferate, and be transported to new regions via precipitation. As the climate cools, any extant Martian organisms that find themselves trapped in a habitable 'oasis' can potentially enter a state of dormancy once again and wait for the next growth opportunity to occur.

Martian Geology

The successful landing of the NASA Mars Exploration rovers, Spirit and Opportunity in January of 2004 (Figure 1.10), and the Phoenix Lander in May of 2008, has fundamentally expanded our understanding of the Martian surface, suggesting that Mars possesses active geologic (Hartmann et al., 1999; Christensen 2003), hydrologic (Baker et al., 1991; Malin et al., 2000; Christensen 2003; Chavdarian et al., 2006) and cryologic

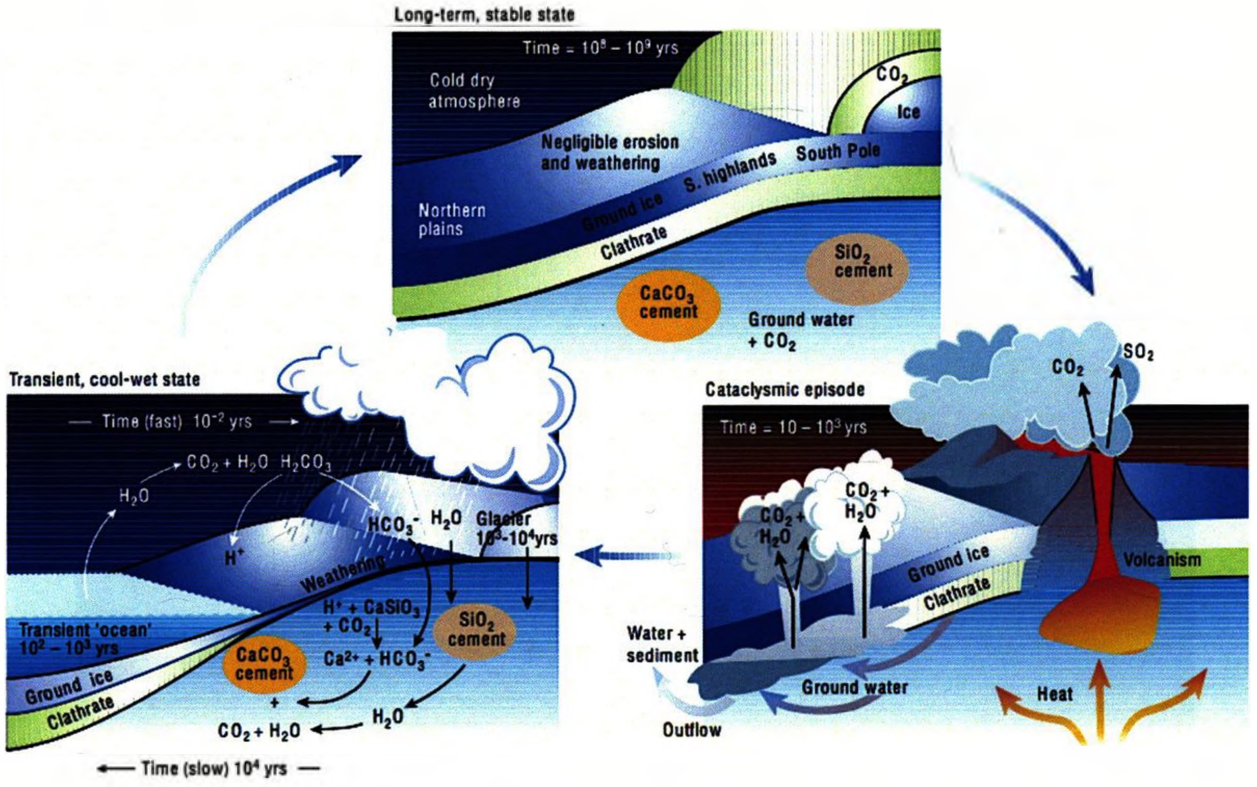

Figure 1.9 – Proposed long-term cold, and short-term warm Martian climate cycles driven by periodic catastrophic volcanic episodes (Baker 2001).

processes (Mellon et al., 2008). Evidence that there was once liquid water (or ice) present at the Martian surface (Mellon et al., 2008), and in the subsurface (Marquez et al., 2005; McLennan el al., 2005; Chavdarian et al., 2006; Squyres et al., 2006), suggests that Mars has/had conditions that may be able to support life (Hiscox 2001; Fairen et al., 2005). Specifically, hematite nodules discovered at Meridiani Planum hosted within massive sulfate deposits, indicate that there were several episodes of near-surface ground water activity in the area, both pre and post deposition (Marquez et al., 2005; Chavdarian et al., 2006).

Results from the Phoenix Lander (Figure 1.11) have shown that if the Martian soil/ice in the northern plains were melted, it would form brine possessing a slightly alkaline pH from the calcite in the soil (Kounaves et al., 2008). Similar to that of extremely arid

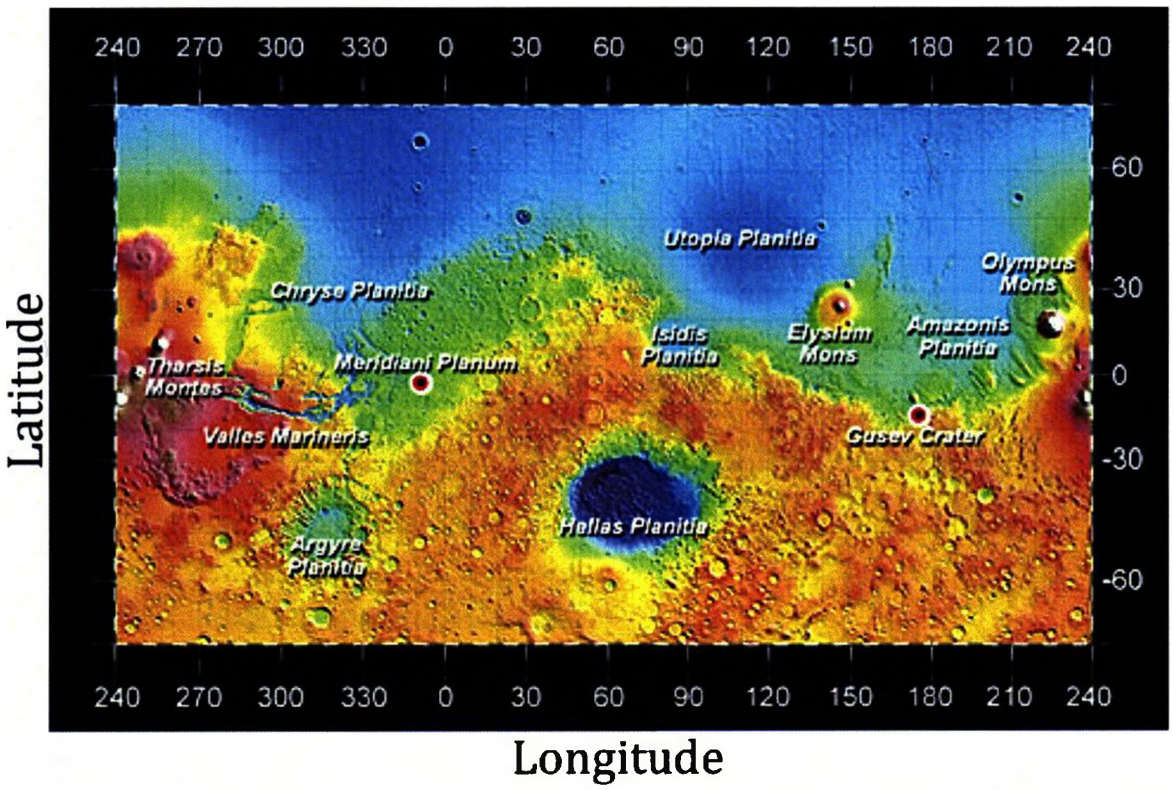

Figure 1.10 – The Mars Exploration Rover landing sites, marked with red and white circles. The Opportunity rover touched down in the hematite-rich plains of Meridiani Planum, while the Spirit rover landed in Gusev crater (Courtesy NASA).

---

environments on Earth (e.g. the Atacama Desert), the soil in the northern plains also contains perchlorates (i.e. any mineral species that contains the ClO_4^- perchlorate anion. Example: $NaClO_4$) (Ericksen 1983, Mellon et al., 2008).

Both of these sites (i.e. Meridiani Planum and the Martian Northern Plains) represent different environments that have resulted from the overall cooling and drying trend throughout Martian history. The Phoenix landing site would seem to represent a frozen sea, or a region possessing extensive ground ice deposits, both of which would have acted as 'traps' for liquid water as the Martian climate cooled. On the other hand, the massive sulfate deposits found by the Opportunity rover at Meridiani Planum, were likely a result of eolian transportation and deposition of sulfate salts formed during the evaporative concentration of Mars' primordial ocean. As the water level receded from its original

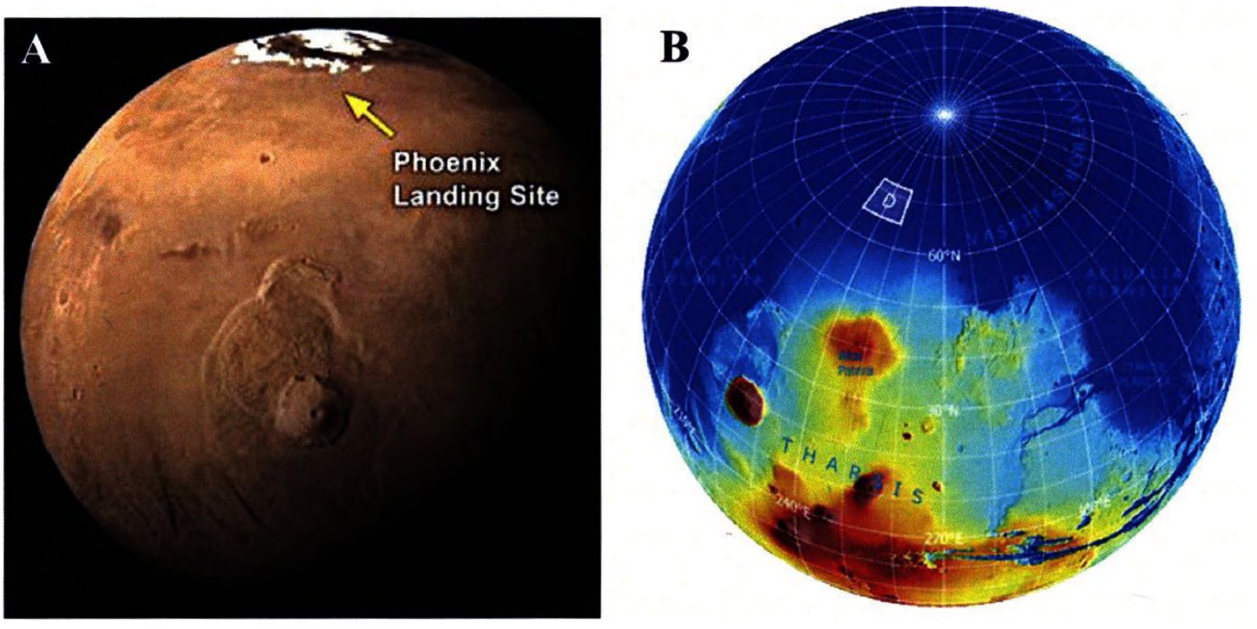

Figure 1.11 – Location of the Phoenix Lander in Vastitas Borealis, a region of the Martian northern plains. (A) Phoenix landing site as seen from orbit. (B) Phoenix landing site on a Mars global elevation map. (Both images courtesy NASA.)

---

shorelines, any local topographic lows would have produced land-locked basins in which seawater could become trapped and concentrated into brines. If drying continued until completion, the result would be the formation of salt covered playas that would slowly desiccate over time. Later eolian processes transported these grains to the Opportunity site, where they were reworked and deposited during brief periods marked by shallow surface water, and ground water flow in the area (Squyres et al., 2006).

Potential Martian Biota

The instability of the Martian climate throughout the last 3.5 Ga has been the driving force behind the geologic history of both of the sites studied herein, and undoubtedly would have had and/or will have had a major impact on any potential Martian biota that may have inhabited the planet. Due to the instability of the post-Noachian climate, it is unlikely that Martian life would have had an opportunity to diversify and proliferate in

the same manner as terrestrial organisms (Klingler et al., 1989; Hiscox 2001; Fairen 2005; Southam et al., 2007), but it does not detract from the possibility of life having developed at some point in Mars past (Klinger et al., 1989; Hiscox 2001; Landis 2001; Pavlov et al., 2006; Southam et al., 2007).

Evidence derived from Earth's geologic record has demonstrated that for the majority of Earth's history, our planet was inhabited exclusively by simple, single-celled organisms (Figure 1.12) (Wacey 2009). In contrast, multicellular life has only existed on Earth for the past 1.5 Ga, and it has only been in the last 542 Ma that terrestrial organisms have undergone an incredible diversification, leading to the evolution of the vast array of species that populate the Earth today (Nicholson 1878; Fortey 1999). In comparison, Earth's climate has been far more stable throughout its history than that of Mars (Studies in Geophysics: Climate in Earth History 1982; Jakosky et al., 1995; Baker et al., 2001; Kasting and Howard 2006), and as a result life has thrived on our world, while it seems to be entirely absent at the Martian surface.

It is for this reason that astrobiological exploration has focused on the relatively simple prokaryotic organisms found in Domain Archaea and Bacteria, as it is unlikely that eukaryotic organisms (those whose cells contain a nucleus), let alone multicellular-life, will have had a chance to evolve on Mars (Schulze-Makuch et al., 2005). Although complex life forms are unlikely to be found, it is possible that simple forms of life may have had the opportunity to evolve and take advantage of the periodic, short-lived, temperate periods that have punctuated Mars' history (Hiscox 2001; Fairen 2005). With

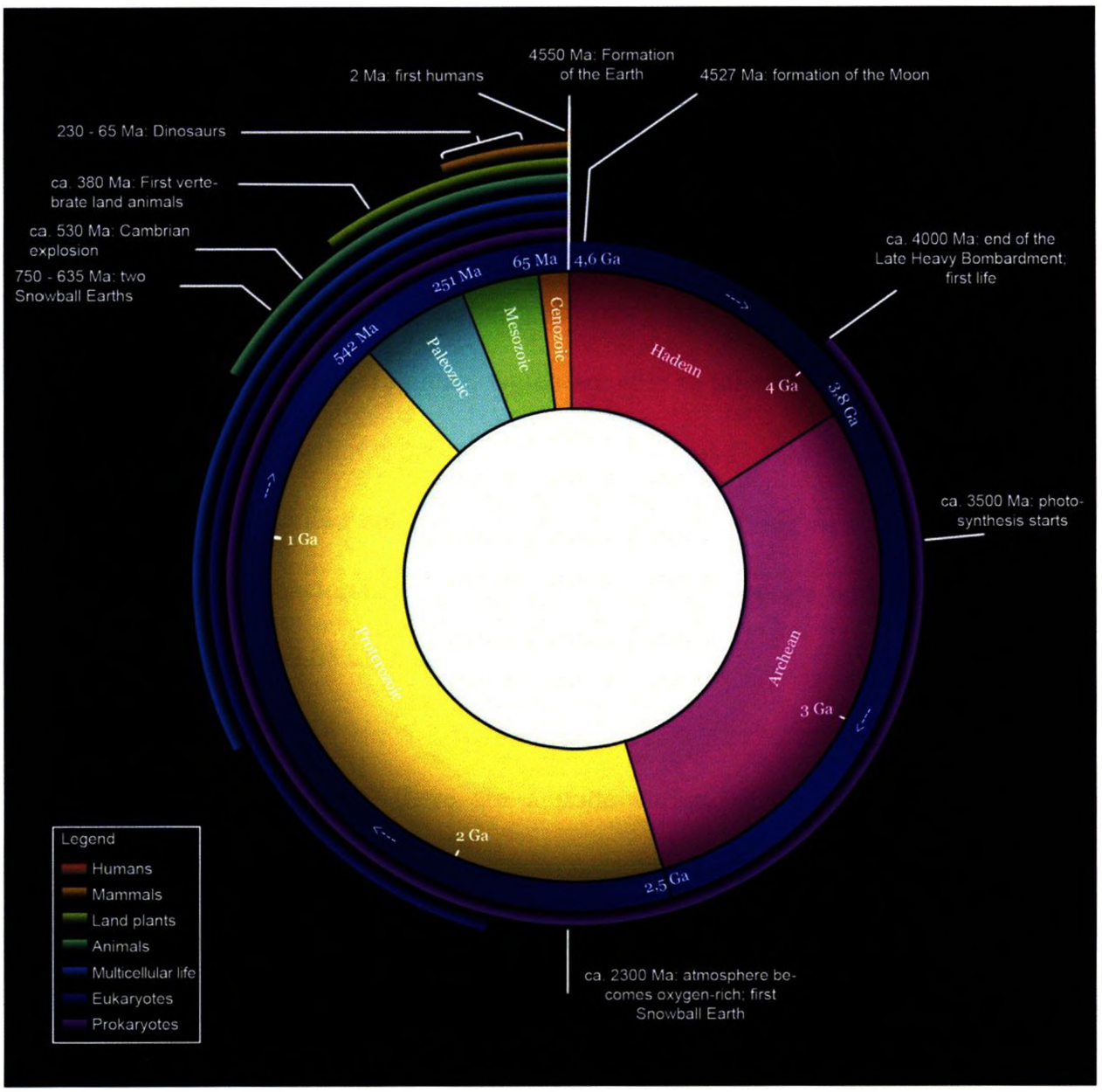

Figure 1.12 – Representative historical summary of the major events that have occurred in Earths geologic and evolutionary past.

---

this in mind, our study will focus primarily on halophilic prokaryotes, as they are the best analogues for proposed organisms on Mars (Landis 2001; DasSarma 2006).

HALOPHILES AS MARTIAN ANALOGUE ORGANISMS

Extreme halophiles, found in both the Domain Archaea and the Domain Bacteria (Landis 2001; DasSarma 2006) are suitable analogs for Martian biota that are capable of surviving

ancient and perhaps contemporary Martian conditions. Defined by Larsen (1962), slight, moderate, and extreme halophiles are organisms that grow best in 2 to 5, 5 to 20 and 20 to 30 weight % salt respectively dissolved in solution, and require salt for growth and reproduction (Edwards 1990). This group of organisms has very low species diversity by comparison to the much more common and diverse halotolerant organisms, comprised primarily of Bacteria and micro algae, which are able to tolerate up to 5.5 mol/L salt but do not require it for growth. Of these organisms the genus *Dunaliella* (Figure 1.13) is the most common single-celled eukaryotic algae, capable of living in brines with 0.03 - 5 mol/L salt, while the bacteria *Halomonas elongata* is the species with the widest single range of salt tolerance, 0.05 - 5.5 mol/L (Edwards 1990).

In addition to salt tolerance, there are a wide variety of halophiles that have also developed tolerances for other extreme environmental conditions, most notably are those with adaptations for alkaline, acidic, high/low temperature, intense UV light and xeric environments (Borowitzka 1981; Javor 1984; Kirkwood and Henley 2006). The type of habitats these organisms inhabit are extremely varied as they can be created by any combination of the aforementioned environmental conditions, but are most commonly found in places such as; tropical to sub-tropical inland closed basins, salt pans, manmade salterns/evaporation ponds, alkali lakes, estuaries/shoreline rock pools, subglacial lakes, and hydrothermal springs.

Figure 1.13 – Color DIC image of the mobile eukaryotic algae *Dunaliella*, found in brine samples from Basque Lake No. 2. Note the two flagella that allow it to propel itself through the brine, the presence of large vesicles, and the small orange clusters of carotenoids in the bottom left of the cell.

Halophile Adaptation Mechanisms

The primary stress encountered by organisms living in habitats with concentrated brine conditions is the constant potential for intracellular water to be lost from the cytosol. The reduction in water content can greatly reduce, or even eliminate the metabolic activity of a cell, lower the influx of ionic species that neutralize electrochemical gradients, and denature/disrupt proteins and macromolecular structures. Conversely, when returning to more dilute conditions, cells risk lysing if their cell walls cannot accommodate the pressure resulting from the influx of water. To overcome the complications of salinity, Bacteria and Archaea have evolved two different evolutionary coping mechanisms. Bacteria have adapted by employing osmotic solutes to balance water activity across the cellular membrane, while Archaea have modified their proteins and cellular machinery to tolerate high internal K^+ concentrations (Edwards 1990; Oren 1999).

During times when salt concentration is high, Bacteria will suspend growth and redirect energy towards accumulating osmotically active compounds such as glycerol ($C_3O_3H_8$) within the cytosol. The accumulation of these solutes will continue until water activity (i.e. the proportion of water molecules available to participate in chemical reactions) is balanced across the cellular membrane and cellular volume is restored, at which point growth can resume. This mechanism requires that the osmotically active compound does not interfere with cellular functioning at high concentrations, must be neutral or negatively charged, and it must be able to be maintained against large concentration gradients. If salinity is reduced, the osmotic solute must also be capable of rapid breakdown, storage into vacuoles, or excretion from the cell. The associated changes in cellular volume that can result from this activity are accommodated by fusing numerous small vesicles to the plasma membrane (Edwards 1990; Oren 1999). This adaptive trait eliminates the need for any irreversible genetic changes to proteins or cellular components, but is energetically costly to the cell.

The strategy developed by Archaea is fundamentally different than that of Bacteria, in that over time they have evolved new proteins, enzymes and macromolecules that are tolerant of high intracellular concentrations of K^+. This increased cellular tolerance of charged species owes itself to alterations made in both the amino acid composition (more acidic residues), and thus the integrated charge domains of proteins, that now require high K^+ levels to prevent repulsion from tearing tertiary structures apart (Edwards 1990). This adaptation has allowed these organisms to survive in high salt environments without any associated energy 'cost' to the cell, as they simply allow K^+ to enter the intracellular space until water activity has reached a new equilibrium across the cellular membrane.

This method of adaptation has rendered these organisms obligate halophiles as they can no longer grow or metabolize without a (species-specific) minimum concentration of salt within the media.

CANADIAN TERRESTRIAL ANALOGUE SITES

As we enter an exciting new age of space exploration, we are constantly challenged to make accurate and informative interpretations of the complex histories and nature of our planetary neighbors. However, in order to conduct thorough and comprehensive studies of extraterrestrial environments, we must first understand how similar environments, or 'terrestrial analogue sites' function on Earth. The Canadian Space Agency currently provides funding for ten different analogue sites (Figure 1.14), which place an emphasis on comparative planetary geology, astrobiology, space utilization/exploration, and public education (Hipkin et al., 2007). The foremost of these sites are: the Haughton-Mars project located on Devon Island, Nunavut, the McGill Arctic Research station on Axel Heiberg Island, Nunavut, and the Pavilion Lake Project in British Columbia (Figure 1.14, labeled red dots). In addition to these major research stations seven additional sites have been funded in Labrador, Ontario, Manitoba, British Columbia, Northwest Territories, and Ellesmere Island (Nunavut).

With Mars currently at the forefront of many astrobiological and exploration efforts, a particular interest has developed in analogue sites which are similar to past or present environments observed on Mars. A number of sites across Canada have been funded to study different aspects of the Martian climate, including polygonal terrain, arctic brine springs, and semi-arid evaporitic basins. Of interest to this study are the semi-arid

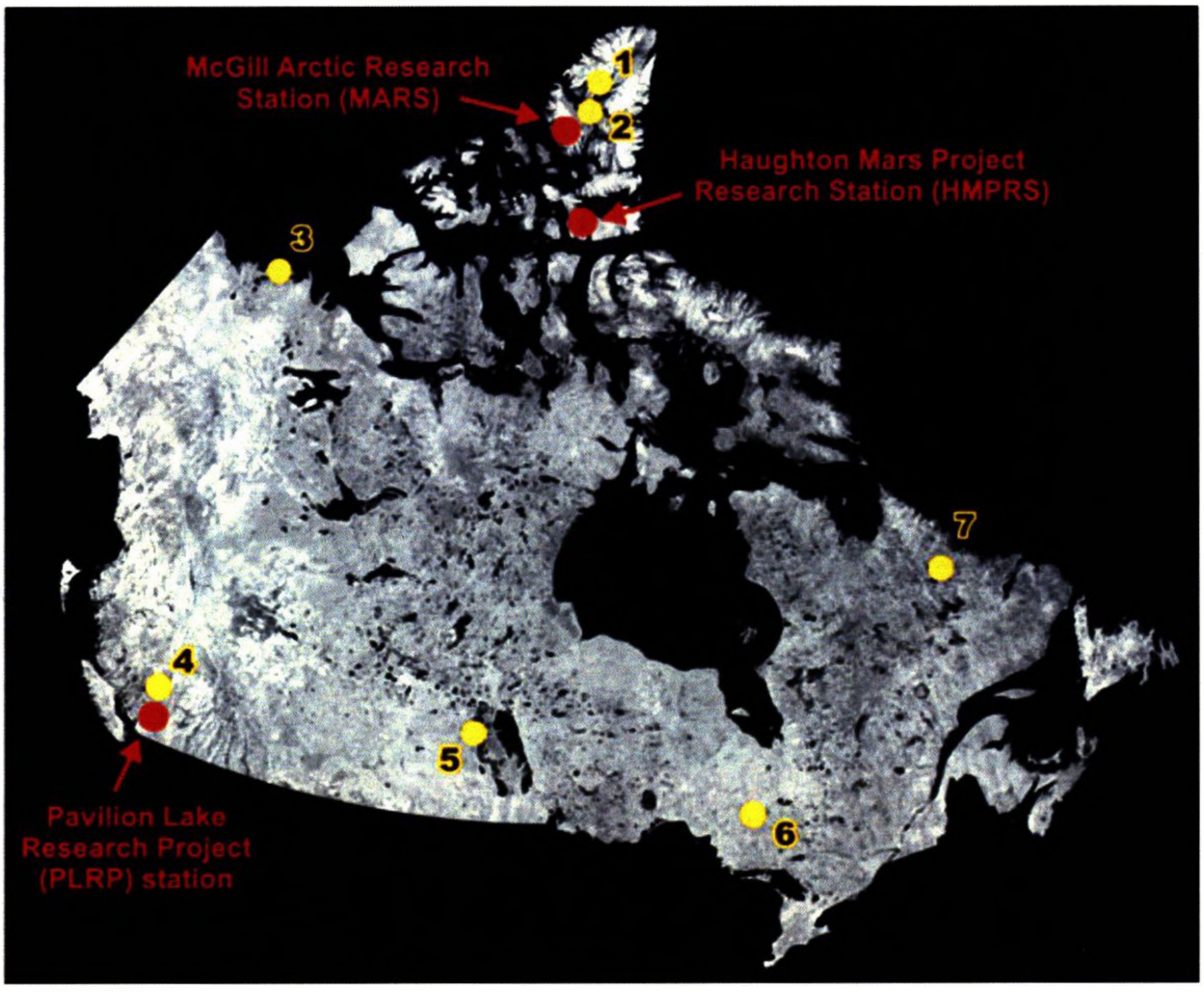

Figure 1.14 – Canadian terrestrial analogue sites funded by the Canadian Space Agency. (1) Borup Fiord, Ellesmere Island, Nunavut. (2) Eureka Sound lowlands, Ellesmere Island, Nunavut. (3) Tuktoyaktuk Peninsula, Northwest Territories. (4) Evaporitic Basins (Basque Lakes, Clinton Lake, Last Chance Lake, Saltwort Pond), British Columbia. (5) East German Creek, Manitoba. (6) Kidd Creek Mine, Ontario. (7) Mistastin impact structure, Labrador and Newfoundland. (Image credit Gordon Osinski.)

---

environments of the British Columbia interior, where low rainfall and high evaporation have resulted in numerous hypersaline lakes and ponds forming in closed-basin settings. These sites represent a number of environments proposed to exist on Mars including subsurface ground water brines (Meridiani Planum, gullies/seeps) and evaporative basins (Terra Meridiani). Both types of environments are of astrobiological interest as they are not only linked to the history of liquid water on Mars, but might also represent a refuge/habitat for past or present Martian life.

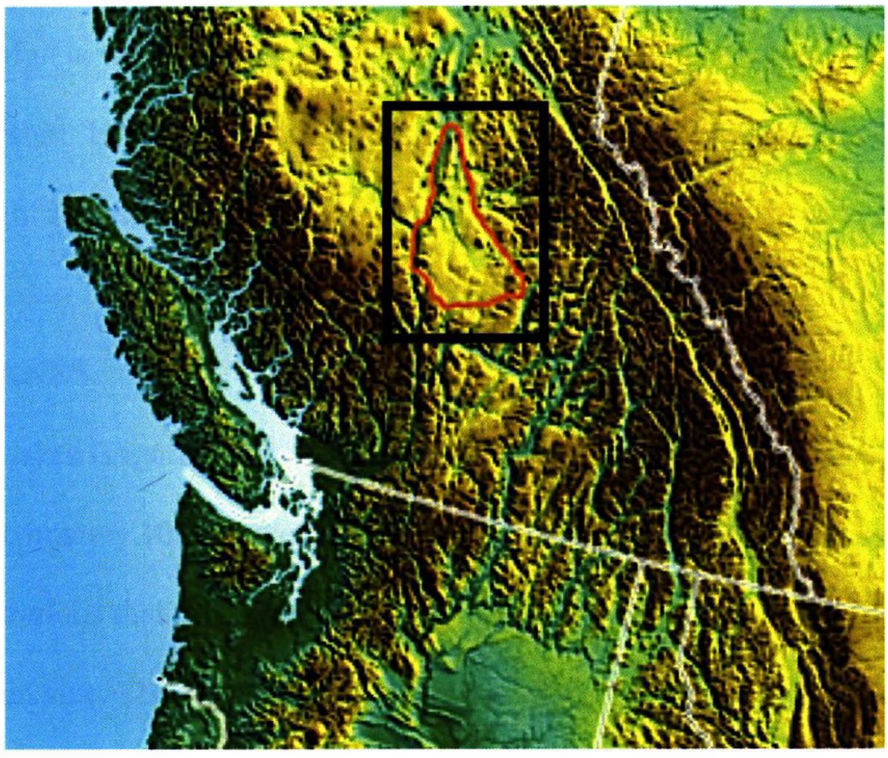

Figure 1.15 – The Cariboo Plateau, located in south-central British Columbia, Canada. This region is home to a variety of hypersaline environments dominated by Mg-Na-sulfate and/or carbonate, a number of which are considered to be terrestrial analogue sites for Mars and the Jovian satellites.

Characterization of Cariboo Plateau

The Cariboo Plateau, located in south-central British Columbia, is a region dominated by flood basalts found within the Rocky Mountain orogenic belt that transverses the entire western coastline of North America (Figure 1.15). The plateau lies at an altitude of 1050 – 1250 m above sea level; and its climate is considered semi-arid to semi-humid receiving only 300 – 400 mm of precipitation per year (Nesbitt 1990). The basement rocks of the region are Neogene-age basalt and ash deposits, as well as metamorphosed greenstones, quartzites, argillites and limestones, all of which have been overlain by a thin veneer of glaciofluvial sediment (Nesbitt 1990). The plateau is a closed basin system with disordered drainage, which has led to the formation of numerous marshes and lakes occupying shallow topographic depressions that range from fresh water to hypersaline in

composition. Notably, the groundwater and brine compositions found in this area contain a very high Mg/Ca ratio of roughly 50:1 making them the most Mg-rich brines in North America (Nesbitt 1990), and therefore one of the best terrestrial analogs for Martian regions thought to possess Mg-rich brines.

BASQUE LAKES

The Basque Lakes (Figure 1.16) are a series of eleven brine pools, mud flats, and playas located approximately 100 km west of Kamloops, British Columbia. The lakes have Mg^{2+} brine concentrations that are among the highest in the world (Nesbitt 1990), and can vary considerably in size. The largest, Basque No. 1, is 195 by 135 m wide while the smallest is Basque No. 4, which consists of a series of 18 small brine pools (Goudge 1924). While Basque No. 5, a historically small pool created by discharge of brine water from Basque No. 1 during mining operations, is currently a Mg-carbonate-sulfate pond, possessing water only after precipitation events. The lake's brine concentrations as well as water levels vary widely throughout the year, ranging from meter deep relatively dilute brines after spring run-off to highly concentrated brines, or completely evaporated ephemeral salt pans, in the late summer. Pools that contain water throughout the year are fed by groundwater discharge as springs (Nesbitt 1990). Commonly a crystal bowl morphology will develop with concentric rings of mineralization, in which the least soluble mineral salts will precipitate out at the edges and the more soluble mineral salts will occur only in the centers. The crystal bowls are typically bounded laterally by an impermeable layer of clay/mud, and overlie a permeable ash layer that typically occurs between ½ to 15 m below the surface, together with sandy lenses they act as an aquifer that feeds the brine

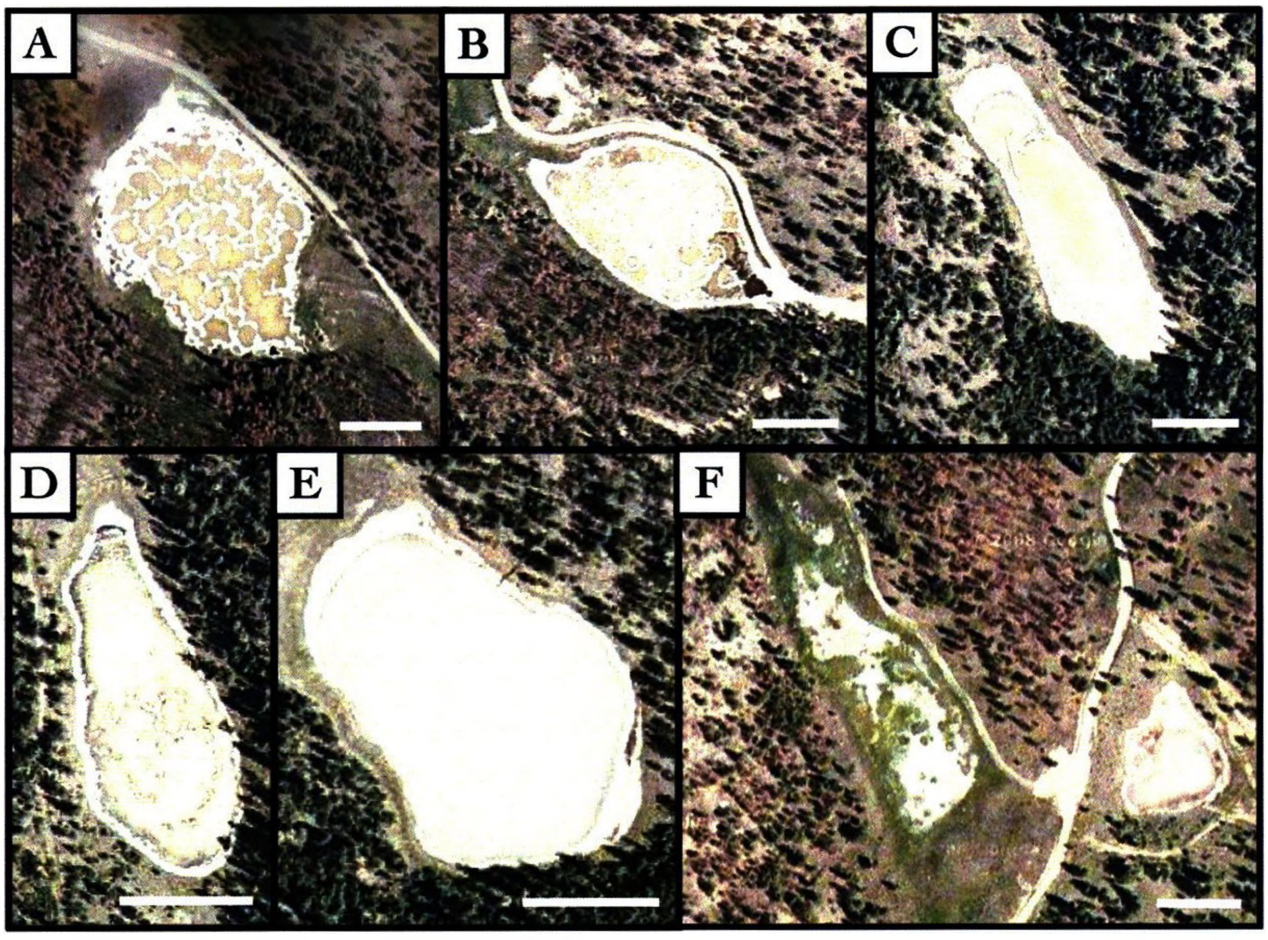

Figure 1.16 – Satellite images of the six largest Basque Lakes sampled in this study. The scale bar is 50 m and North is up in each image. (A) Basque Lake No. 1. (B) Basque Lake No. 2. (C) Basque Lake No. 2W. (D) Basque Lake No. 3. (E) Basque Lake No. 4. (F) Basque Lake No. 5 (Courtesy Google Maps).

---

springs (Nesbitt 1990). The Mg^{2+} and SO_4^{2-} rich brine associated with the Basque Lakes achieves its extremely high ionic concentrations from the weathering of basaltic minerals and underlying volcanic and metamorphic rocks. The dissolved ions are then concentrated at upwelling areas as water is evaporated in the closed basin's arid setting (Cole 1926; Cummings 1940; Nesbitt 1990; Renaut 1990).

PRESERVATION OF ORGANIC MATERIAL IN SALT

Astrobiological exploration of other planetary bodies relies heavily on the ability of natural processes to preserve organic material and biosignatures in a recognizable state

over geologically relevant timescales. Tuovila et al., (1987) demonstrated that ATP in hypersaline environments could survive unhydrolysed indefinitely even after extreme UV exposure had eliminated all viable cells, while recent experiments performed by Aubrey et al., (2006) have concluded that amino acids from a variety of terrestrial locations can be preserved in sulfates over geologic time, and could potentially have been preserved for billions of years on Mars. Renaut (1993) documented that although microbial mat preservation in the form of microbolite (stromatolites) was not likely in modern terrestrial hypersaline environments due to predation, preservation of small mat fragments and organic-rich mineral residues readily occurs in the hydromagnesite deposits of the Cariboo Plateau, British Columbia, Canada. Furthermore, Vreeland et al., (2000) reported the isolation and growth of three strains of viable, halophilic bacteria, from 250 million year old fluid inclusions contained within a primary salt crystal.

BIOSIGNATURES

A biosignature can be defined as any evidence, chemical or physical, that indicates the past or present existence of life. Accordingly, a good biosignature in astrobiological terms would be any chemical compound (DNA), or physical feature (fossilized bacteria) that is indicative solely of life-based processes. In addition, a good biosignature should be a relatively common molecule capable of survival over geologically relevant periods of time in a recognizable state. A study performed by Marshall et al., (2006) has proposed that several organic molecules such as chlorophyll, carotenoids, cell membranes, bacteriorhodopsin, bacterioruberin and algaenan would be suitable biosignatures because they are easily identified and are resistant to degradation. Other suitable biosignatures

may include biogenically related chemical species such as kerogen (Moreau et al., 2004), microfossils (Hugo 2005), and distinctive combinations of molecules (oxygen [O_2] and methane [CH_4] for example) that are incompatible on a long-term basis in a planet's atmosphere (Lovelock 1965). Since our experiments focus on the reflectance IR spectral features produced by molecules related to halophilic organisms, good biosignatures must also be life-specific (i.e., not overprinted by inorganic features), and most importantly, strong enough to be detected within sulfate host minerals.

REFLECTANCE IR AS A TECHNIQUE FOR ASTROBIOLOGICAL STUDY

To plan and execute a successful astrobiological mission to Mars, or any other astrobiologically interesting body, we must first identify target sites that have a high probability of hosting or preserving organic and inorganic molecules required/produced by life. To do this effectively, and in a timely manner, we require a technique that can be scaled from a regional to outcrop scale, while providing fast, and accurate chemical information about its target. Diffuse Reflectance Infrared Fourier Transform Spectroscopy (DRIFTS), here referred to as reflectance IR, has a long and successful history of use on a variety of space missions including the Galileo spacecraft, the Earth monitoring Aura satellite, Cassini, the Hubble telescope, Mars Global Surveyor, Mars Express, the Mars Exploration rovers, the Mars Odyssey spacecraft, the Mars Reconnaissance Orbiter, and the New Horizons spacecraft, to name a few. As early as 1856 reflectance IR has been used to characterize planetary surface materials (the Moon), and is currently a planned instrument on the Wide-Field Infrared Survey Explorer intended to study the solar system, our galaxy and the universe; aboard the James Webb

Space Telescope set to study the assembly of galaxies and planetary system formation; and as part of the European Space Agency's ExoMars mission to both search for signs of life on Mars, and to characterize its surface materials.

Currently several satellites orbiting Mars are equipped with reflectance IR instruments, and phyllosilicates, sulfates, hydrated silicates, carbonates, serpentine and others have been identified on the Martian surface using this technique (Bandfield et al., 2003; Gendrin et al., 2005; Bishop et al., 2007; Bishop et al., 2008; Mustard et al., 2008; Carter et al., 2009; Ehlmann et al., 2009; Wiseman et al., 2009). Reflectance IR has also been successful in identifying macromolecular compounds in the Zagami Mars meteorite (Anderson et al., 2005), as well as in Martian surface analogue materials (Esposito et al., 2000; Anderson et al., 2005). Together this demonstrates the capability of reflectance IR to detect both inorganic and organic compounds by bulk spectral analysis on a regional, local and sample scale. This versatility, as well as its sensitivity to water content, and non-destructive nature (Andersen et al., 2005), suggests reflectance IR may be an ideal tool for orbital or site-specific, in-situ, remote-sensing objectives.

STUDY OBJECTIVES

The goal of this study is to characterize organic material that has been trapped and preserved in magnesium sulfate salt deposits obtained from the Basque Lakes of British Columbia, Canada, using a biomass assay, confocal/light microscopy, and reflectance IR spectroscopy. Laboratory enrichment samples are used to highlight the types of organisms present in the environment, and to characterize the inherent biosignatures

produced by a consortium of halophilic organisms within a magnesium sulfate matrix. Natural salt samples are examined via biomass assay, and confocal/light microscopy is used to confirm the presence of cells and organics within the sample. Diffuse Reflectance Infrared Fourier Transform Spectroscopy (DRIFTS), referred to here as reflectance IR, will be employed to determine if the detection of organic material within natural salt samples is possible using reflectance IR techniques. Experimental results are then used to evaluate the suitability of reflectance IR as an astrobiological remote sensing tool, and to develop a sampling/analysis strategy that could be used on both Mars and the Jovian satellites.

REFERENCES

Acuna, M. H., Connerney, J. E. P., Ness, N. F., Lin, R. P., Mitchell, D., Carlson, C. W., McFadden, J., Anderson, K. A., Reme, H., Mazelle, C., Vignes, D., Wasilewski, P., Cloutier, P., 1999. Global distribution of crustal magnetization discovered by the Mars Global Surveyor MAG/ER experiment. *Science* 284, 790-793.

Anderson, M. S., Andringa, J. M., Carlson, R. W., Conrad, P., Hartford, W., Shafer, M., Soto, A., Tsapin, A. I., 2005. Fourier transform infrared spectroscopy for Mars science. *Review of Scientific Instruments* 76, 34101-1-34101-9.

Ansan, V., and Mangold, N., 2006. New observations of Warrego Valles, Mars: Evidence for precipitation and surface runoff. *Planetary and Space Science* 54, 219-242.

Aubrey, A., Cleaves, H. J., Chalmers, J. H., Skelley, R. A., Mathies, R. A., Grunthaner, F. J., Ehrenfreund, P., Bada, J. L., 2006. Sulfate minerals and organic compounds on Mars. *Geology* 34, 357-360.

Baker, V. R., Strom, R. G., Gulick, V. C., Kargel, J. S., Komatsu, G., Kale, V. S., 1991. Ancient oceans, ice sheets and the hydrological cycle on Mars. *Nature* 352, 589-594.

Baker, V. R., 2001. Water and the Martian landscape. *Nature* 412, 228-236.

Banfield, J. F., Glotch, T. D., Christensen, P. R., 2003. Spectroscopic identification of carbonate minerals in the Martian dust. *Science* 301, 1084-1087.

Bishop, J. L., Murchie, S. L., Brown, A. J., Pelkey, S. M., Roach, L. A., Mustard, J. F., Bibring, J.-P., and the CRISM Team, 2007. Sulfates in Juventae Chasma as seen by CRISM. *Lunar and Planetary Science* XXXVIII, 1338, 2252.

Bishop, J. L., Noe Dobrea, E. Z., McKeown, N. K., Parente, M., Ehlmann, B. L., Michalski, J. R., Milliken, R. E., Poulet, F., Swayze, G. A., Mustard, J. F., Murchie, S. L., Bibring, J.-P., 2008. Phyllosilicate diversity and past aqueous activity revealed at Mawrth Vallis, Mars. *Science* 321, 830-833.

Borowitzka, L. J, 1981. The microflora: Adaptations to life in extremely saline lakes. *Hydrobiologia* 81, 33-46.

Carter, J., Poulet, F., Bibring, J.-P., Murchie, S., Langevin, Y., Mustard, J. F., Gondet, B., 2009. Phyllosilicates and other hydrated minerals on Mars: 1. Global distribution as seen by MEx/OMEGA. *Lunar and Planetary Science* XL, 2028.

Catling, D., (2009). Atmospheric Evolution of Mars, *Encyclopedia of Paleoclimatology and Ancient Environments, Encyclopedia of Earth Sciences Series* XXVIII. Springer.

Chavdarian, G. V., Sumner, D. Y., 2006. Cracks and fins in sulfate sand: Evidence for recent mineral-atmospheric water cycling in Meridiani Planum outcrops? *Geology* 34, 229-232.

Christensen, P. R., 2003. Formation of recent Martian gullies through melting of extensive water-rich snow deposits. *Nature* 466, 45-48.

Cockell, C. S., Catling, D. C., David, W. L., Snook, K., Kepner, R. L., Lee, P., McKay, C. P., 2000. The ultraviolet environment of Mars: Biological implications past, present, and future. *Icarus* 146, 343-359.

Connerney, J. E. P., Acuna, M. H., Keleteschka, G., Ness, N. F., Mitchell, D. L., Lin, R. P., 1999. Tectonic implications of Mars crustal magnetism. *Lunar and Planetary Science XXXVI*, 1401.

Connerney, J. E. P., Acuna, M. H., Wasilewski, P. J., Kletetschka, G., 2001. The global magnetic field of Mars and implications for crustal evolution. *Geophysical Research Letters* 21, 4015-4018.

Cole, L. H., 1926. Sodium sulfate of Western Canada: Occurrence, uses and technology. *Canada Department of Mines* 72-129.

Cummings, J. M., 1940. Saline and hydromagnesite deposits of British Columbia. *British Columbia Department of Mines: Bulletin No. 4.*

DasSarma, S., 2006. Extreme halophiles are models for astrobiology. *Microbiology* 1, 120-126.

Dohm, J. M., Anderson, R. C., Baker, V. R., Ferris, J. C., Rudd, L. P., Hare, T. M., Rice, J. W., Casavant, R. R., Strom, R. G., Zimbleman, J. R., Scott, D. H., 2001. Latent outflow activity for western Tharsis, Mars: Significant flood record exposed. *Journal of Geophysical Research* 106, 12301-12314.

Dohm, J. M., Baker, V. R., de Pablo, M. A., Ruiz, J., Ferris, J. C., Anderson, R. C., 2003. Tharsis-triggered flood inundations of the lowlands of Mars. *Lunar and Planetary Science XXXIV*, 1093.

Dohm, J. M., Anderson, R. C., Barlow, N. G., Miyamoto, H., Davies, A. G., Taylor, G. J., Baker, V. R., Boynton, W. V., Keller, J., Kerry, K., Janes, D., Fairen, A. G., Schulze-Makuch, D., Glamoclija, M., Marinangeli, L., Ori, G. G., Strom, R. G., Williams, J.-P., Ferris, J. C., Rodriguez, J. A. P., de Pablo, M. A., Karunatillake, S., 2008. Recent geological and hydrological activity on Mars: The Tharsis/Elysium corridor. *Planetary and Space Science* 56, 985-1013.

Edwards, C., 1990. *Microbiology of Extreme Environments.* United States: McGraw-Hill.

Ehlmann, B. L., Mustard, J. F., Murchie, S. L., 2009. Detection of serpentine on Mars by MRO-CRISM and possible relationship with olivine and magnesium carbonate in Nili Fossae. *Lunar and Planetary Science* XXXX, 1787.

Ericksen, G. E., 1983. The Chilean nitrate deposits. *American Scientist* 71, 366-374.

Esposito, F., Colangeli, L., Palomba, E., 2000. Infrared reflectance spectroscopy of Martian analogues. *Journal of Geophysical Research* 105, 17643-17654.

Fairen, A. G., Dohm, J. M., Baker, V. R., de Pablo, M. A., Ruiz, J., Ferris, J. C., Anderson, R. C., 2003. Episodic flood inundations of the northern plains of Mars. *Icarus* 165, 53-67.

Fairen, A. G., Dohm, J. M., Uceda, E. R., Rodriguez, A. P., Baker, V. R., Fernandez-Remolar, D., Schulze-Makuch, D., Amils, R., 2005. Prime candidate sites for astrobiological exploration through the hydrogeological history of Mars. *Planetary and Space Science* 53, 1355-1375.

Fassett, C. I., Head, J. W., 2008. Valley network-fed, open-basin lakes on Mars: Distribution and implications for Noachian surface and subsurface hydrology. *Icarus* 198, 37-56.

Forsberg-Taylor, N. K., and Howard, A. D., 2004. Crater degradation in the Martian highlands: Morphometric analysis of the Sinus Sabaeus region and simulation modeling suggest fluvial processes. *Journal of Geophysical Research* 109, E05002.

Fortey, R., 1999. *Life: A natural history of the first four billion years of life on Earth.* United States: Vintage Books.

Gendrin, A., Mangold, N., Bibring, J.-P., Langevin, Y., Gondet, B., Poulet, F., Bonello, G., Quantin, C., Mustard, J., Arvidson., R., LeMouelic, S., 2005. Sulfates in

Martian layered terrains: The OMEGA/Mars Express view. *Science* 307, 1587-1591.

Goudge, M. F., 1924. Magnesium sulfate in British Columbia. *Canada Department of Mines, Investigations of Mineral Resources and the Mining Industry*, 62-101.

Greenwood, J. P., Itoh, S., Sakamoto, N., Vicenzi, E. P., Yurimoto, H., 2008. Hydrogen isotope evidence for loss of water from Mars through time. *Geophysical Research Letters* 35, L05203.

Harrison, K. P., and Chapman, M. G., 2008. Evidence for ponding and catastrophic floods in central Valles Marineris, Mars. *Icarus* 198, 351-364.

Hartmann, W. K., Malin, M., McEwen, A., Carr, M., Soderblom, L., Thomas, P., Danielson, E., James, P., Veverka, J., 1999. Evidence for recent volcanism on Mars from crater counts. *Nature* 397, 586-589.

Hartmann, W. K., and Neukum, G., 2001. Cratering chronology and the evolution of Mars. *Space Science Reviews* 96, 165-194.

Hartmann, W. K., 2005. Martian cratering 8: Isochron refinement and the chronology of Mars. *Icarus* 174, 294-320.

Hiscox, J. A., 2001. An overview of the origin of life: The case for biological prospecting on Mars. *Earth, Moon and Planets* 87, 191-212.

Hugo, B.-C., 2005. Microfossils as biosignatures. *Astrobiology and Planetary Missions* 5906, 217-226.

Irwin, L. N., Schulze-Makuch, D., 2003. Europa: Strategy for modeling putative multilevel ecosystems on Europa. *Astrobiology* 3, 813-821.

Jakosky, B. M., and Carr, M. H., 1985. Possible precipitation of ice at low latitudes of Mars during periods of high obliquity. *Nature* 315, 559-561.

Jakosky, B. M., Henderson, B. G., Mellon, M. T., 1995. Chaotic obliquity and the nature of the Martian Climate. *Journal of Geophysical Research* 100, 1579-1584.

Jakosky, B. M., Phillips, R. J., 2001. Mars' volatile and climate history. *Nature* 412, 237-244.

Javor, B. J., 1984. Growth potential of halophilic bacteria isolated from solar salt environments: Carbon sources and salt requirements. *Applied and Environmental Microbiology* 48, 352-360.

Kass, D. M., Yung, Y. L., 1995. Loss of atmosphere from Mars due to solar wind-induced sputtering. *Science* 286, 697-699.

Kasting, J. F., and Howard, M. T., 2006. Atmospheric composition and climate on the early Earth. *Philosophical Transactions of the Royal Society B: Biological Sciences* 361, 1733-1742.

Kirkwood, A. E., and Henley, W. J., 2006. Algal community dynamics and halotolerance in a terrestrial, hypersaline environment. *Journal of Phycology* 42, 537-547.

Klingler, J. M., Mancinelli, R. L., White, M. R., 1989. Ecological considerations for possible Martian biota. *Exobiology and Future Mars Missions* 38, 416-417.

Kounaves, S. P., Hecht, M. H., Quinn, R., West, S. J., Young, S. M., Clark, B. C., Ming, D. W., Boynton, W. V., Gospodinova, K., Kapit, J., Deflores, L. P., Smith, P. H., and Team A, 2008. The aqueous chemistry of the soils at the Phoenix landing site. *American Geophysical Union,* Fall Meeting 2008, U14A-05.

Kumar, A., Koaski, M., Lee, H. M., Kim, K. S., 2008. Photoexcitation and photoionization dynamics of water photolysis. *Journal of Physical Chemistry A* 112, 5502-5508.

Lammer, H., Stumptner, W., Bauer, S. J., 1996. Loss of H and O from Mars: Implications for the planetary water inventory. *Geophysical Research Letters* 23, 3353-3356.

Lammer, H., Lichtenegger, H. I. M., Kolb, C., Ribas, I., Guinan, E. F., Abart, R., Bauer, S. J., 2003. Loss of water from Mars: Implications for the oxidation of the soil. *Icarus* 165, 9-25.

Landis, G. A., 2001. Martian water: Are there extant halobacteria on Mars? *Astrobiology* 1, 161-164.

Langlais, B., and Amit, H., 2008. The past Martian dynamo. *Science* 321, 1784-1785.

Lillis R. J., Frey, H. V., Roberts, J. H., Kuang, W., Manga, M., 2008. Giant impacts and the death of the Martian dynamo: Where data meet models. *Lunar and Planetary Science XXXIX 1391,* 1173-1174.

Larsen, H., 1962. *The bacteria, vol. 4: Halophilism*. United States: Academic Press.

Laskar, J., Levrard, B., Mustard, J. F., 2002. Orbital forcing of the Martian polar deposits. *Nature* 419, 375-377.

Lovelock, J., 1965. A physical basis for life detection experiments. *Nature* 207, 568-570.

Malin, M. C., Edgett, K. S., 2000. Evidence for recent groundwater seepage and surface runoff on Mars. *Science* 288, 2330-2335.

Mancinelli, R. L., Fahlen, T. F., Landheim, R., Klovstad, M. R., 2004. Brines and evaporites: analogues for Martian life. *Advances in Space Research* 33, 1244-1246.

Makay, C. P., 1997. The search for life on Mars. *Origins of Life and Evolution of the Biosphere* 27, 263-289.

Marion, G. M., Fritsen, C. H., Eicken, H., Payne, M. C., 2003. Europa: The search for life on Europa: Limiting environmental factors, potential habitats, and Earth analogues. *Astrobiology* 3, 785-811.

Marquez, A., angel de Pablo, M., Oyarzun, R., Viedma, C., 2005. Evidence of gully formation by regional groundwater flow in the Gorgonum-Newton region (Mars). *Icarus* 179, 398-414.

Marshall, C. P., Carter, E. A., Leuko, S., Javaux, E. J., 2006. Vibrational spectroscopy of extant and fossil microbes: Relevance for the astrobiological exploration of Mars. *Vibrational Spectroscopy* 41, 182-189.

McLennan, S. M., Bell, J. F., Calvin, W. M., Christensen, P. R., Clark, B. C., Souza, P. A., Farmer, J., Farrand, W. H., Fike, D. A., Gellert, R., Ghosh, A., Glotch, T. D., Grotzinger, J. P., Hahn, B., Herkenhoff, K. E., Hurowitz, J. A., Johnson, J. R., Johnson, S. S., Jolliff, B., Klingelhofer, G., Knoll, A. H., Learner, Z., Malin, M. C., McSween, H. Y., Pocock, J., Ruff, S. W., Soderblom, L. A., Squyers, S. W., Tosca, N. J., Watters, W. A., Wyatt, M. B., Yen, A., 2005. Provenance and diagenesis of the evaporite-bearing Burns Formation, Meridiani Planum, Mars. *Earth and Planetary Science Letters* 240, 95-121.

Mege, D., Cook, A. C., Garel, E., Lagabrielle, Y., Cormier, M.-H., 2003. Volcanic rifting at Martian grabens. *Journal of Geophysical Research* 108, 1-33.

Mellon, M. T., Boynton, W. V., Feldman, W. C., Arvidson, R. E., Titus, T. N., Bandfield, J. L., Putzig, N. E., Sizemore, H. G., 2008. A pre-landing assessment of the ice-

table depth and ground-ice characteristics in Martian permafrost at the Phoenix landing site. *Journal of Geophysical Research* 113, E00A25.

Moreau, J. W. and Sharp T. G., 2004. A transmission electron microscopy study of silica and kerogen biosignatures in ~1.9 Ga Gunflint microfossils. *Astrobiology* 4, 196-210.

Mustard, J. F., Murchie, S. L., Pelkey, S. M., Ehlmann, B. L., Milliken, R. E., Grant, J. A., Bibring, J.-P., Poulet, F., Bishop, J., Noe Dobrea, E., Roach, L., Seelos, F., Arvidson, R. E., Wiseman, S., Green, R., Hash, C., Humm, D., Malaret, E., McGovern, J. A., Seelos, K., Clancy, T., Clark, R., Marais, D. D., Morris, R., Robinson, M., Roush, T., Smith, M., Swayze, G., Taylor, H., Titus, T., Wolff, M., 2008. Hydrated silicate minerals on Mars observed by the Mars Reconnaissance Orbiter CRISM instrument. *Nature* 454, 305-309.

Nesbitt, H. W., 1990. Groundwater evolution, authigenic carbonates and sulfates, of Basque Lake No. 2 basin, Canada. *Fluid Mineral Interactions: A Tribute to H. P. Eugster, The Geochemical Society, Special Publication No. 2,* 355-369.

Nicholson, H. A., 1878. *Ancient Life-History of the Earth.* United States: D. Appleton & Company

Nyquist, L. E., Bogard, D. D., Shih, C.-Y., Greshake, A., Stoffler, D., Eugster, O., 2001. Ages and geologic histories of Martian meteorites. *Chronology and Evolution of Mars* 96, 105-164.

Oren, A., 1999. Bioenergetic aspects of halophilism. *Microbiology and Molecular Biology Reviews* 63, 334-348.

Pavlov, A. K., Blinov, A. V., Konstaninov, A. N., 2002. Sterilization of Martian surface by cosmic radiation. *Planetary and Space Science* 50, 669-673.

Poulet, F., Bibring, J.-P., Mustard, J. F., Gendrin, A., Mangold, N., Langevin, R. E., Arvidson, A. E., Gondet, B., Gomez, C., and the Omega Team, 2005. Phyllosilicates on Mars and implications for early Martian climate. *Nature* 438, 623-627.

Raulin, F., Owen, T., 2002. Organic chemistry and exobiology on Titan. *Space Science Reviews* 104, 377-394.

Renaut, R. W., Stead, D., 1990. Recent magnesite-hydromagnesite sedimentation in playa basins of the Cariboo Plateau, British Columbia. *Geological Fieldwork 1991-1,* 279-288

Renaut, R. W., 1993. Morphology, distribution and preservation potential of microbial mats in the hydromagnesite-magnesite playas of the Cariboo Plateau, British Columbia, Canada. *Hydrobiologia* 267, 75-98.

Schon, S. C., Fassett, C. I., Head, J. W., 2008. Meander loops and point bar sequences: Evidence of a stable delta plain environment in Jezero Crater. *Lunar and Planetary Science* XXXIX 1391, 1354.

Schulze-Makuch, D., Irwin, L. N., Lipps, J. H., LeMone, D., Dohm., J. M., Fairen, A. G., 2005. Scenarios for the evolution of life on Mars. *Journal of Geophysical Research* 110, E12S23.

Sleep, N. H., 1994. Martian plate tectonics. *Journal of Geophysical Research* 99, 5639-5655.

Southam, G., Rothschild, L. J., Westall, F., 2007. The geology and habitability of terrestrial planets: Fundamental requirements for life. *Space Science Reviews* 129, 7-34.

Squyres, S. W., Knoll, A. H., Arvidson, R. E., Clark, B. C., Grotzinger, J. P., Jolliff, B. L., McLennan, S. M., Tosca, N., Bell Ill, J. F., Calvin, W. M., Farrand, W. H., Glotch, T. D., Golombek, M. P., Herkenhoff, K. E., Johnson, J. R., Klingelhofer, G., McSween, H. Y., Yen, A. S., 2006. The Opportunity rover's Athena science investigation at Meridiani Planum, Mars. *Nature* 306, 1698-1703.

Stevenson, D. J., 2001. Mars' core and magnetism. *Nature* 412, 214-219.

Studies in Geophysics, 1982. *Climate in Earth history*. United States: National Academy Press.

Tanaka, K. L., Skinner, J. A., Hare, T. M., Joyal, T., Wenker, A., 2003. Resurfacing history of the northern plains of Mars cased on geologic mapping of Mars Global Surveyor data. *Journal of Geophysical Research* 108, 24-1-32.

Terada, N., Kulikov, Y. N., Lammer, H., Lichtenegger, H. I. M., Tanaka, T., Shinagawa, H., Zhang, T., 2009. Atmosphere and water loss from early Mars under extreme solar wind and extreme ultraviolet conditions. *Astrobiology* 9, 55-70.

Tuovila, B. J., Dobbs, F. C., LaRock, P.A., and Siegel, B. Z., 1987. Preservation of ATP in hypersaline environments. *Applied and Environmental Microbiology* 53, 2749-2753.

Vreeland, R.H., Rosenzwelg, W. D., Powers, D. W., 2000. Isolation of a 250 Million-year-old halotolerant bacterium from a primary salt crystal. *Nature* 407, 897-900.

Wacey, D., 2009. *Early life on Earth, a practical guide*. Springer Science and Business Media B.V.

Ward, W. R., 1974. Climatic variations on Mars: 1. Astronomical theory of insolation. *Journal of Geophysical Research* 79, 3375-3386.

Werner, S. C., 2009. The global Martian volcanic evolutionary history. *Icarus* 201, 44-68.

Wiseman, R. E., Arvidson, R. E., Morris, R. V., Murchie, S. L., Seelos, F. P., Andrews-Hanna, J. C., and the CRISM team, 2009. Hydrated sulfate deposits detected within Schiaparelli Crater, Mars. *Lunar and Planetary Science* XL, 1798.

Wood, L. J., 2006. Quantitative geomorphology of the Mars Eberswalde delta. *GSA Bulletin* 118, 557-566.

CHAPTER 2

CHARACTERIZATION OF HALOPHILIC MICROORGANISMS IN NATURAL MAGNESIUM SULFATE SALTS AND LABORATORY ENRICHMENT SAMPLES: ASTROBIOLOGICAL IMPLICATIONS

INTRODUCTION

There is ample evidence indicating that parts of the Martian surface are rich in sulfate salts, and therefore likely had sulfate-rich surface/near-surface solutions or brines (e.g., review in King et al., 2004). Magnesium sulfates likely make up a large portion of these minerals, based on data from lander missions (Viking, Pathfinder, the Mars Exploration rovers and Phoenix), and remote sensing from orbit (e.g., OMEGA/Mars Express and CRISM) (Bishop et al., 2007; Roach et al., 2007; Bishop et al., 2008; Wiseman et al., 2008; Wiseman et al., 2009). Because Mg-sulfate salts are so widespread on the Martian surface, it is critical to understand if and how they may preserve potential biosignatures, and how those biosignatures might be detected.

If life exists (or existed) on Mars, it is most likely in the form of extremophilic bacteria and Archaea, based on analogy with extreme terrestrial environments (McKay et al., 1992; Gross 1998). In magnesium sulfate-bearing regions of the Martian surface it is likely that any bacteria or Archaea found in these areas would be 'salt-loving' or halophilic organisms (Landis 2001; DasSarma 2006). Halophiles are capable of surviving both extremes of salinity and temperature, and contain ultraviolet-opaque pigments, or live near minerals such as: calcite ($CaCO_3$), epsomite ($MgSO_4 \cdot 7H_2O$), gypsum ($CaSO_4 \cdot 2H_2O$) and halite (NaCl), that protect them from ultraviolet radiation (Rothschild 1990; Rothschild et al., 1994; Rothschild and Mancinelli 2001; Cockell et al., 2002; Boison et al., 2004; Cockell and Raven 2004; Parnell et al., 2004; Martinez-Frias et al., 2006). All of these characteristics indicate that halophiles are compatible with sulfate-rich environments, and are good candidates for surviving the extreme conditions on Mars.

Despite the rationale presented above, there are relatively few studies of halophiles in terrestrial Mg-sulfate-rich brines (e.g., Prieto-Ballesteros et al., 2003). Furthermore, we know of no studies of halophiles in Mg-sulfate playa systems that cycle through wet-dry-icy conditions with rapid changes in salinity, temperature, and UV radiation. In these systems, like Mars, the water availability and composition change drastically over the year causing large fluctuations in the availability of nutrients, energy sources for metabolism, and habitability (e.g., changeable redox, pH and activity of water; e.g., Tosca et al., 2008).

Although Mg-sulfate playa systems episodically become inhospitable, the potential for preserving biosignatures is high as halophiles can become trapped in sulfate salts, which preserve organic compounds and allow their preservation over geologically significant periods of time (Vreeland et al., 2000; Parnell et al., 2004; Edwards et al., 2005; Villar et al., 2005; Aubrey et al., 2006; Marshall et al., 2006; Villar and Edwards 2006). An analysis of ancient sulfate deposits by Aubrey et al., (2006) showed that amino acids may be preserved for 4-40 million years, while Tuovila et al., (1987) demonstrated that adenosine triphosphate (ATP) could remain unhydrolysed indefinitely in hypersaline environments; even after extreme UV exposure had rendered the cells nonviable. Also, spectroscopic methods (infrared and Raman spectroscopy) have shown that specific organic macromolecules are preserved in sulfates (Parnell et al., 2004; Villar et al., 2005; Marshall et al., 2006; Villar and Edwards 2006). Using both pure-cultures and molecular isolates Marshall et al., (2006) identified chlorophyll, carotenoids, cell membranes,

bacteriorhodopsin, bacterioruberin, and algaenan suggesting that these are ideal biosignatures as they are easily identified and resistant to degradation. The potential to entrap bacteria and preserve organic compounds make salts good candidate materials in the search for extant or extinct life on Mars.

In this paper, we present data on halophilic organisms collected from the Mg-sulfate Basque Lakes (playas) of British Columbia, Canada. These playas cycle through wet-dry-icy conditions and contain deposits of dominantly Mg-sulfates, but also Ca-, Na-, and mixed sulfates (e.g., Hardie and Eugster 1970; Nesbitt 1990; Peterson et al., 2008; Appendix C). The lakes represent excellent analog environments for Mars from an inorganic chemical perspective, and importantly, they also contain abundant halophilic organisms. We have examined the halophilic microorganisms and their inherent, organic, constituent macromolecules found within the salts from the Basque Lakes by: 1) characterizing brines, salts and microbial mats containing halophiles using inorganic chemistry, biomass assay, confocal microscopy, and reflectance infrared spectroscopy; and 2) producing laboratory enrichments of halophiles for detailed characterization with light microscopy, confocal microscopy, biomass assay, and reflectance infrared spectroscopy. This multi-faceted approach permits the absolute concentration of biomass in a sample (biomass assay), the location of the biomass in the sample (confocal microscopy), and the spectral signatures of halophiles (reflectance IR spectroscopy) to be determined.

SITE DESCRIPTION AND FIELD METHODS

The Basque Lakes are a series of ten hypersaline lakes, playas, and brine pools, located in the Cariboo Plateau, southwest of Ashcroft, British Columbia, Canada (see Figure 1 for the five lakes studied here). The plateau lies at an altitude of 1050 – 1250 m above sea level and has a semi-arid climate, receiving 300 – 400 mm of precipitation per year (Nesbitt 1990). The basement rocks in the area contain basalt and ash deposits, as well as metamorphosed greenstones, quartzites, argillites, and limestones, all of which are overlain by a thin veneer of glaciofluvial sediment (Nesbitt 1990).

The Basque Lakes are considered to be near-closed basin systems, with each lake being bound by clay banks and deposits on the downhill side (Nesbitt 1990). Water chemistry varies widely among the ten lakes; in some cases, waters are effectively fresh, whereas in others, waters are enriched in Mg-carbonate, Mg-sulfate and/or Na-Mg-sulfate. This paper concerns only four of the Mg-sulfate lakes (Basque Lakes No. 1, 2, 3, 4) and one Na-Mg-sulfate lake (Basque Lake No. 2W).

The lakes studied contain highly concentrated brines that consist primarily of Mg^{2+} and SO_4^{2-} ions derived from groundwater induced chemical weathering of either mafic minerals or volcanic glass and sulfides. The groundwater and evaporitic brines at this site possess a very high Mg/Ca ratio of approximately 50:1, making them among the most Mg-rich brines in the world (Hardie and Eugster 1970; Nesbitt 1990), and therefore a good terrestrial analog for Mg-rich brines on Mars. Minerals in the lakes include epsomite ($MgSO_4 \cdot 7H_2O$ that may transform to hexahydrite $MgSO_4 \cdot 6H_2O$, Starkeyite

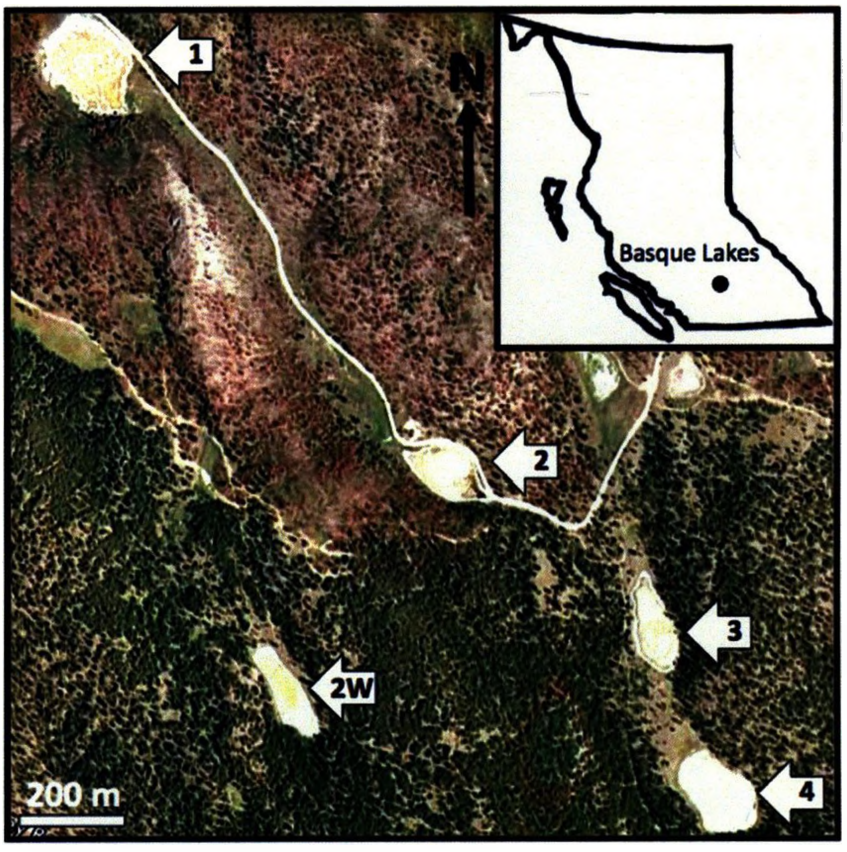

Figure 2.1: Satellite image of the Basque Lakes area (from Google Maps). Each Basque Lake is identified with its corresponding number.

$MgSO_4 \cdot 4H_2O$, kieserite $MgSO_4 \cdot H_2O$ or meridianiite $MgSO_4 \cdot 11H_2O$), gypsum $CaSO_4 \cdot 2H_2O$, protodolomite $CaMg(CO_3)_2$, thenardite Na_2SO_4 (in Basque Lake 2W), bischofite $MgCl_2 \cdot 6H_2O$, magnesite $MgCO_3$, Hydromagnesite $Mg_5(CO_3)_4(OH)_2 \cdot 4H_2O$, Loweite $Na_{12}Mg_7(SO_4)_{13} \cdot 15H_2O$ and clay minerals (Nesbitt 1990; Peterson et al., 2008; Appendix C). Brine pools within each lake occur where upwelling groundwater meets the surface (Figure 2C), and dissolved ionic species are concentrated by evaporation in the basin's arid setting (Cummings 1940, Nesbitt 1990). Each near-circular brine pool is lined with salt crystals and forms an area on average 0.5 – 2 m across and 0.1 m deep, separated by muddy banks.

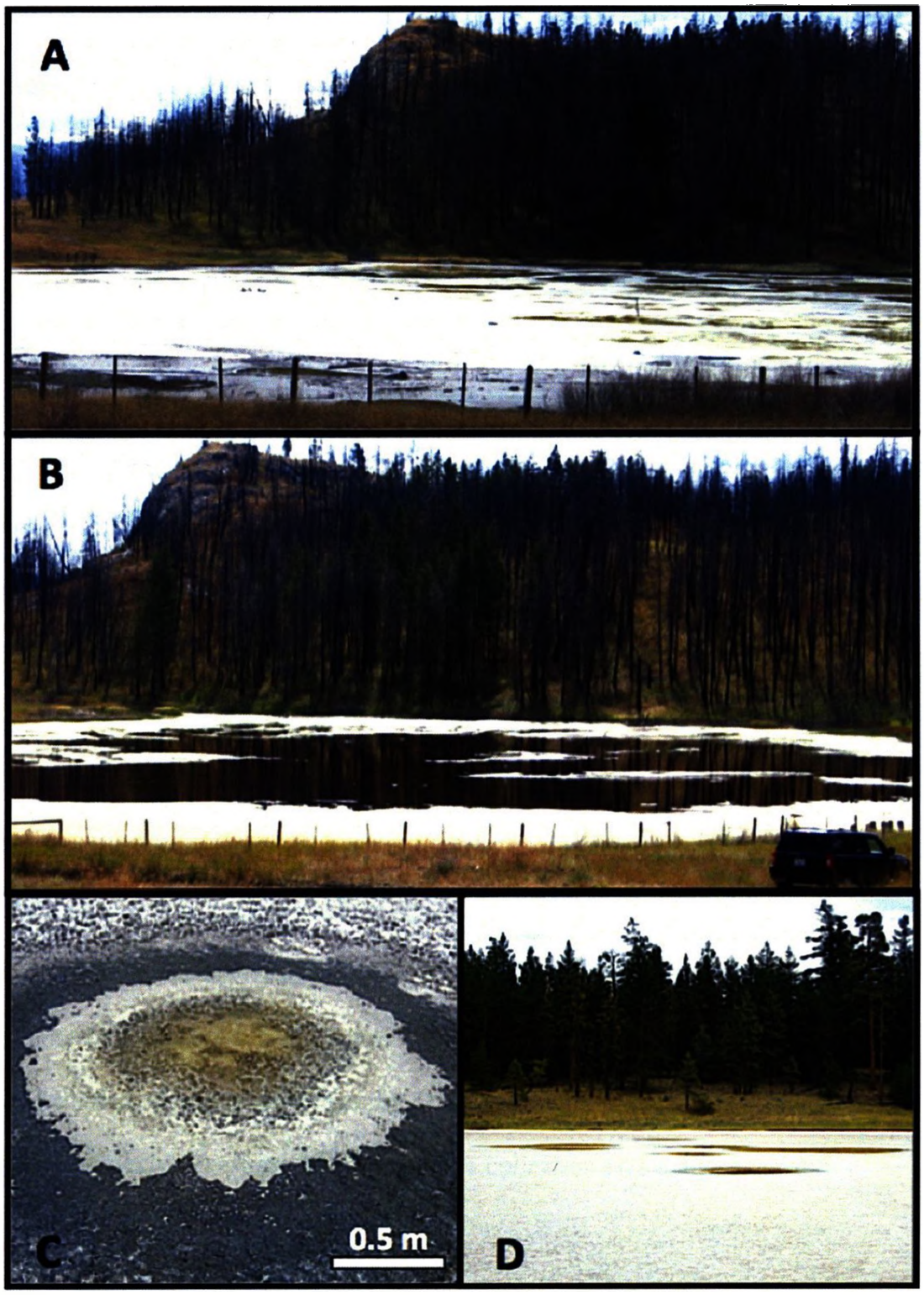

Figure 2.2: Basque Lake mud flats and brine pools. (A) Basque Lake No. 1 mud flats and brine pools as observed from the north in August of 2006. (B) Basque Lake No.1 as seen from the north in August of 2007, exhibiting extensive ≥ 1 cm thick green floating microbial mats, and brine approximately 1.2 m deep at the lake's center. (C) A typical Basque Lake No. 4 brine pool exhibiting concentric rings of sulfate minerals, defined by differing levels of crystallinity and entrained water, located within a dry mud flat in August of 2006. (D) Wet brine pools within the Basque Lake No. 4 mud flat as observed in August of 2007.

During sampling trips in August of 2006, May of 2007 and August of 2007 water levels as well as brine concentrations changed dramatically. In August of 2006, the lakes were almost completely evaporated ephemeral salt-pans (Figure 2A), and all lakes were accessible by foot; although Basque Lake No. 3 was too wet to venture far from the lake's edge. In May of 2007, the lakes were up to ~ 2 m deep and all lakes were sampled from a boat; and we verified that there were no large gradients in water composition or physical properties across the surface of each lake. In August of 2007, Basque Lake No. 1 was accessed by boat (Figure 2B), and the others by foot, except for Basque Lake No. 3. The latter lake was not sampled in August of 2007 as we observed a dramatic increase in water level in the lake through overland flow of brine water being piped artificially out of Basque Lake No. 2.

Environmental data as well as GPS positions were gathered at each sampling site using a handheld GPS, a SPER Scientific 800014 Humidity Temperature Datalogger, and a multimeter with pH, conductivity, and dissolved oxygen probes (Table 1). $Temperature_{air}$/$Temperature_{water}$ and $Temperature_{air}$/RH data loggers, as well as a rain gauge, were deployed in August of 2007 at Basque Lake No. 1 to monitor environmental conditions throughout the remainder of the summer and the following winter. The loggers were retrieved in February of 2008 for data collection and analysis.

MATERIALS AND METHODS

Sampling

Samples of salt, microbial mats, mud, and brine were collected from areas in and around brine pools for analysis. Three core samples, one from a ridge between pools, one from the center of a pool, and one from the edge of a pool, were also obtained by driving a 4 cm wide clear polyethylene tube down into the sediment with a rubber mallet, and then extracting the sample by hand. All other samples were grab samples collected by hand and placed into 50 mL Falcon tubes that were subsequently sealed with parafilm, and packed in an ice-chilled cooler for transport. It was not possible to filter samples in the field due to the extremely high density of the brines.

Chemical Analysis of Natural Brines

Ion Coupled Plasma Spectrometry (ICP; Perkin-Elmer Optima 3300 Dual View atomic emission spectrometer equipped with a Cetac ASX-500 auto-sampler) and Ion Cathode Spectrometry (IC; Dionex ICS-3000 reagent-free system equipped with a gradient pump and AS50 auto-sampler) were performed at The University of Western Ontario on laboratory-filtered brine samples to examine their cation and anion content, respectively. Samples for ICP analysis were acidified to a pH of 2 using nitric acid. Molarity values were calculated for each constituent, for each site. Synthetic bulk brine samples were prepared based on the ICP/IC data, and stored to serve as experimental controls for biological culturing.

Microbiology

A low oxygen resuscitation was performed on all sample material prior to inoculation, by placing approximately 1 g or 1 mL of sample into a 15 mL Falcon tube containing 10 mL of a 2 mol/L brine buffer solution consisting of 3 g/L KCl, 6 g/L NaCl, 60 g/L Na_2SO_4, 0.2 g/L $CaSO_4 \cdot 2H_2O$, 355 g/L $MgSO_4 \cdot 7H_2O$ and 20.9 g/L 3-morpholinopropanesulfonic acid (MOPS). The tube was then topped off with buffer and capped to exclude oxygen, and placed in a fridge at 4°C for 2 hr.

Preliminary samples were cultured in 3.6 to 4.2 mol/L brines, based on the highly evaporated field chemistry conditions measured at Basque lakes 1, 2, 3 and 4 in August of 2006, respectively (see Table 1). These brines were supplemented with 0.116 g/L Yeast Extract, 0.116 g/L Tryptone, 0.116 g/L Casamino acids, 0.5 g/L Dextrose, 0.5 g/L Soluble starch, 0.3 g/L K_2HPO_4, 0.3 g/L Na-Pyruvate, 3 g/L Na_3-Citrate, 6.065 g/L Tris-Hydroxymethyl-Aminomethane, 1 mL/L trace elements (Table 2), and inoculated with 1 mL resuscitated cells. The latter brine cultures fared poorly under both aerobic and anaerobic conditions and produced a range of enrichments from minimal turbidity to cultures possessing faintly orange or pink enrichments (aerobic). For anaerobic cultures, the media was made anoxic by the addition of 0.1 g Ascorbic Acid ($C_6H_8O_6$) per 100 mL media.

Samples subsequently resuscitated and cultured under aerobic and anaerobic conditions at 0.5 mol/L intervals from 3.5 down to 1.0 mol/L 'field brine' revealed optimal bacterial enrichment conditions (i.e., high diversity combined with high biomass), at 2.0 mol/L, which was selected as the Brine Basal Medium (BBM) used in this study: 3 g/L KCl, 6

Table 2: Modified SHAND Media

Ingredient		g/L
Deionized Water		1000
Yeast Extract		0.116
Tryptone		0.116
Casamino Acids		0.116
Dextrose		0.5
Soluble Starch		0.5
K_2HPO_4		0.3
Na-Pyruvate		0.3
Na_3 Citrate		3
Trace Elements		1 ml
Tris-Hydroxymethyl-Aminomethane		6.065
2.0 M Synthetic Basque Lake Brine	**mol/L**	**g/L**
KCl	0.040	3
NaCl	0.103	6
Na_2SO_4	0.422	60
$CaSO_4.2H_2O$	0.001	0.2
$MgSO_4.7H_2O$	1.440	355

g/L NaCl, 60 g/L Na_2SO_4, 0.2 g/L $CaSO_4 \cdot 2H_2O$, 355 g/L $MgSO_4 \cdot 7H_2O$. The pH for field site specific BBM was adjusted using 1 mol/L H_2SO_4 or NaOH to match each lake (Table 1), and filter sterilized (0.45 μm filter).

Laboratory enrichment cultures were grown in 155 mL serum bottles possessing 80 mL BBM for the aerobic cultures and 150 mL BBM for the anaerobes. Each culture was inoculated with 1 mL of resuscitated sample and then capped with a butyl rubber stopper and crimped shut using an Aluminum seal (anaerobes) or covered loosely with Aluminum foil (aerobes). Samples were cultured at RT for up to 3 months, i.e., until abundant growth was observed. These laboratory enrichment cultures were then examined using Differential Interference Contrast (DIC) light microscopy (Zeiss Imager.Z1) and selected for further analysis based on their macroscopic phenotype (i.e., green for cyanobacteria, red for Archaea and black for dissimilatory sulfate reducing bacteria), and their microscopic cellular morphology.

Preparation of Samples for Analysis

Natural Brines

For determination of dissolved organic content in natural brines, and for use in reflectance IR as a natural salt matrix, brine samples collected from Basque lakes 1 and 2 (Figure 2.3) were laboratory filtered (0.45 μm pore size) to remove particulate organic constituents, placed in separate plastic dishes and dried in an oven at 70˚C for 24 hours. Upon removal, the resulting salts were powdered by mortar and pestle and stored in sealed glass vials for later reflectance IR analysis. These samples are referred to as FBS-B1 and FBS-B2.

Laboratory Enrichments

Laboratory enrichments were selected for further analysis based on their strong growth characteristics (i.e., high biomass) and the presence of green and red pigmented autotrophs, as well as dissimilatory sulfate reducing bacteria, as determined by macroscopic and microscopic observations. Thirty-six mL of each enrichment culture was concentrated by centrifugation (12,000 X g) for 5 minutes to produce condensed pellets of cells that were removed and placed into a sterile 7 mL vial, which was then filled with 7 mL organic free 2.0 mol/L Mg-sulfate brine to produce a concentrated cell suspension. Each sample was then poured into its own dish and allowed to dry in an oven at 70°C for 24 hours. The dried material from each sample was then weighed and ground into a fine powder by mortar and pestle, and stored in sterile glass vials for biomass and reflectance

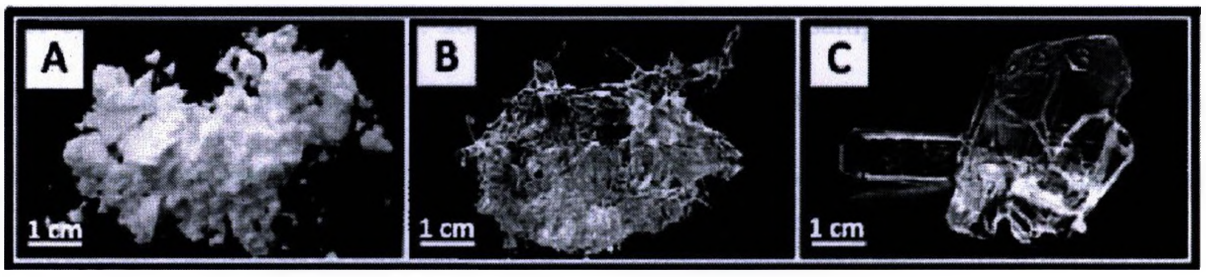

Figure 2.3: Magnesium-sulfate sample control crystals. (A) Dried 99.9% pure $MgSO_4$ powder. Referred to as laboratory epsomite. (B) Small acicular salt crystals, precipitated from filtered Basque Lake No. 1 field brine. Referred to as FBS-B1. (C) Large, tabular, intergrown salt crystals, precipitated from Basque Lake No. 2 filtered field brine. Referred to as FBS-B2.

IR analysis. From each enrichment type (cyanobacteria, Archaea, and SRB) three different samples were selected based on phenotypic and microscopic observations, and a separate number was assigned to each.

Natural Microbial Mats

Three microbial mats, collected from Basque Lake No. 2 and No. 2W (BL2 and BL2W prefixes), were selected for analysis based on microbial habit and visual macroscopic differences. Each sample was separated into an aliquot for whole mat analysis (0.25 cm x 2 cm, 2-3 mm thick sample) and an aliquot that was separated into cellular (particulate) vs. soluble constituents.

For whole mat analysis, samples were placed into 7 mL glass vials that were subsequently filled with 7 mL of sterile, organic free, 2 mol/L $MgSO_4$ brine. Samples were then poured into aluminum dishes, placed into an oven at 70°C and allowed to dry for 24 hours. Once dry, samples were powdered by mortar and pestle and placed in sterile 7 mL glass vials for storage until analysis.

For separation into cellular vs. soluble constituents, each sample of mat was weighed, then placed in a 7 mL glass vial and suspended in 7 mL of 2 mol/L organic free $MgSO_4$ brine, and vortexed twice for 30 seconds at a 5-minute interval. The resulting cell suspension was placed in microfuge tubes and centrifuged for 5 min to separate the solid microbial pellet from the supernatant brine. The supernatants from each of the mats sampled were then pipetted from the microfuge tubes and collected separately in a 7 mL glass vial. The sample pellets were then resuspended in fresh brine containing no organics, and placed in a separate 7 mL glass vial. Both samples, supernatant and pellet, were placed in separate dishes and dried in an oven for 24 hours at 70°C. Once removed from the oven, the samples were weighed, powdered by mortar and pestle, and stored in glass vials for biomass and reflectance IR analysis.

Natural Salt Crystals

Forty-nine individual, natural salt crystals were selected for further analysis from all five lakes/playas. The samples were labeled using the lake name as a prefix (e.g., samples from Basque Lake No. 1 have a prefix of BL1). Each salt crystal was cleaned of surface mud and debris by hand, and washed for 5 seconds in two consecutive sterile 2 mol/L $MgSO_4$ solutions, followed by two consecutive washes in sterile deionized water, and a final rinse for 2 seconds in saturated $MgSO_4$ brine. Fresh solutions were used for each salt crystal. Sample crystals were then placed into sterile falcon tubes for storage prior to examination using confocal microscopy, and subsequent grinding (mortar and pestle) and drying (70°C/24h) for the biomass assay, and for reflectance IR analysis.

Biomass Assay

Determination of the total biomass contained in natural brines, microbial mats, and within salt crystals obtained from each site, was estimated using a Modified Lowry Protein Assay (Sandermann and Strominger 1971) and absorption values were read at 650 nm using a Bausch & Lomb Spectronic 20 spectrophotometer. Representative salt crystals were selected for each site and crushed into a fine powder/paste, which was then split into three portions, and weighed for triplicate analysis against a 2.0 mol/L $MgSO_4$ and yeast extract (Difco) solution, representing a (0 to 0.5 mg/mL) biomass calibration curve.

Confocal Microscopy

Confocal microscopy was performed with a Zeiss LSM 5 Duo, on natural salt crystal samples containing a range of organic material between 0.078 and 4.21 $mg_{biomass}/g_{salt}$, to visualize microbial cells, microcolonies, or layers of mat trapped within the crystal. Sample holders for confocal microscopy were constructed by drilling 1 cm diameter holes through the bottom of 45 mm plastic Petri dishes, and gluing a VWR No. 1 glass coverslip over the hole, to allow for mounting on an inverted microscope. For each sample, the largest flat crystal face was placed downward onto the glass coverslip, and a few of drops of immersion oil were added to coat the salt crystal and fill any space between the glass coverslip and the crystal. As the refractive index of epsomite (N=1.433-1.461) is close to that of immersion oil (N=1.56) it allows imaging of material within the salt crystal with no discernable distortion. Natural salts were then irradiated with an excitation wavelength of 543 nm and 633 nm and autotrophic pigments vs. UV protection

emission bands were detected using a multi-channel long-pass 505 and 650 nm filter, respectively, for use in 2D and 3D imaging.

Reflectance Infrared Spectroscopy

Based on preliminary reflectance IR data and biomass analysis of laboratory red Archaea enrichments, it was observed that samples containing biomass values below 0.75 $mg_{biomass}/g_{salt}$ produced only weak or ambiguous IR biosignatures that were not suited for further study (data not shown). As a result only field salt samples possessing a biomass content $\geq$ 0.75 $mg_{biomass}/g_{salt}$ were selected for reflectance IR analysis to allow for biosignature detection. Powdered, dried (70°C/24 hr) salts were mounted in three separate steel sample cups for triplicate analysis. Care was taken to prevent preferential grain alignment, as well as pitting/clumping, by gently tapping sample material into place until the surface was smooth. Gloves were worn at all times during sample preparation to prevent contamination.

Mounted samples were placed in a Nicolet Nexus 670 Fourier Transform Infrared Spectrometer with a Pike Technology automated diffuse reflectance attachment. We used a Globar source, KBr beamsplitter and DTGS detector. Each sample was analyzed for 500 scans, with a spectral resolution of 4 cm^{-1}, over a range of 400 - 5600 cm^{-1}. The reflectance IR unit was purged with dry air prior to analysis for at least 45 minutes. This process effectively eliminated atmospheric absorption features resulting in spectral features related only to the sulfate mineral and/or its contained biological component. Background spectra were collected under the same conditions before analysis on a

polished Aluminum disc. Data were plotted, and converted to % Reflectance values using the Omnic software program, for analysis by visual identification and comparison of absorption features to known organic and inorganic materials.

RESULTS

Water Chemistry

The Basque Lakes are characterized by the evaporative concentration of brines released from springs producing hypersaline waters dominated by Mg^{2+}, Na^{+} and SO_4^{2-} (Table 1). In contrast to the 2006 water chemistry, the 2007 samples highlighted brines that were only a fraction (1/2 to $1/10^{th}$) as concentrated as those observed in 2006.

Microbiology

All resuscitated field samples inoculated into the Brine Based Media (BBM) produced laboratory enrichments displaying positive biphasic growth, typified by a rapid growth period within the first week, followed by gradual color development, as pigmented autotrophs became more abundant after the initial, presumably heterotrophic bloom. Although most sample salts had no obvious coloration, each sample resulted in an enrichment that was dominated by either green (cyanobacteria or eukaryotic algae) or red (Archaea) autotrophic species, or in rare cases, non-pigmented cells (not analyzed further). These results would suggest that there is a degree of heterogeneity within the natural environment, and that these organisms are both closely associated and in competition with one another.

Table 1: Basque Lakes Physical Conditions and Chemical Compositions

Physical Conditions										
Sample Site	**Basque Lake No. 1**		**Basque Lake No. 2**		**Basque Lake No. 3**		**Basque Lake No. 4**		**Basque Lake No. 2W**	
GPS Coordinants	50° 36.017 N	121° 21.527 W	50° 35.593 N	121° 20.916 W	50° 35.520 N	121° 20.680 W	50° 35.330 N	121° 20.599 W	50° 35.408 N	121° 21.169 W
Sample Year	**August 2006**	**August 2007**	**August 2006**	**August 2007**	**August 2006**	**August 2007**	**August 2006**	**August 2007**	**May 2007**	**August 2007**
pH	8.31	8.70	7.54	n.c.	7.58	8.40	8.05	7.28	9.06	9.0
Relative Humidity %	24.30	42.00	24.30	36.00	n.c.	44.00	n.c.	38.00	n.c.	n.c.
Water Temperature °C	27.80	20.19	27.80	n.c.	n.c.	n.c.	n.c.	n.c.	n.c.	n.c.
Chemical Compositions (ppm)										
Ca^{2+}	110	490	100	150	120	360	110	90	260	380
K^{+}	3 340	690	1 530	4 100	3 860	370	4 680	1 200	1 570	2 170
Mg^{2+}	37 020	15 160	34 400	36 080	26 920	5 790	27 400	13 210	2 840	11 150
Na^{+}	18 560	3 980	27 000	31 040	33 170	1 950	26 490	8 690	5 100	19 150
Cl^{-}	2 670	330	4 040	2 160	860	210	625	390	320	470
SO_4^{2-}	339 670	99 680	281 740	394 960	305 300	34 910	281 900	94 700	24 400	113 550

Mineralogy of Dried Crystal Samples Containing Black and Brown Sediments From Basque Lake No. 2 and No. 4

Carbonates		
Eitelite - $Na_2Mg(CO_3)_2$	Hydromagnesite - $Mg_5(CO_3)_4(OH)_2 \cdot 4H_2O$	Magnesite - $MgCO_3$ and $(Mg,Fe)CO_3$
Oxides		
Hematite - Fe_2O_3		
Silicates		
Anorthite - $(Ca,Na)(Al,Si)_2Si_2O_8$	Clinochlore - $Mg_{4.88}Fe_{0.22}Al_{1.88}Si_{2.95}O_{10}(OH)_8$	Heulandite - $CaAl_2Si_7O_{18} \cdot 6H_2O$
Kanemite - $NaHSi_2O_4(OH)_2 \cdot 2H_2O$	Kaolinite - $Al_2(Si_2O_5)(OH)_4$	Laumontite - $Ca_{0.89}(Al_2Si_4O_{12})(H_2O)_{1.88}$
Muscovite - $KAl_3Si_3O_{10}(OH)_2$	Quartz - SiO_2	
Sulfides		
Rasvumite - KFe_2S_3	Troilite - FeS	
Sulfates		
Blodite - $Na_2Mg(SO_4)_2 \cdot 4H_2O$	Gypsum - $CaSO_4 \cdot 2H_2O$	Hexahydrite - $MgSO_4 \cdot 6H_2O$
Kieserite - $MgSO_4 \cdot H_2O$	Krausite - $KFe(SO_4)_2 \cdot H_2O$	Loweite - $Na_{12}Mg_7(SO_4)_{13} \cdot 15H_2O$
Mendozite - $NaAl(SO_4)_2 \cdot 11H_2O$	Romerite - $Fe_3(SO_4)_4 \cdot 14H_2O$	Starkeyite - $MgSO_4 \cdot 4H_2O$

n.c. = Data not collected.

All cultures grown aerobically produced active bacterial enrichments, regardless of sample container size or growth conditions. By contrast, most samples grown under anoxic conditions fared poorly, producing only minimal to no visible growth after 2-3 weeks. Anoxic samples that did provide enrichments were commonly milky-looking, or rich in SRB, which produced a black, FeS precipitate that lined the sample container walls and precipitated out of solution.

Differential Interference Contrast (DIC) light microscopy of the bacterial enrichments revealed microorganisms from all three domains of life; Bacteria (Figure 2.4 and 2.6), Archaea (Figure 2.5) and Eukarya. Observations were made of single cells and colonies, mobile photosynthetic algae, diatoms, and complex animals such as brine shrimp and nematodes, suggesting that these brine pools support complex ecosystems. Due to the likelihood that any life on Mars would occur as 'simple' (i.e., prokaryotic-like) organisms, further analysis focused on bacteria and Archaea enrichments.

As a result of the relationship between salt precipitation and microorganism entrapment, special attention was paid to microscopic biofilms, and tabular as well as acicular salt crystals were observed to nucleate and grow outward from microbial enrichment colonies (Figure 2.7), as well as on top of microbial mats observed in the field (Figure 2.8). It was also noted that although crystallization did not occur in abiotic brine controls, it proved to be quite common in the biofilms.

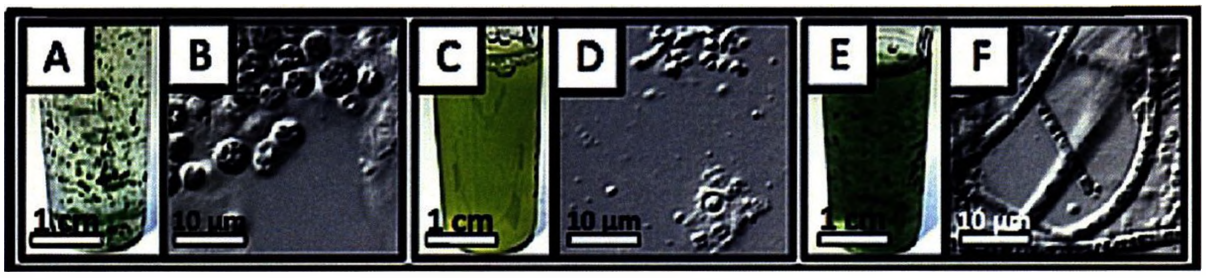

Figure 2.4: Laboratory enrichments dominated by green-photosynthetic bacteria. (A) Cyano1 enrichment culture containing colonial single-celled green photosynthetic autotrophs. (B) DIC microscopy image of single-celled autotrophic bacteria (dark spheres ~5 µm), associated heterotrophs and extracellular polymers found in laboratory sample Cyano1. (C) Cyano2 enrichment culture dominated by green single-celled planktonic autotrophs. (D) DIC microscopy image of single-celled autotrophs and heterotrophs in laboratory sample Cyano2. (E) Cyano3 laboratory enrichment dominated by filamentous cyanobacteria. (F) DIC microscopy image of filamentous cyanobacteria and associated heterotrophs (1-2 µm cocci) in laboratory sample Cyano3.

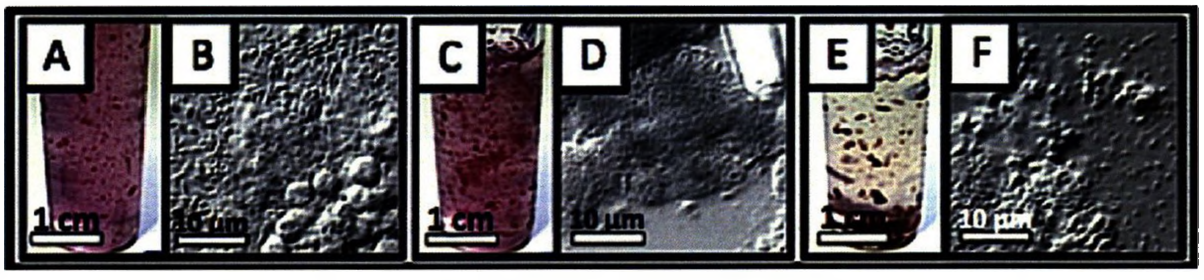

Figure 2.5: Laboratory enrichments dominated by red-photosynthetic Archaea. (A) Red colonial Archaea comprising laboratory model sample Arch1. (B) DIC microscopy imaging of red, single-celled autotrophic bacteria and associated heterotrophs found in laboratory sample Arch1, 3-4 µm cocci cells appear in the bottom right surrounded by 1 µm rods towards the top left. (C) Enrichment of red colonial and filamentous Archaea found in laboratory model sample Arch2. (D) DIC microscopy imaging of red autotrophs (1µm cocci) observed in laboratory sample Arch2, note the large salt crystal growing within the colony in the upper right corner of the image. (E) Red Archaea mats and associated heterotrophs comprising sample Arch3. (F) DIC microscopy of red Archaea microbial mats (1-2 µm cocci in the bottom left), and associated planktonic autotrophic/heterotrophic organisms (1µm cocci on the right side of the image) in laboratory sample Arch3.

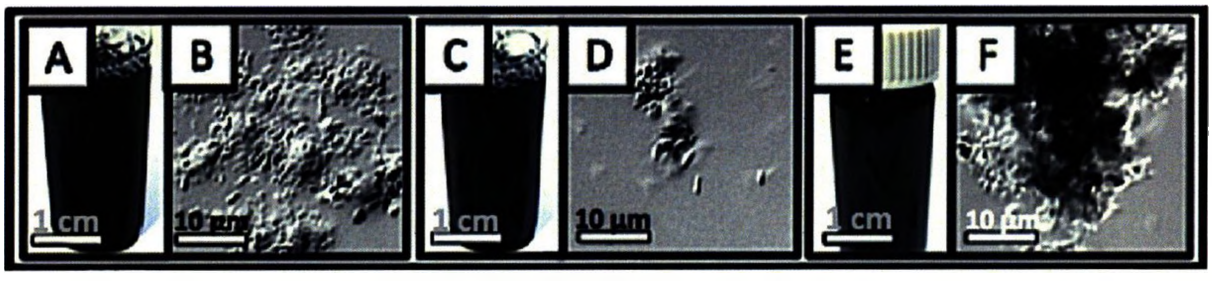

Figure 2.6: Laboratory enrichments dominated by dissimilatory sulfate reducing bacteria (SRB). (A) Dissimilatory SRB concentrated for use in laboratory model sample SRB1. (B) DIC microscopy imaging of a heterotrophic microcolony containing 1-2 µm rod shaped bacteria, found in laboratory sample SRB1. (C) Concentrated SRB enrichment culture used to create laboratory model sample SRB2. (D) DIC microscopy imaging of planktonic and colonial rod-shaped heterotrophs as observed in laboratory sample SRB2. (E) SRB3 enrichment culture containing dissimilatory SRB. (F) DIC microscopy of a heterotrophic microcolony comprised of rod-shaped bacteria, coated in black sediments.

Figure 2.7: Diffuse Interference Contrast (DIC) imagery of salt crystals growing outward from a microcolony of pink-colored Archaea in a Basque Lake No. 4 laboratory enrichment culture.

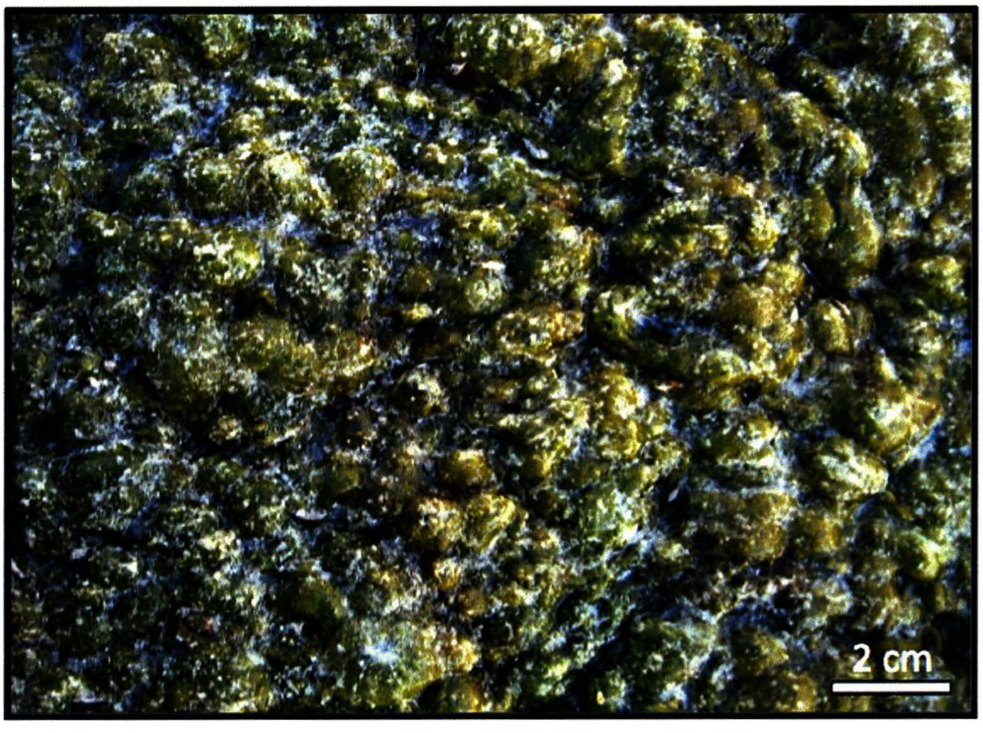

Figure 2.8: A ≥ 1 cm thick, green microbial mat, containing air pockets that are trapped within the biofilm, and mm size white salt crystals scattered on the surface of the floating microbial mat; this mat was observed at Basque Lake No. 1 in August of 2007.

Table 3: Laboratory Enrichments Selected for Reflectance IR Analysis.

Sample ID	Sample Type	Sample Source	Sample Description	Biomass Content ($mg_{biomass}/g_{salt}$)
Cyano1	Basque Lake Cyanobacteria Enrichment	Basque #1	Benthic unicellular cyanobacteria	11.53
Cyano2	Basque Lake Cyanobacteria Enrichment	Basque #4	Pelagic unicellular cyanobacteria	2.23
Cyano3	Basque Lake Cyanobacteria Enrichment	Basque #1	Filamentous cyanobacteria	22.01
Arch1	Basque Lake Archaea Enrichment	Basque #1	Filamentous red unicellular Archaea	8.46
Arch2	Basque Lake Archaea Enrichment	Basque #2	Colonial red unicellular Archaea	8.44
Arch3	Basque Lake Archaea Enrichment	Basque #1	Pink unicellular Archaea biofilms	4.70
SRB1	Basque Lake Sulfate Reducing Bacteria Enrichment	Basque #1	Unicellular sulfate reducing bacteria	18.57
SRB2	Basque Lake Sulfate Reducing Bacteria Enrichment	Basque #4	Unicellular sulfate reducing bacteria	26.28
SRB3	Basque Lake Sulfate Reducing Bacteria Enrichment	Basque #4	Unicellular sulfate reducing bacteria	26.88

Biomass Assay

Biomass assay results obtained for the laboratory enrichment samples ranged from 2.23 $mg_{biomass}/g_{salt}$ in Cyano2, to 26.88 $mg_{biomass}/g_{salt}$ found in SRB3, and confirmed the presence of abundant biomass within each of the prepared model samples (Table 3). Biomass values obtained from field salts were far lower, with, a range from 0.078 $mg_{biomass}/g_{salt}$ in BL4-0 a Basque Lake No. 4 sample (data not shown) to 4.213 $mg_{biomass}/g_{salt}$ in BL4-7 (Table 4), indicating a range of approximately 7.80×10^8 cells to 4.21×10^9 cells/g_{salt}, using a 0.5 x 1 μm bacillus wet cell weight of 10^{-9} mg/cell (Neidhardt et al., 1990).

Biomass values for natural microbial mats range from 8.54 to 13.39 $mg_{biomass}/g_{salt}$ (Table 4), and are composed of approximately 78-88% solid biomass and 12-22% soluble biomass. Samples of crystallized brine from Basque Lake No. 1 and No. 2 also contain comparable amounts of soluble biomass, 1.15 and 1.51 $mg_{biomass}/g_{salt}$, respectively.

Confocal Microscopy

Natural salt crystals containing visible sediment (usually black), and occasionally green

Table 4: Field Sample Salts Selected for Reflectance IR Analysis

Sample ID	Sample Source	Sample Description	Biomass Content ($mg_{biomass}/g_{salt}$)
		Microbial Mats	
Mat1	Basque No. 2W	Green pelagic surface biofilm Solid biomass = 78.3% Soluble organic carbon = 21.70%	10.59
Mat2	Basque No. 2	Thick green and red coherent pool bottom mat Solid biomass: 87.20% Soluble organic carbon = 12.80%	13.39
Mat3	Basque No. 2W	Layered red green and white lake shore mat Solid biomass = 88.20% Soluble organic carbon = 11.80%	8.54
		Precipitated Salt from Filtered Field Brine	
FBS-B1	Basque No. 1	Dried brine taken from a brine pool	1.15
FBS-B2	Basque No. 2	Dried brine taken from a brine pool	1.51
		Field Samples Selected for DRIFTS Analysis	
BL1-1	Basque No. 1	Large salt crystals from the mud below a brine pool	1.55
BL2-1	Basque No. 2	Top section of core taken from a brine pool	0.78
BL2-2	Basque No. 2	Middle section of core taken from a brine pool	0.94
BL2-3	Basque No. 2	Massive salt crystals on the bottom of a brine pool	1.00
BL2-4	Basque No. 2	Crystals found on the banks around several brine pools	1.03
BL2-5	Basque No. 2	Bottom section of core taken from a brine pool	1.09
BL2-6	Basque No. 2	Small tabular crystals from a green coloured brine pool	1.49
BL2-7	Basque No. 2	Top section of core taken from an 80% dry brine pool	1.67
BL2-8	Basque No. 2	Bottom section of core taken from an almost dry brine pool	2.36
BL4-1	Basque No. 4	Salt crystals growing in a biofilm	1.06
BL4-2	Basque No. 4	Salt crystals from the top layer of a brine pool	1.10
BL4-3	Basque No. 4	Brown-black crystals in the mud near a brine pool	1.46
BL4-4	Basque No. 4	Crystals from the mud below a brine pool	1.78
BL4-5	Basque No. 4	Sediments and crystals from below a brine pool	2.20
BL4-6	Basque No. 4	Crystals from the black mud below a brine pool	3.12
BL4-7	Basque No. 4	Large crystals from the mud below a brine pool	4.21

material, were selected from field samples containing abundant, moderate, or minimal biomass, based on biomass assay results, for characterization of biomass trapped within magnesium sulfate crystals. Using natural pigment excitation wavelengths of 543 nm and 633 nm (Marine et al., 2004), images of regions with dense clusters of biomass containing

suspended cells were commonly observed throughout the crystals (Figure 2.9A). Three-dimensional images show that the areas of biomass are 10's to 100's of μm in size, with irregular morphologies comprised of amorphous central regions, which tapered off toward the edges of void spaces commonly forming flat plains (Figure 2.9B). The outer regions of these voids occasionally appeared as sharp plains a few microns across, occurring at distinct angles from the main void cavity. In addition to large biomass clusters, numerous small microcolonies and single cells were observed in isolated planar regions, 10's of μm long and 5-10 μm wide, generally occurring deep within the magnesium sulfate crystals.

Low-biomass field salt samples analyzed consisted of small single crystals or agglomerates of sub-millimeter crystals with overall dimensions = 2-10 mm long and 1-5 mm wide, with either faint green or no obvious coloration in hand sample. When exposed to 543 and 633 nm radiation all crystals were found to contain individual cells and/or small microcolonies disseminated throughout the crystal (Figure 2.9A), or in open spaces between other small salt crystals. In contrast, crystals containing moderate or large amounts of biomass, contained relatively few small disseminated areas of biomass, however large planar regions filled with cells and organic material, and characterized by sharp boundary edges were common (Figure 2.9B). Using transmitted light microscopy the small diffuse regions were identified as fluid inclusions, typically occurring as long tabular voids with euhedral morphologies that mimicked the salt crystals habit, while large planar regions with sharp edges were identified as angular void spaces between interlocking salt crystal grains.

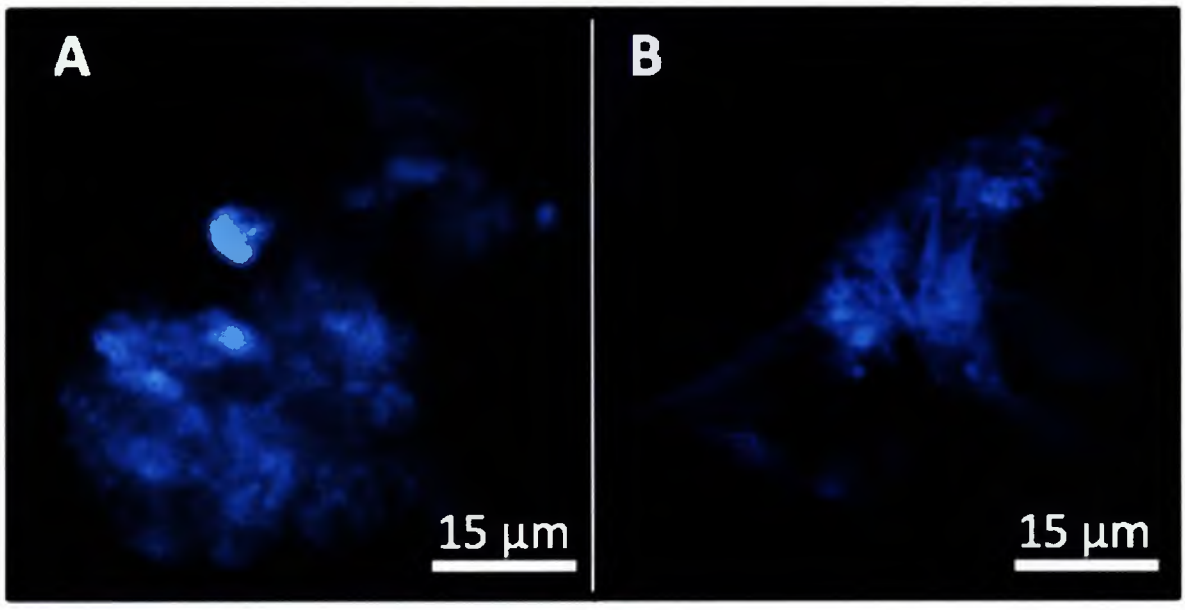

Figure 2.9: Confocal microscopy images of halophiles and extracellular organics trapped within magnesium sulfate crystals. (A) A globular fluid inclusion filled with cells and extracellular polymers. Several large round cells are visible among smaller cells and organic material. (B) An irregularly shaped void space created between intergrown salt crystals, which is filled with several small bright cells nested within extracellular polymers. Note that the extracellular material branches outward along flat planes filling the space created along salt crystal faces.

The 543 nm excitation wavelength highlighted cells and extracellular/disseminated biomass, while only green autotrophs were observed using 633 nm radiation. Cocci are the most common cell type in all samples imaged, while occasional coccobacilli and vibrio (or curved) bacteria were also observed. No filamentous or large bacillus species were noted in the samples examined despite their common occurrence in field samples and laboratory enrichments.

Reflectance Infrared Spectroscopy

Reflectance IR of Laboratory Salt and Natural Brines

Spectra obtained for laboratory epsomite samples containing no organic molecules possess absorption features at 710, 1025, 1170, 1280±10, and 1965-2400 cm^{-1}

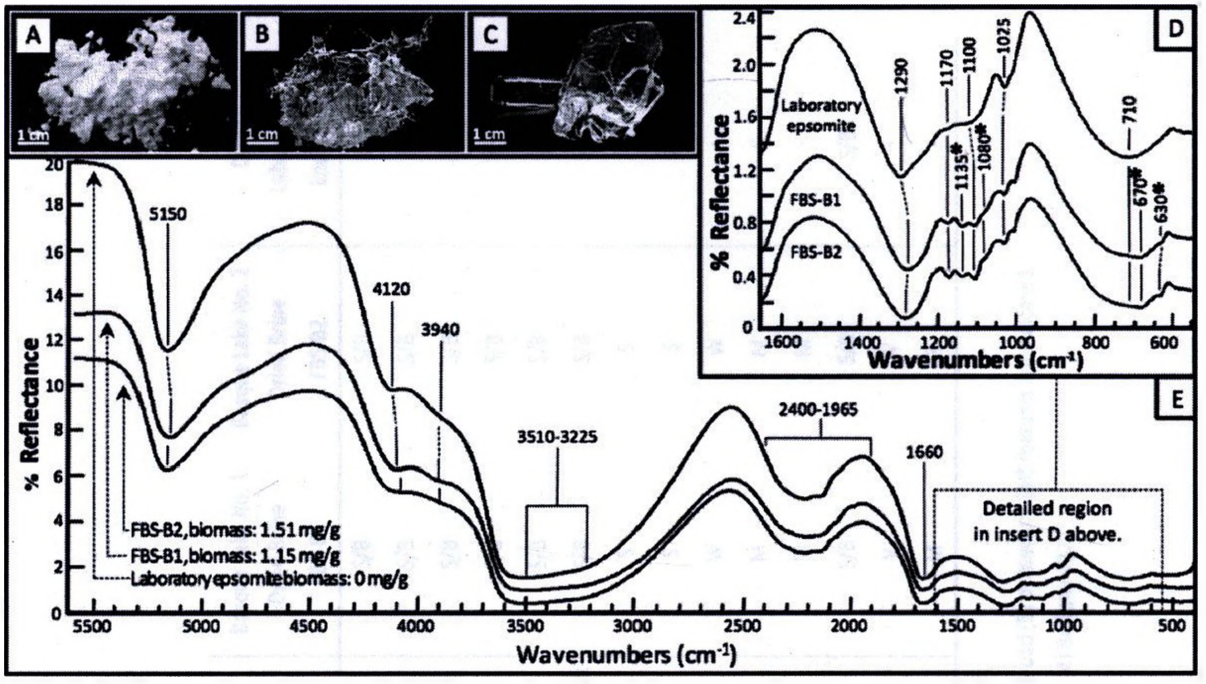

Figure 2.10: Reflectance IR spectra of dried laboratory grade epsomite, and dried salt crystals formed from the crystallization of filtered Basque Lake No. 1 (labeled FBS-B1) and No. 2 brine (labeled FBS-B2). (A) Laboratory epsomite $MgSO_4 \cdot xH_2O$. (B) Basque Lake No. 1 crystals. (C) Basque Lake No. 2 crystals. (D) Detailed reflectance IR spectral region between 1650 and 550 cm^{-1}. All three salt spectra show bands that are related to sulfate and water features in the minerals. Salt spectra from the crystallized, filtered, field brines also show features, marked with an asterisk, related to dissolved organic species. (E) Reflectance IR spectra of dried laboratory and filtered field brine salts, between 5600 and 400 cm^{-1}. Discernable features from the organic molecules in sample FBS-B1 and FBS-B2 are only observable in the region between 1650 and 550 cm^{-1}.

---

corresponding to SO_4^{2-} vibrations, and features at 1100-1135, 1660, 3225-3510, 3940 and 4120 cm^{-1} related to –OH and H_2O vibrations (Figure 2.10 D, E, and Table 5). These results match well with those obtained from previous studies by Cloutis et al., (2006), and Lane (2007), and are used as background spectra for laboratory enrichment samples. In addition, samples of filtered, crystallized brine, taken from Basque Lake No.1 and No.2 (identified as FBS-B1 and FBS-B2) possess several additional absorbance features related to the dissolved organic molecules present in the brine. These features are located at 630 cm^{-1} corresponding to C-N, C-S, C-H, N-H, -OH and SO_4^{2-} found in amino acids, amines, and amides, 670 cm^{-1} corresponding to C-H, C-S, and –OH in glycoproteins and amino

Table 5: DRIFTS Spectral Assignments for Dried Laboratory Brine and Basque Lake Field Brine Salt Samples			Basque Lake No. 1 Dried Brine	Basque Lake No. 2 Dried Brine	Dried Laboratory
Wavenumber (cm-1)	Vibrational Assignment	Macromolecule	FBS-B1	FBS-B2	Epsomite
4120	OH^{-} [3], H_2O [1], S-O [1]	Hydroxide, Water, and Sulfate Overtones	S/B	S/B	S/B
3940	OH^{-} [3], H_2O [1], S-O [1]	Hydroxide, Water, and Sulfate Overtones	S/B	S/B	S/B
3225-3510	OH^{-} [3] [3], H_2O [1]	Hydroxide and Water Absorptions in Hexahydrite	S/B	S/B	S/B
1965-2400	SO_4^{2-} [1]	Sulfate Overtones and Combination Absorption Bands	S/B	S/B	S/B
1660	H_2O [1]	H_2O Bending in Hexahydrite	S/B	S/B	S/B
1275-1290	SO_4^{2-} [1], PO^{2-} [3]	Sulfate Christiansen Feature, Nucleic Acids, Phospholipids	S/B	S/B	S/B
1170	SO_4^{2-} [1]	Sulfate Bending	S	S	W
1100-1135	SO_4^{2-} [1] [2] [4]	Sulfate Bending	S	S	S/B
1080	C-N [4], PO_4^{3-} [4]	Amine I, Phospholipids	W	W	•
1025	SO_4^{2-} [1]	Sulfate Bending	M	M	S
985-1000	SO_4^{2-} [1]	Sulfate Stretching	M	M	•
710	SO_4^{2-} [1]	Sulfate Bending	S/B	S/B	S/B
670	C-H [4], C-S [4], -OH [4]	Glycoproteins, Amino Acids	V	V	•
630	C-N [4], N-H [4], C-H [4], C-S [4], -OH [4], SO_4^{-2} [4]	Amino Acids, Amide II, Proteins	M	V	•

S, strong; W, weak; V, very weak; • not detected

* Most Organic structures produced narrow absorption features, those structures that produced broad (B) or medium (M) features are indicated.

[1] Cloutis et al. 2006, [2] Marshall et al. 2006, [3] Garip et al. 2007, [4] Bellamy 1975

acids, and 1080 cm^{-1} corresponding to C-N, N-H and PO_4^{3-} found in amines, amino acids, adenosine triphosphate (ATP), phospholipids and DNA (Figure 2.10 D, E, and Table 5). These spectral features are used as a 'background' for field samples, allowing us to differentiate biosignature features directly related to the non-soluble cellular component of the samples, from those related to soluble organic molecules derived from either organic or inorganic chemical processes.

Reflectance IR of laboratory Enrichments

Reflectance IR spectra of laboratory enrichments demonstrated our ability to detect abundant organic matter within an $MgSO_4$ matrix in every sample analyzed. A total of twenty spectral absorbance features are observed between 550-1650 cm^{-1} and 2400-3000 cm^{-1}, which can be correlated with the following types of organic molecular bonds: C-C, C-O, C-H, C-N, C-S, C-OH, -OH, N-H, and P-O (Figure 2.11G, H, 2.12G, H, 2.13G, H, and Table 6). These types of bonds are found in amino acids, phospholipids, DNA, amines, amides, fatty acids, glycoproteins, and pigments. Additionally, two biosignature features can be identified that occurred in every sample analyzed, these are the 1040-1050 cm^{-1} C-N, C-OH and PO_4^{3-}, and the 1425-1465 cm^{-1} C-CH_3, C-CH_2-C, and CH_2 features (see Table 6). Samples containing green-pigmented autotrophs are found to possess an average of 13 biosignature features, while Archaea and SRB samples averaged 14 and 7 respectively (range = 6-19).

Samples with abundant biomass are not observed to consistently have more biosignatures than those of moderate samples (R^2 = 0.43); however, each group (cyanobacteria,

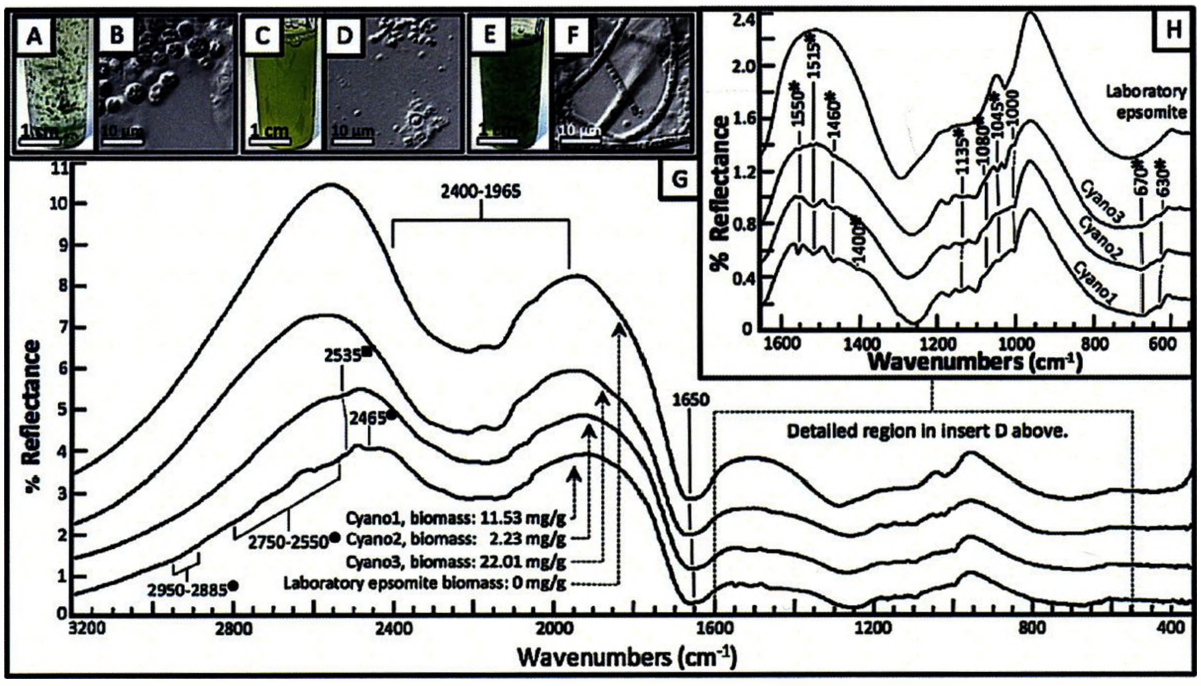

Figure 2.11: Reflectance IR spectra of laboratory enrichments dominated by green-photosynthetic autotrophs. (A) Cyano1 enrichment culture. (B) DIC microscopy image of laboratory sample Cyano1. (C) Cyano2 enrichment culture. (D) DIC microscopy image of laboratory sample Cyano2. (E) Cyano3 enrichment culture. (F) DIC microscopy image of laboratory sample Cyano3. (G) Reflectance IR spectra of dried laboratory epsomite, and laboratory enrichment samples Cyano1, Cyano2, and Cyano3, between 3200 and 400 cm^{-1}. All four spectra contain absorption bands related to sulfate and water features in the minerals. Discernable features from the organic molecules in sample Cyano3 can only be seen in the region between 1650 and 550 cm^{-1}, while Cyano2 possess a feature related to -COOH at 2535 cm^{-1}, and Cyano1 possesses several features between 2465 and 2950 cm^{-1} related to –COOH, CH_2 and CH_3. (H) Close-up of the reflectance IR spectral region between 1650 and 550 cm^{-1}. Salt spectra for laboratory samples Cyano1, Cyano2, and Cyano3 possess biosignatures, marked with an asterisk, that do not appear in the epsomite control. The 1550, 1515 and 1080 cm^{-1} features were found to be diagnostic of samples dominated by cyanobacteria and Archaea.

Archaea, SRB) tend to have similar high intensity biosignature features, e.g. 620-630 cm^{-1} in samples containing cyanobacteria (Figure 2.11G, H), 1040-1050 cm^{-1} in samples dominated by Archaea (Figure 2.12G, H), and 1425-1465 cm^{-1} observed in SRB samples (Figure 2.13G, H, and Table 6). The strongest bands observed for samples dominated by cyanobacteria are the 620-635, 1160-1175, 1230-1275, and 1425-1465 cm^{-1} features. Samples dominated by Archaea possessed strong features at 1040-1050, 1085-1135, 1060-1175, 1230-1275 cm^{-1}, and those dominated by SRB had their strongest absorption features at 1085-1135, 1060-1175, 1230-1275, and 1425-1465 cm^{-1} (Table 6). Although

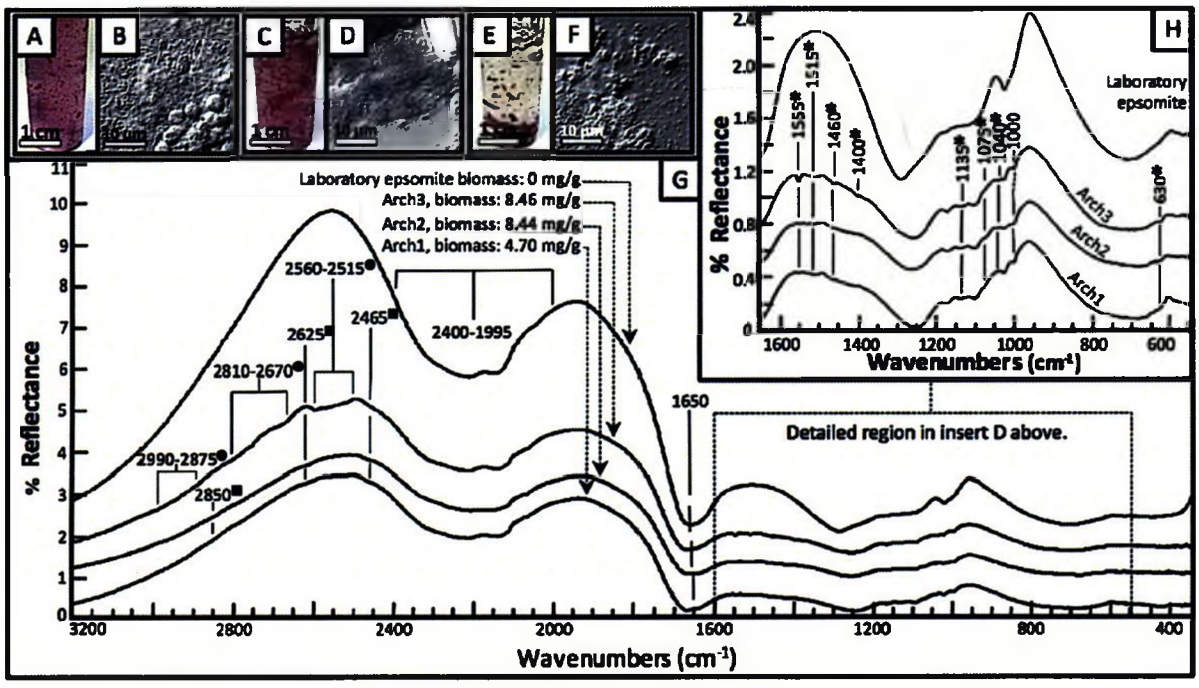

Figure 2.12: Reflectance IR spectra of laboratory enrichments dominated by red-photosynthetic Archaea autotrophs. (A) Laboratory model sample Arch1. (B) DIC microscopy imaging laboratory sample Arch1. (C) Laboratory model sample Arch2. (D) DIC microscopy imaging of laboratory sample Arch2. (E) Laboratory model sample Arch3. (F) DIC microscopy of laboratory model sample Arch3. (G) Reflectance IR spectra of dried laboratory epsomite, and laboratory enrichment samples Arch1, Arch2, and Arch3, between 3200 and 400 cm^{-1}. All four spectra contain absorption bands related to sulfate and water features in the minerals. Discernable features from the organic molecules in sample Arch1 and Arch2 are marked with squares, while Arch3 possess several features, marked with circles, related to –COOH, CH_2 and CH_3 bonds. (H) Close-up of the reflectance IR spectral region between 1650 and 550 cm^{-1}. Salt spectra for laboratory samples Arch1, Arch2, and Arch3 possess biosignatures, marked with an asterisk, that do not appear in the epsomite control. The 1550, 1515 and 1080 cm^{-1} features were found to be diagnostic of samples dominated by cyanobacteria and Archaea.

these samples were not pure cultures (all samples were enrichment consortia dominated by either cyanobacteria, Archaea or SRB), these results suggest that there may be spectral features that are diagnostic for each culture type.

Reflectance IR of Microbial mats

Reflectance IR spectra obtained for microbial mat samples (identified as Mat1, Mat2 and Mat 3) all have similar absorption features (Figure 2.14G, H, and Table 6) and average 14

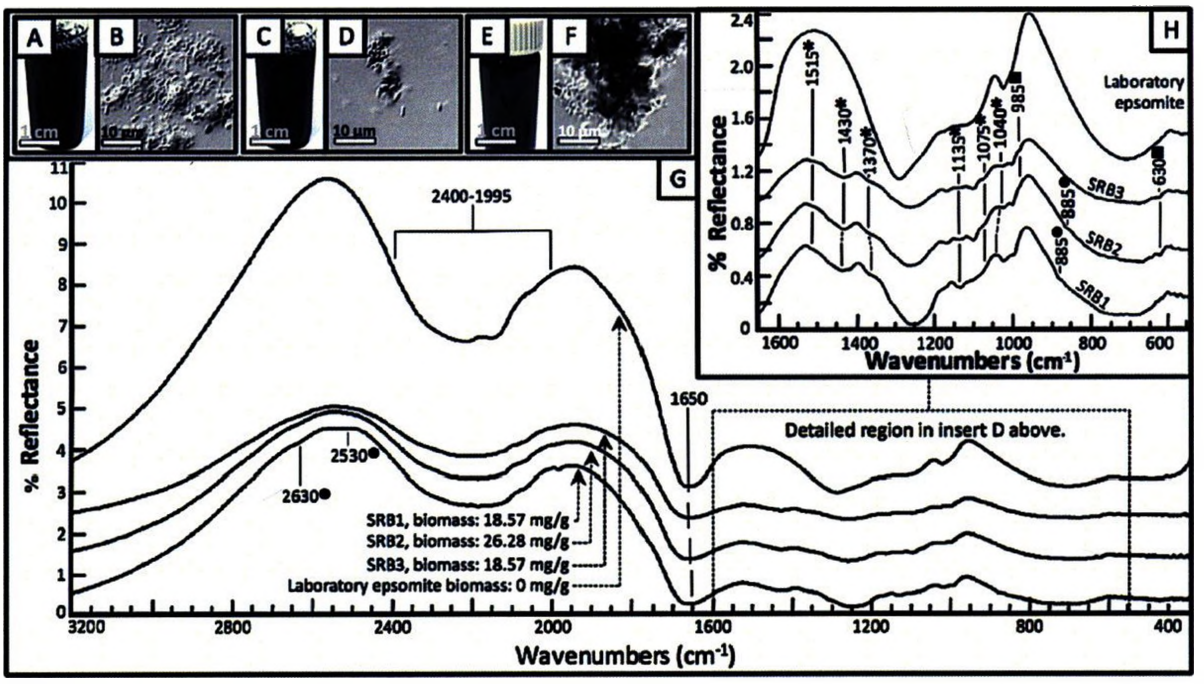

Figure 2.13: Reflectance IR spectra of laboratory enrichments dominated by dissimilatory sulfate reducing bacteria (SRB). (A) Laboratory model sample SRB1. (B) DIC microscopy image of laboratory sample SRB1. (C) Laboratory model sample SRB2. (D) DIC microscopy image of laboratory sample SRB2. (E) Laboratory enrichment culture SRB3. (F) DIC microscopy of laboratory sample SRB3. (G) Reflectance IR spectra of dried laboratory epsomite, and laboratory enrichment samples SRB1, SRB2, and SRB3, between 3200 and 400 cm^{-1}. All four spectra contain absorption bands related to sulfate and water features in the minerals. Discernable features from the organic molecules in sample SRB1 can be observed at 2530 and 2630 cm^{-1} corresponding to -COOH, while features in SRB2 and SRB3 can only be observed in the region between 1650 and 550 cm^{-1}. (H) Close-up of the reflectance IR spectral region between 1650 and 550 cm^{-1}. Salt spectra for laboratory samples SRB1, SRB2, and SRB3 possess common biosignatures, marked with an asterisk, and unique features, marked with a circle or square, that do not appear in the epsomite control. The 1370 cm^{-1} feature is diagnostic of samples dominated by SRB or containing microbial mats.

---

absorption features per sample (range = 12-16), 12 of which were common to all three samples (Table 6). Additionally, each sample contains 6 strong spectral features located at, 1040-1050, 1230-1275, 1430-1465, 2465-2470, 2595-2625, and 2630-2690 and cm^{-1} that correspond to C-OH, C-N, PO_4^{3-}, -C-$(CH_3)_3$, and -COOH (see Figure 14G, H, and Table 6).

Reflectance IR of Natural Salts

Spectra obtained for natural salts highlighted our ability to detect biomass greater than or

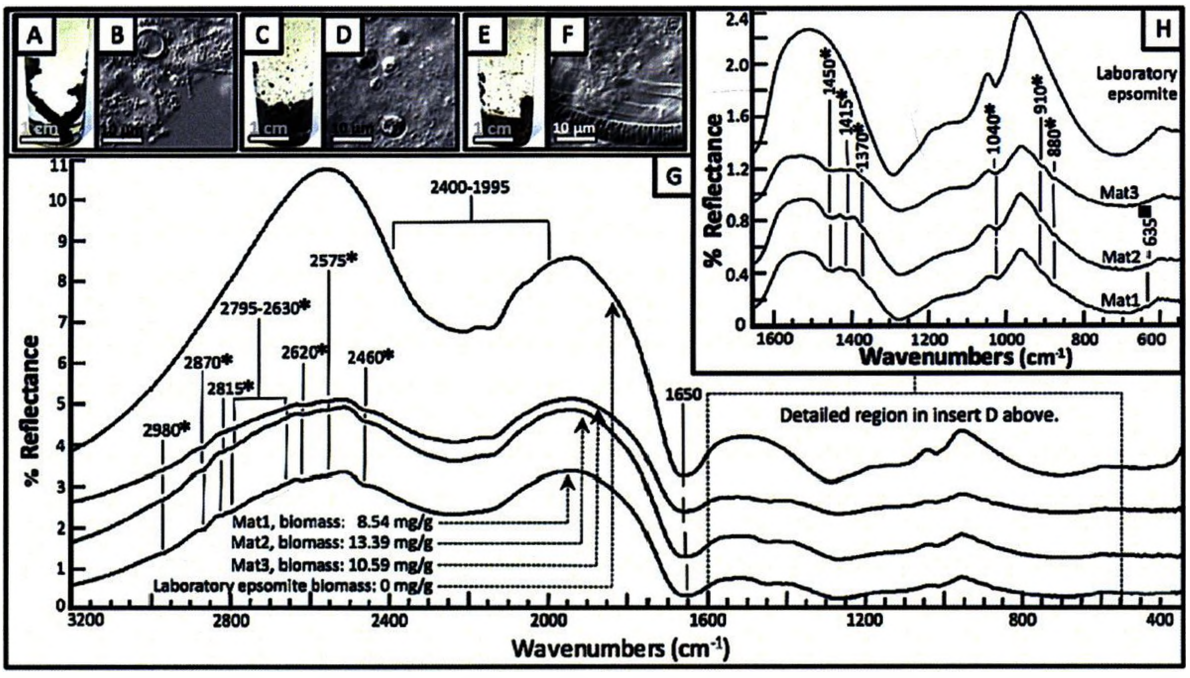

Figure 2.14: Reflectance IR spectra of natural microbial mats obtained form Basque Lake No. 2 and No. 2W. (A) Green microbial mat material suspended within 2 mol/L magnesium sulfate brine, comprising field mat sample Mat1. (B) DIC microscopy imaging of a consortia of single-celled, and filamentous autotrophs, associated heterotrophic species, and extracellular organics found in sample Mat1. (C) Dark green and red natural microbial mat suspended in 2 mol/L Mg-sulfate brine, comprising sample Mat2. (D) DIC microscopy imaging of red and green single-celled autotrophs, as well as heterotrophic species and extracellular organic material observed in sample Mat2. (E) Light green microbial mat material suspended in 2 mol/L Mg-sulfate brine comprising field mat sample Mat3. (F) DIC microscopy of two types of green filamentous autotrophs, associated heterotrophs, diatoms, and extracellular organic material found in sample Mat3. (G) Reflectance IR spectra of dried laboratory epsomite, and natural mat samples Mat1, Mat2, and Mat3, between 3200 and 400 cm^{-1}. All four spectra contain absorption bands related to sulfate and water features in the minerals. Discernable features from the organic molecules in all samples occur between 2460 and 2980 cm^{-1} corresponding to –COOH, CH_2 and CH_3 bonds. (H) Close-up of the reflectance IR spectral region between 1650 and 550 cm^{-1}. Salt spectra for natural microbial mat samples Mat1, Mat2, and Mat3 possess common biosignatures, marked with an asterisk, and one unique feature, marked with a square, that do not appear in the epsomite control. The 1370 and 885 cm^{-1} features are indicative of samples dominated by SRB, or containing microbial mats, while the 910 cm^{-1} feature is found only in samples containing microbial mats.

---

equal to concentrations of 0.78 $mg_{biomass}/g_{salt}$ within a salt matrix. The most common biosignatures identified in the field salt samples are the absorption features at 620-635, 1040-1050, 1080-1140, 1425-1465, and 1530-1570 cm^{-1}, corresponding to C-N, C-S, C-H, N-H, -OH, SO_4^{2-}, C-OH, PO_4^{3-}, CO-O-C, C-CH_3, C-CH_2-C, CH_2, and –COOH (Figure 2.15C, F, I, and Table 7). As in the laboratory enrichments, we saw the same features in all field salts regardless of possessing low biomass, however, the absorption features in

Table 6: DRIFTS Spectral Assignments for Model Laboratory Enrichment Samples

		Sample Biomass (mg$_{cells}$/g$_{sed}$)	11.53	2.23	22.01	8.46	8.44	4.7	18.57	26.28	26.88	10.59	13.39	8.54
Wavenumber (cm^{-1})	Vibrational Assignment	Biological Component	Cyano1	Cyano2	Cyano3	Arch1	Arch2	Arch3	SRB1	SRB2	SRB3	Mat1	Mat2	Mat3
4620-4720	H_2O [1]	Bound Water	M	V/B	-	-	-	M	M	-	-	-	-	-
4400-4500	H_2O [1]	Bound Water	S	M	W	M	M	S	W/B	V/B	W/B	S/B	S/B	S/B
2930-2955	CH_2 [2] [3], CH_3 [4]	Fatty Acids	W	-	-	-	-	W	-	-	-	W	V	-
2885-2900	CH_2 [4]	Fatty Acids	V	-	-	-	V	W	-	-	-	V	-	-
2850-2870	CH_2 [2] [3], CH_3 [4]	Fatty Acids	-	-	-	V	V	-	-	-	-	M	W	M
2795-2825	$(CH_3)_2N$ [4]	Amino Acids	V	-	-	-	-	W	-	-	-	S	W	-
2750-2770	$(CH_3)_2N$ [4], Dimeric -COOH [4]	Amino Acids	W	-	-	-	-	W	-	-	-	W	-	-
2630-2690	Dimeric -COOH [4]	Amino Acids	M	-	-	-	-	M	W/B	V	-	M	M	M
2595-2625	Dimeric -COOH [4]	Amino Acids	S	-	-	W	V	S	-	-	-	S	S	S
2540-2560	Dimeric -COOH [4]	Amino Acids	W/B	-	-	V	-	M	-	-	-	W	W	W
2515-2535	Dimeric -COOH [4]	Amino Acids	W	M	-	-	-	M	W/B	-	-	-	-	-
2465-2470	Dimeric -COOH [4]	Amino Acids	S	-	-	W	W	W	-	-	-	S	M	M
1530-1570	C-N [2] [3], N-H [2] [3], -COOH [4]	Amide II, Amino Acids	S	W	W	W	W	S	-	-	-	-	-	-
1480-1515	CO_3^{2-} [1]	Carbonate	S	S	V	V	V	W	-	-	-	-	-	-
1425-1465	C-CH_3 [4], C-CH_2-C [4], CH_2 [2] [3]	Fatty Acids	S	M	W	W	W	M	S/B	S/B	S/B	S/B	S/B	S/B
1400-1415	C-N [2], N-H [2]	Amide IV	V	-	-	-	-	W	V	-	-	M	M	V
1365-1375	C-CH_3 [4]	Fatty Acids	-	-	-	-	-	-	W/B	W/B	W/B	V	V	V
1230-1275	H_2O [1], C-OH [1], -C-$(CH_3)_3$ [1], PO_4^{3-} [3]	Amide III, Glycoproteins	S/B	S/B	S/B	S/B	S/B	S/B	S/B	S/B	S/B	S/B	S/B	S/B
1160-1175	C-N [4], N-H [4], C-$(CH_3)_2$ [4], SO_4^{2-} [1]	Amine II, Fatty Acids	S	M	S	M	M	M	W	M	M	-	-	-
1085-1135	CO-O-C [3], C-N [4], N-H [4], SO_4^{2-} [1] [2] [4]	Amine II	M	W	W	M	M	M	S	M	W	-	-	-
1070-1080	C-N [4], N-H [4], PO_4^{3-} [3]	Amine I, Phospholipids	W	W	V	V	W	V	-	-	-	-	-	-
1040-1050	C-OH [4], C-N [4], PO_4^{3-} [4]	Amine I, Glycoproteins	W	V	S	S	M	M	S	M	V	S	S	S
910	C-CH_2 [4]	Fatty Acids	-	-	-	-	-	-	-	-	-	V	V	W
865-890	=CH_2 [4], CO_3^{2-} [4]	Carbonate, Fatty Acids	-	-	-	-	-	-	-	-	-	W	V	M
620-635	C-N [4], N-H [4], C-H [4], C-S [4], -OH [4], SO_4^{2-} [4]	Amino Acids, Amide II, Proteins	S	M	W	-	W	M	-	M	-	-	-	-

S, strong; W, weak; V, very weak; - not detected

* Most Organic structures produced narrow absorption features, those structures that produced broad (B) or medium (M) features are indicated.

[1] Cloutis et al. 2006, [2] Marshall et al. 2006, [3] Garip et al. 2007, [4] Bellamy 1975

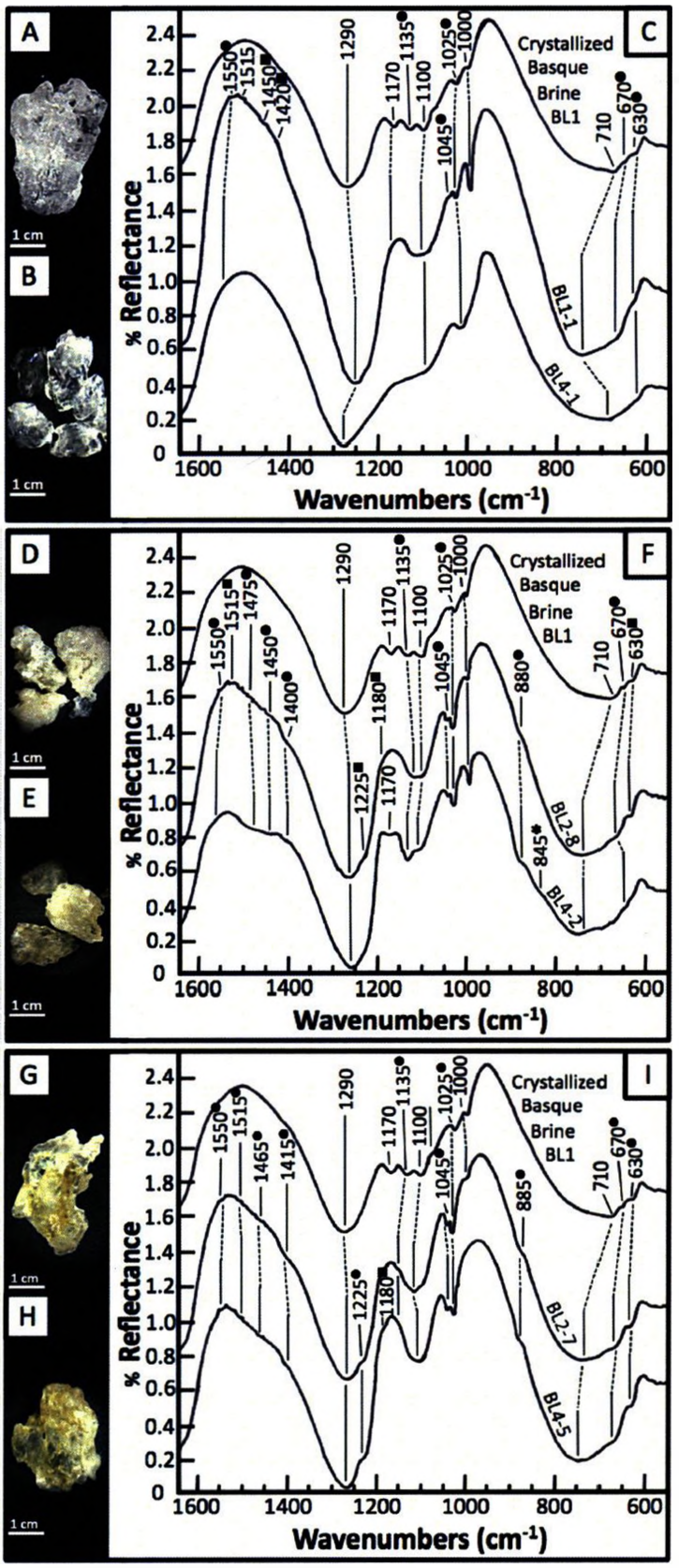

Figure 2.15: Reflectance IR spectra between 1650 and 550 cm^{-1} of natural salts and crystallized, filtered, field brines obtained form the Basque Lakes. (A) A relatively clear BL1-1 salt crystal containing 1.55 $mg_{biomass}/g_{salt}$. (B) Several small, clear BL4-1 salt crystals containing 1.06 $mg_{biomass}/g_{salt}$. (C) The three salt spectra show bands that are related to sulfate and water features in the minerals. Both field salt samples possess common biosignatures, marked with circles, while field salt sample BL1-1 also possesses unique biosignatures, marked with squares. (D) Translucent-beige colored BL2-8 salt crystals containing 2.36 $mg_{biomass}/g_{salt}$. (E) Slightly green-colored, translucent BL4-2 salt crystals containing 1.10 $mg_{biomass}/g_{salt}$. (F) The three salt spectra show bands that are related to sulfate and water features in the minerals. Both field salt samples possess common biosignatures, marked with circles, while salt sample BL2-8 also possesses unique biosignatures, marked with squares. Field salt sample BL4-2 possesses only one additional feature at 845 cm^{-1}. (G) A translucent, yellow-brown BL2-7 crystal riddled with dissolution cavities, containing 1.67 $mg_{biomass}/g_{salt}$. (H) A translucent yellow-green-brown colored BL4-5 crystal containing 2.20 $mg_{biomass}/g_{salt}$. (I) The three salt spectra show bands that are related to sulfate and water features in the minerals. Both field salt samples possess common biosignatures, marked with circles, while field salt sample BL4-5 also possesses one additional biosignature at 1080 cm^{-1}.

Table 7: DRIFTS Spectral Assignments for Natural Biomass Containing Salts

Sample Biomass ($mg_{biomass}/g_{salt}$)		1.55	0.78	0.94	1.00	1.03	1.09	1.49	1.67	2.36	1.06	1.10	1.46	1.78	2.20	3.12	4.21
Wavenumber (cm^{-1})	Vibrational Assignment	BL1-1	BL2-1	BL2-2	BL2-3	BL2-4	BL2-5	BL2-6	BL2-7	BL2-8	BL4-1	BL4-2	BL4-3	BL4-4	BL4-5	BL4-6	BL4-7
4600-4700	H_2O [1]	•	V/B	V/B	V/B	V/B	W/B	V/B	M	W/B	•	•	•	W/B	W/B	W/B	V
4400-4500	H_2O [1]	V	•	W/B	V/B	V/B	W	V	W/B	W	•	V/B	•	W	V/B	W/B	•
2930-2955	CH_2 [2] [3], CH_3 [4]	•	•	•	•	•	•	•	•	•	•	•	•	•	•	•	V
2850-2870	CH_2 [2] [3], CH_3 [4]	•	•	•	•	•	•	•	•	•	•	•	•	•	•	•	V
2630-2690	Dimeric -COOH [4]	•	V	•	•	•	•	•	•	•	•	W/B	•	•	•	•	•
2515-2535	Dimeric -COOH [4]	•	•	•	•	V/B	•	•	M	W/B	•	W/B	•	S/B	S/B	M	S/B
1530-1570	C-N [2] [3], N-H [2] [3], -COOH [4]	V	V	W	W	W	M	W	W	W	V	V	W	W	W	W	W
1480-1515	CO_3^{2-} [1]	V	•	V	V	V	W	V	V	V	•	•	M/B	V	V	V	V
1425-1465	C-CH_3 [4], C-CH_2-C [4], CH_2 [2] [3]	V	V	•	V	V/B	W/B	V	V	V	•	S/B	W	W/B	V	V	S/B
1400-1415	C-N [2], N-H [2]	•	W	•	•	W/B	•	•	W	W	•	W	S	W	W	W	W
1230-1275	H_2O [1], C-OH [1], -C-$(CH_3)_3$ [1] PO_4^{3-} [3]	•	•	•	W	•	W/B	W	W	W	•	•	•	W	M	•	•
1180-1190	C-N [4], C-$(CH_3)_2$ [4]	•	M	•	V	W	•	W	•	W	•	•	•	W	W	V	M
1160-1175	C-N [4], N-H [4], C-$(CH_3)_2$ [4], SO_4^{2-} [1]	V	•	•	•	•	V	•	V	V	•	W	•	•	•	•	•
1085-1140	CO-O-C [3], C-N [4], N-H [4], SO_4^{2-} [1] [2] [4]	S/B	S/B	S/B	S/B	S/B	S/B	S/B	S	S	S	S	S/B	S/B	S	S/B	S/B
1040-1050	C-OH [4], C-N [4], PO_4^{3-} [4]	W	W	W	W	M	W	S	M	W	W	S	•	W	•	M	M
875-890	$=CH_2$ [4], CO_3^{2-} [4]	•	W	V	•	W	•	•	W	W	•	M	V	S	W	M	S
840-845	$=CH_2$ [4]	•	•	•	•	•	•	•	•	•	•	W	•	•	•	•	•
665-680	C-H [4], C-S [4], -OH [4]	W	W	W/B	M	M	M/B	M	W	M	•	V	•	M	M	M	•
620-635	C-N [4], N-H [4], C-H [4], C-S [4], -OH [4], SO_4^{-2} [4]	W	S	W/B	S	S	M/B	S/B	S	S	V	•	V	S	M	S	M

S, strong; W, weak; V, very weak; • not detected

* Most Organic structures produced narrow absorption features, those structures that produced broad (B) or medium (M) features are indicated.

[1] Cloutis et al. 2006, [2] Marshall et al. 2006, [3] Garip et al. 2007, [4] Bellamy 1975

high biomass samples have larger band depths overall. The strongest observable features in the field salt samples are the 620-635 cm^{-1} C-N, C-S, C-H, N-H, -OH, SO_4^{2-} feature, and the 665-680 cm^{-1} C-S, C-H, -OH feature 1040-1050 cm^{-1} C-N, C-OH, PO_4^{3-} feature which corresponds to proteins, carbohydrates, phospholipids, glycoproteins, and nucleic acids (Figure 2.15C, F, I, and Table 7).

DISCUSSION

Entrapment of Halophiles in Salts: a Martian Preservation Analogue

The Basque Lakes of British Columbia, Canada (Figure 2.1 and 2.2), represent an important Mars analogue on Earth. In addition to possessing geological and chemical similarities to Mars, they are of astrobiological interest because they are inhabited by halophilic organisms that are capable of surviving high salinity, fluctuations in temperature, and high UV conditions. Under these evaporative, supersaturated conditions, the halophiles that grow in the brine pools at the Basque Lake sites encounter active salt crystallization (Figure 2.7) and are often closely associated with salt crystals (Figure 2.8), which can lead to entrapment. The entrapment of cells within salts during evaporation (Figure 2.9), would help protect these organisms from total desiccation, high UV exposure during dry periods, and ice crystal formation during freezing conditions on Earth, and by analogy, on Mars as well. Alternately, if water availability increases and salt dissolution begins, the trapped organisms may be released back into the environment where growth can resume.

The entrapment of bacteria in salt suggests that any Martian halophiles growing under comparable evaporative conditions would also be entrained within the salts on Mars. In samples studied from the Basque Lakes both cells and extracellular organic compounds are easily identifiable within the evaporites. When combined with the preservation of organic macromolecules (Tuovila et al., 1987; Aubrey et al., 2006), and viable cells (Vreeland et al., 2000) in halite, the preservation of biosignatures in these magnesium sulfate crystals supports a general, evaporite-biosignature preservation process. Important to astrobiology, this process appears to function on geologically relevant periods of time (Vreeland et al., 2000).

Biomass Assay and Confocal Microscopy Results

Biomass assay results obtained for natural salts from the Basque Lakes, have indicated that a range of biomass from 0.078 to 4.21 $mg_{biomass}/g_{salt}$ (Table 4) can become trapped within salt crystals, and that the average amount of biomass trapped is 0.74 $mg_{biomass}/g_{salt}$ ± 0.7 $mg_{biomass}/g_{salt}$. Samples found to contain the most biomass were usually sampled from the black mud found underneath the brine pools, where organic material can become trapped between intergrown salt crystals. Samples with moderate amounts of biomass were most often found on the bottom of the brine pools, or growing in, on, or around microbial mats. The samples that contained the least biomass were usually found at the brine-pool-atmosphere interface where active evaporation was occurring, or as encrustations around completely dry pools.

To determine the approximate cell content of these salts we used a model bacillus 1 μm x 0.5 μm possessing a wet mass of 10^{-9} mg/cell (Neidhardt et al., 1990), and an average salt biomass content of 0.74 $mg_{biomass}/g_{salt}$, resulting in an average population of 7.4 x 10^8 cells/g_{salt}. While the co-preservation of cells and soluble, extracellular biomass (12-22%), indicates that the actual cell count would be proportionately less, i.e., 5.7-6.5 x 10^8 cells/g_{salt}, both cell numbers correspond well with viable microbial populations observed by Chan et al., (2005) who reported an average of 1.2 x 10^8 cfu/g (colony forming units) recovered from an ephemeral, oligotrophic desert environment.

Imaging of field salts using confocal and light microscopy demonstrated that the majority of biomass was contained within relatively large (10's to 100's of μm), generally amorphous regions where crystal intergrowth or defects had created void spaces (Figure 2.9B). The remainder of the biomass is located in small isolated fluid inclusions (Figure 2.9A). In samples containing little organic material, the biomass occurred as single cells and microcolonies located within fluid inclusions with minimal or no associated extracellular organic material.

Microbial Adaptations to Hypersaline Environments:

Implications for Astrobiological Remote Sensing Targets

To survive desiccation, terrestrial halophilic species have evolved mechanisms that allow for survival in highly concentrated brines, and tolerance to fluctuating brine concentrations throughout the year, caused by brine dilution during spring runoff to supersaturated conditions in the midsummer. Archaea accumulate (and tolerate) K^+ in the

cytoplasm to counter osmotic stress (Oren 1999). As such these organisms will possess approximately the same amount of biomass per cell and general composition as non-halophilic species. In contrast, Bacteria expend energy to produce osmotic solutes such as glycerol ($C_3H_8O_3$) to balance osmotic pressure across the cellular membrane (Oren 1999). By employing this strategy, a comparable population of bacteria would be fundamentally easier to detect, as they possess higher concentrations of biomass per cell than Archaea or other non-halophilic species. The amount of solute produced by these organisms is proportional to the external brine molarity. More importantly, up to 20% of the cell biomass can be composed of this compatible solute (Ono et al., 1998), which could produce dominant organic biosignatures such as CH_2 absorptions at 2880 and 2930 cm^{-1} and 1°/2° C-OH absorption features at 1045, 1110 and 1220 cm^{-1} that may be identified using reflectance IR.

Reflectance IR

Reflectance IR as an Astrobiological Technique

The detection of organic macromolecules by reflectance IR analysis is directly related to the concentration of the molecular bonds in the sample. Cells consist of a wide variety of macromolecules, e.g., enzymatic catalysts, phospholipids, peptidoglycan, nucleic acids, and water, most of which can be simplified down to relatively few bond types. Although life as we know it on Earth is incredibly diverse (Pace 1997), it requires the same basic set of 'building blocks' (Henderson 1913; Bowen 1979; Li 1984; Cooper 2000).

While Earth is the only planet we know of that harbors life, and thus our understanding of life is inevitably biased towards what we know from Earth, there is good reason to believe life on other planets would require similar environmental conditions (Henderson 1913), and be comprised of similar elements, i.e., C, O, H, N, S, and P (Henderson 1913; Bowen 1979; Li 1984; Cooper 2000). However, if there is life on Mars, and its organic macromolecules differ from life on Earth, we may still be able to locate it by identifying areas containing organic molecular bonds, which would intuitively support a Martian biosphere. Thus we can narrow down the general types of bonds we need to look for to: C-C bonds, C-N bonds, C-O bonds, C-H bonds, C-OH bonds, N-H bonds, C-S bonds, and P-O bonds. However, to determine whether or not a reflectance IR absorption feature is useful as a biosignature, we must determine which of these bonds do not produce absorbance features that overlap with any inorganic, matrix signatures.

To determine if we can detect these organic molecular bonds within an abiotic salt matrix using reflectance IR analysis, we first established the spectral features of the host mineral (Figure 2.10D, E and Table 5), and verified that the instrument sensitivity was high enough to detect realistic microbial populations. These parameters are especially important when attempting to detect small amounts of biological material within an abiotic matrix (the most common situation in a natural environment), as mineral absorption signatures will almost always be more prominent than the biosignature absorption features available.

The reflectance IR beam samples a 1-1.5 mm diameter area, which falls on only a small area of the 6 mm diameter sample cup. In addition the IR beam cannot penetrate deeply into the sample (<1 mm), resulting in only a fraction of the total sample being analyzed. To determine a mass estimate of sample exposed to the IR beam we assume that the infrared beam has a depth of penetration = 530 μm (Moradi et al., 1999), and the diameter of the beam is = 1.5 mm, producing an analysis volume of 0.63 mm^3. With a cup volume of 113.1 mm^3, the amount of material (salt + biomass) being analyzed is ~ 0.55 % of the original sample. Thus, the actual range of biomass analyzed will fall between 4.1 μg for samples containing 0.78 $mg_{biomass}/g_{salt}$ and 22.3 μg for samples containing 4.21 $mg_{biomass}/g_{salt}$, corresponding to an absolute cell number of 4.1 X 10^6 to 2.23 X 10^7 cells assuming 100% of the constituent organics are cells.

Reflectance IR of Laboratory Enrichments

Our reflectance IR analysis of laboratory enrichment samples highlights a variety of biosignature absorption features. The most common of these are the 1040-1050 cm^{-1} C-OH, C-N, PO_4^{3-} feature, the 1230-1275 cm^{-1} H_2O, C-OH, C-$(CH_3)_3$, PO_4^{3-} feature and the 1425-1465, cm^{-1} feature which corresponds to C-CH_3, C-CH_2-C, and CH_2 (Table 6). These features would imply that macromolecules like fatty acids, phospholipids, amino acids, proteins, DNA and peptidoglycan are major contributors to the absorption features. In addition, several unique biosignatures can be observed in the enrichment samples, which are the 1070-1080 cm^{-1} C-N, N-H, PO_4^{3-} feature, 1480-1515 cm^{-1} CO_3^{2-} feature and 1530-1570 cm^{-1} C-N, N-H, -COOH feature found only in cyanobacteria and Archaea

samples (Figure 2.11 and 2.12, and Table 6), and the 1365-1375 cm^{-1} $C\text{-}CH_3$ feature observed only in samples containing SRB (Figure 2.13 and Table 6).

Reflectance IR of Natural Salts

Spectra obtained for natural salts highlighted our ability to detect biomass greater than or equal to concentrations of 0.78 $mg_{biomass}/g_{salt}$ within a salt matrix. On average each natural salt crystal analyzed contained 11 biosignatures (range = 4-15), however, the number of biosignatures present in a sample was not related to the amount of biomass present (R^2 = 0.19), despite the range in biomass concentrations. Conversely, the overall strength (band depth) of these absorption features was found to be moderately correlated to the amount of biomass (R^2 = 0.45) present, resulting in very weak, or ambiguous biosignatures in each salt sample (Figure 2.15 and Table 7).

The presence of the 1530-1570 cm^{-1} feature in all samples suggests that they may contain both cyanobacteria and Archaea, which is further supported by the additional presence of the 1480-1515 cm^{-1} feature in 13 of the 16 samples (see Table 7). A second diagnostic feature, the 875-890 cm^{-1} absorption, indicative of microbial mats, would also suggest that 11 of the 16 field salt samples also contain mat-like material in addition to cyanobacteria and Archaea (Table 7).

Reflectance IR of Microbial Mats

Reflectance IR analysis of microbial mats obtained from Basque Lake No. 2 and No. 2W possess many of the absorption features observed in the laboratory enrichments,

indicating that they are likely an amalgamation of all three types of organisms (green/red autotrophs and SRB). The natural mats also possess two unique absorbance features, one at 910 cm^{-1}, and the other at 850-890 cm^{-1} corresponding to C-CH_2, and =CH_2, CO_3^{2-} respectively. That these biosignature regions were not observed in the laboratory enrichments suggesting that there are also differences between the laboratory and natural salts. One possibility that may account for the prominent CH_2 and CH_3 features in the natural microbial mats is that they have been depleted in N and P relative to intact cells. N and P are limiting in natural systems and will be consumed preferentially, before all of the C-based organic materials, during the decay of organic matter.

Factors Affecting Biosignature Presence, and Depth

Because the amount of biomass present in a sample has a minimal affect on the number of biosignatures observed, and only moderately affects their intensity, it suggests that there are other factors present which have a negative or positive effect on biosignature detectability. Differences in sample grain size, grain orientation, pitted surfaces, water content, organic molecule concentration, and sample heterogeneity can all affect both the position, and intensity, of the absorption peaks. However, since our samples were dried at 70°C and ground with a mortar and pestle, our results indicate that there is also a limit of detection for organic material within a salt matrix. Therefore it is important to be able to distinguish between samples containing small amounts of organic material that appear to have very few, or no reflectance IR biosignatures, from those that do not contain any organics at all (Figure 2.15C sample BL4-1 vs. Figure 2.10D laboratory epsomite).

Complimentary Techniques for Detecting and Identifying Organic Material in Salts

Based on the results of this study we find that no single technique serves as a standalone method to identify life in these samples; ideally, details in structure and chemistry are required. It is therefore useful to consider each technique's advantages and disadvantages, as it pertains to the role it can play in astrobiological exploration. Confocal and light microscopy provides a visual discrimination of soluble organics, as well as in-situ observation of biomass within the salt matrix. While neither technique provides quantitative chemical data, visual inspection was instrumental in determining whether the biomass within the salts contained cells, or if it is entirely disseminate organic material. In this respect visual microscopy techniques will be immensely important in determining whether a sample contains cells, as they allow for easy detection of the complex structures that characterize living systems.

The Lowry protein assay, adapted for detection of biomass content, provides a relatively simple method of quantitatively determining the bulk biomass content of a sample. In addition, the presence or absence of a signal indicates whether a sample contains detectable concentrations of protein, which can be used to infer the likelihood of finding cells in the sample, as all cells will contain proteins, while disseminated, extracellular organic macromolecules may not. The main disadvantage of this technique is the number of chemical reagents required, as well as the need to completely disaggregate the sample matrix material to expose cells and organics, while fully breaking down cell envelopes to release cellular proteins into solution.

While IR analysis does not detect specific molecules, it does detect the molecular bonds, within major organic and inorganic phases within a sample. As such, it can provide fast, non-destructive, semi-quantitative, and real-time chemical data, making it an ideal tool for screening remote, in-situ, targets. This versatility makes IR (and Raman) spectroscopy an ideal tool to use for advance screening of potential study sites, as well as identifying areas of interest where organic material is presently exposed at the surface.

CONCLUSION

The Basque Lakes of British Columbia, Canada are an excellent terrestrial analogue for Mg-sulfate deposits on Mars, and represent an environment where active salt precipitation and crystal growth traps halophilic organisms and their constituent organics in sulfate salts. A biomass assay was performed on natural salts obtained from this site, and they contain between 0.078 and 4.21 $mg_{biomass}/g_{salt}$. Confocal light microscopy confirmed the presence of cells within these samples, and we have shown that detection of organic macromolecules is possible using reflectance IR analysis of inherent biosignatures, advocating its use for astrobiological objectives on Mars.

ACKNOWLEDGMENTS

This project was funded by a Canadian Space Agency (CSA) CARN and SSEP grants to PLK, NSERC Discovery grants to GS, and an Ontario Graduate Student Scholarship and Natural Sciences and Engineering Research Council Graduate Student Scholarship to ISF. The authors would like to thank Charlie Wu and Lachlan MacLean for technical support for the ICP and IC analysis respectively, and Katrina Moser and Driton Nushaj for their valuable contributions in the field.

REFERENCES

Aubrey, A., Cleaves, H. J., Chaimers, J. H., Skelley, A. M., Mathies, R. A., Grunthaner, F. J., Ehrenfreund, P., Bada, J, L., 2006. Sulfate minerals and organic compounds on Mars. *Geology* 34, 357-360.

Bellamy, L. J., 1975. *The infrared spectra of complex molecules*. New York: Wiley.

Bishop, J. L., Lane, M. D., Darby Dyar, M., Parente, M., Roach, L. H., Murchie, S. L., Mustard, J. F., 2008. Sulfates on Mars: How recent discoveries from CRISM, OMEGA and the MERs are changing our view of the planet. *Geochimica et Cosmochimica Acta* 72, A86.

Bishop, J. L., Murchie, S. L., Brown, A. J., Pelkey, S. M., Roach, L. A., Mustard, J. F., Bibring J. P., and the CRISM Team, 2007. Sulfates in Juventae Chasma as seen by CRISM. *Lunar and Planetary Science XXXVIII*, 2252.

Boison, G., Mergel, A., Jolkver, H., and Bothe, H., 2004. Bacterial life and dinitrogen fixation at a gypsum rock. *Applied and Environmental Microbiology* 70, 7070-7077.

Bowen, H. J. M., 1979. *Environmental chemistry of the elements*. New York: Academic Press.

Chan, M. A., Moser, K., Davis, J. M., Southam, G., Hughes, K., Graham, T., 2005. Desert potholes: Ephemeral aquatic microsystems. *Aquatic Geochemistry* 11, 279-302.

Cloutis, A. E., Hawthorne, F. C., Mertzman, S. A., Krenn, K., Craig, M. A., Marcino, D., Methot, M., Strong, J., Mustard, J. F., Blaney, D. L., Bell III, J. F., Vilas, F., 2006. Detection and discrimination of sulfate minerals using reflectance spectroscopy. *Icarus* 184, 121-157.

Cockell, C. S., Lee, P., Osinski, G., Horneck, G., and Broady, O., 2002. Impact-induced microbial endolithic habitats. *Meteoritics & Planetary Science* 37, 1287–1298.

Cockell, C. S. and Raven, J. A., 2004. Zones of photosynthetic potential on Mars and the early Earth. *Icarus* 169, 300-310.

Cooper, G. M., 2000. *The Cell: A Molecular Approach, Second Edition*. Massachusetts: Sinauer.

Cummings, J. M., 1940. Saline and hydromagnesite deposits of British Columbia. *British Columbia Department of Mines: Bulletin no. 4.*

DasSarma, S., 2006. Extreme halophiles are models for astrobiology. *Microbiology* 1, 120-126.

Edwards, H. G. M., Jorge Villar, S. E., Parnell, J., Cockell, C. S., and Lee, P., 2005. Raman spectroscopic analysis of cyanobacterial gypsum halotrophs and relevance for sulfate deposits on Mars. *Analyst* 130, 917-923.

Garip, S., Bozoglu, F., Severcan, F., 2007. Differentiation of mesophilic and thermophilic bacteria with fourier transform infrared spectroscopy. *Applied Spectroscopy* 61, 186-192.

Gross, M., 1998. *Life on the Edge: Amazing Creatures Thriving in Extreme Environments*. New York: Plenum Press.

Hardie, L. A. and Eugster, H. P., 1970. The evolution of closed-basin brines. *Mineralogical Society of America Special Paper* 3, 273-290.

Henderson, L. J., 1913. The fitness of the environment, an inquiry into the biological significance of the properties of matter. *The American Naturalist* 47, 105-115.

King, P. L., Lescinsky, D. T., Nesbitt, H. W., 2004. The composition and evolution of primordial solutions on Mars, with application to other planetary bodies. *Geochemica et Cosmochimica Acta* 68, 4993-5008.

Landis, G. A., 2001. Martian water: are there extant halobacteria on Mars? *Astrobiology* 1, 161-164.

Lane, M. D., 2007. Mid-infrared emission spectroscopy of sulfate and sulfate-bearing minerals. *American Mineralogist* 92, 1-18.

Li, Y. H., 1984. Why are the chemical compositions of living organisms so similar? *Schweizerische Zeitschrift fur Hydrologie - Swiss Journal of Hydrology* 46, 177-184.

McKay, C. P., Friedmann, E. I., Wharton, R. A., and Davis, W. L., 1992. History of water on Mars: a biological perspective. *Advances in Space Research* 12, 231-238.

Marine, M. H., Clavero, E., Roldan, M., 2004. Microscopy methods applied to research on cyanobacteria. *Limnetica* 23, 179-186.

Martinez-Frias, J., Amaral, G., and Vázquez, L., 2006. Astrobiological significance of minerals on Mars surface environment. *Reviews in Environmental Science and Biotechnology* 5, 219-231.

Marshall, C. P., Carter, E. A., Leuko, S., Javaux, E. J., 2006. Vibrational spectroscopy of extant and fossil microbes: Relevance for the astrobiological exploration of Mars. *Vibrational Spectroscopy* 41, 182-189.

Moradi, K., Depecker, C., Barbillat, J., Corset, J., 1999. Diffuse reflectance infrared spectroscopy: An experimental measure and interpretation of the sample volume size involved in the light scattering process. *Spectrochimica Acta Part A* 55, 43-64.

Neidhardt, F. C., Ingraham, J. L., Schaechter, M., 1990. *Physiology of the bacterial cell – A molecular approach.* Massachusetts: Sinauer.

Nesbitt, H. W., 1990. Groundwater evolution, authigenic carbonates and sulfates, of Basque Lake No. 2 basin, Canada. *Fluid Mineral Interactions: A Tribute to H. P. Eugster,* The *Geochemical Society, Special Publication* 355-369.

Ono, H., Okuda, M., Tongpims, S., Koima, I., Shinmyo, A., Sakuda, S., Kaneko, Y., Murooka, Y., and Takano, M., 1998. Accumulation of compatible solutes, ectoine and hydroxyectoine, in a moderate halophile, *Halomonas elongata* KS3 isolated from dry salty land in Thailand. *Journal of Fermentation and Bioengineering* 85, 362-368

Oren, A., 1999. Bioenergetic aspects of halophilism. *Microbiology and Molecular Biology Reviews* 63, 334-348.

Pace, N. R., 1997. A molecular view of microbial diversity and the biosphere. *Science* 276, 734-740.

Parnell, J., Lee, P., Cockell, C. S., and Osinski, G. R., 2004. Microbial colonization in impact-generated hydrothermal sulphate deposits, Haughton impact structure, and implications for sulphates on Mars. *International Journal of Astrobiology* 3, 247–256.

Peterson, R. C., Nelson, W., Madu, B., and Shurvell, H. F., 2008. Meridianiite: a new mineral species observed on Earth and predicted to exist on Mars. *American Mineralogist* 92, 1756-1759.

Prieto-Ballesteros, O., Rodriguez, N., Kargel, J. S., Gonzalez Kessler, C., Amils, R., Fernandez Remolar, D., 2003. Tirez Lake as a terrestrial analog of Europa. *Astrobiology* 3, 863-877.

Roach, L. H., Mustard, J. F., Murchie S., Weitz C. M., Ehlmann, B. L., Pelkey, S., Seelos, F. P., Seelos, K., Bibring, J.-P., and the CRISM Team, 2007. Sulfate identification in East Candon, Valles Marineris with CRISM visible-infrared spectra. *Lunar and Planetary Science XXXVIII, 2106.*

Rothschild, L. J., 1990. Earth analogs for Martian life. Microbes in evaporites, a new model system for life on Mars. *Icarus* 88, 246-260.

Rothschild, L. J., Giver, L. J., White, M. R., Mancinelli, R. L., 1994. Metabolic activity of microorganisms in gypsum-halite crusts. *Journal of Phycology* 30, 431-438.

Rothschild, L. J. and Mancinelli, R. L., 2001. Life in extreme environments. *Nature* 409, 1092-1101.

Sandermann, H.J., Strominger J.L., 1971. Purification and properties of C_{55}-isoprenoid alcohol phosphokinase from *Staphylococcus aureus*. *The Journal of Biological Chemistry 247, 5123-5131.*

Tosca, N. J., Knoll, A. H., and McLennan, S. M., 2008. Water activity and the challenge for life on early Mars. *Science* 320, 1204-1207.

Tuovila, B. J., Dobbs, F. C., LaRock, P.A., and Siegel, B. Z., 1987. Preservation of ATP in hypersaline environments. *Applied and Environmental Microbiology* 53, 2749-2753.

Villar, S. E., Edwards, H. G., and Cockell, C. S., 2005. Raman spectroscopy of endoliths from Antarctic cold desert environments. *Analyst* 130, 156-162.

Villar, S. E. J. and Edwards, H. G. M., 2006. Raman spectroscopy in astrobiology. *Analytical and Bioanalytical Chemistry* 384, 100-113.

Vreeland, R. H., Rosenzwelg, W. D., Powers, D. W., 2000. Isolation of a 250 million-year-old halotolerant bacterium from a primary salt crystal. *Nature* 407, 897-90

Wiseman, S. M., Arvidson, R. E., Poulet, F., Murchie, S., Morris, R. V., Seelos, F. P., Andrews-Hanna, J. C., 2008. Phyllosilicate and hydrated sulfate deposits: Recorders of water-rock interactions throughout Sinus Meridiani, Mars. *Geological Society of America Abstracts with Programs* 40, 206.

Wiseman, S. M., Arvidson, Morris, R. V., Murchie S. L., Seelos, F. P., Andrews-Hanna, J. C. and the CRISM Team, 2009. Hydrated sulfate deposits detected within Schiaparelli Crater, Mars. *Lunar and Planetary Science XL, 1798.*

CHAPTER 3

GENERAL DISCUSSION OF SULFATE SALTS AND HALOPHILIC MICROORGANISMS IN THE BASQUE LAKES SYSTEM: AN ASTROBIOLOGICAL PERSPECTIVE

The ability to detect indications of halophilic organisms within a magnesium sulfate matrix using both structural and chemical-based techniques (Chapter 2) has direct implications for astrobiology, remote sensing, and the search of life in our solar system. Specifically, hypersaline environments hosting halophiles possess a heterogeneous distribution of organic matter and biomass. This, in turn, suggests several different processes by which halophilic organisms are preserved in sulfate salts, and can guide the development of a sampling strategy and procedure which could be employed in the search for life on Mars and the Jovian satellites.

'Contemporary' Martian Water and its Relationship to Hypersaline Conditions

Mars is currently too cold, and the atmospheric pressure too low, to support liquid water anywhere on the planet's surface. However, the geneses of many of Mars' observable features are most readily attributed to the action of liquid water (Baker et al., 1991; Baker 2001; Dohm et al., 2001; Jakosky and Philips 2001; Fairen et al., 2003; Fairen et al., 2005; Ansan and Mangold 2006). They also seem to be geologically young, possessing crater counts (Hartmann 1999; Baker 2001; Fairen et al., 2003; Tanaka et al., 2003; Dohm et al., 2008), and geologic relationships (Baker et al., 1991; Baker 2001; Fairen et al., 2003; Schon et al., 2008; Wood 2006), that imply that at least some of these features are only millions of years old. If this is true, then there must have been periods throughout Martian history when the planet's surface was significantly warmer and wetter than that which we observe today. If life ever did arise on Mars, these warm periods may have been crucial lifelines for Martian biota, as they would have provided

opportunities for growth/reproduction, and facilitated their survival through Mars' variable climate history.

At present Mars appears to be in a state of liquid water dormancy at the surface. However, there is mounting evidence that there may in fact be an active subsurface hydrologic cycle, at least in some regions of the planet today. Evidence for present-day liquid groundwater comes from the occurrence of Martian gullies (Figure 3.1), found along cliff faces and crater walls, at a variety of locations across the planet (Christensen 2003; Marquez et al., 2005; Heldmann et al., 2007; Reiss et al., 2008). In addition, striking images obtained from orbital satellites have documented several of these features forming (Figure 3.2) and evolving over the course of only a few years (NASA MGS MOC press release). While the idea of past groundwater flow on Mars has already been suggested for sites such as Meridiani Planum (Figure 3.3) (Marquez et al., 2005; McLennan el al., 2005; Squyres et al., 2006; Chavdarian et al., 2006), it has only recently been claimed that, due to the cryospheric conditions on Mars, groundwater flow would be enhanced in areas that possess subsurface brines. The occurrence of magnesium sulfates in a number of locations across the planet and their highly soluble nature, suggests that groundwater systems active today would intuitively be enriched in both magnesium and sulfate ions.

In comparable hypersaline terrestrial environments, such as the Basque Lakes, one can observe both brine-rich groundwater flow, and the formation of sulfate salts in the surface and near-subsurface environment (Figure 3.4). Here, groundwater upwelling sites

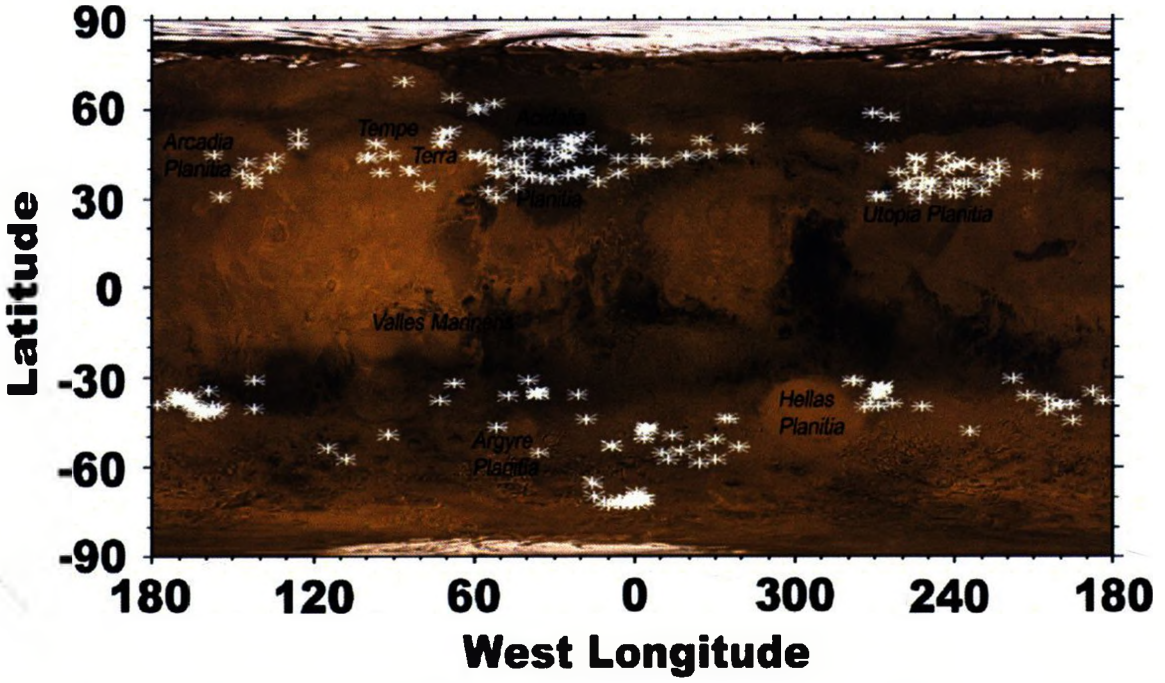

Figure 3.1 – Distribution of MGS MOC images found to show clear evidence of gullies. Each unambiguous location is marked with a white star (Heldmann and Mellon 2004).

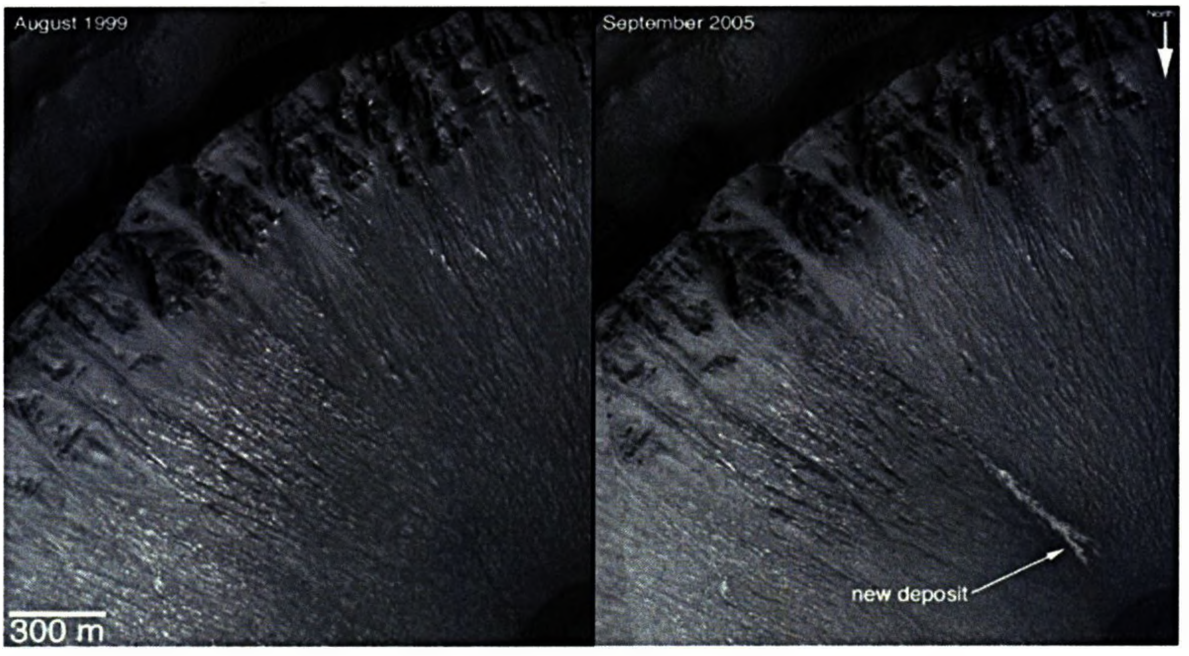

Figure 3.2 – (A) MGS MOC images of a Centauri Montes region crater, which indicates the location of a newly formed gully-deposit that occurred sometime between 1999 and 2005 (Credit NASA, Release No. MOC2-1619).

Figure 3.2 – (B) MGS MOC images of a Terra Sirenum region crater indicating a new gully-deposit has formed sometime during the five-year time span between 2001 and 2005 (Credit NASA, Release No. MOC2-1618-a).

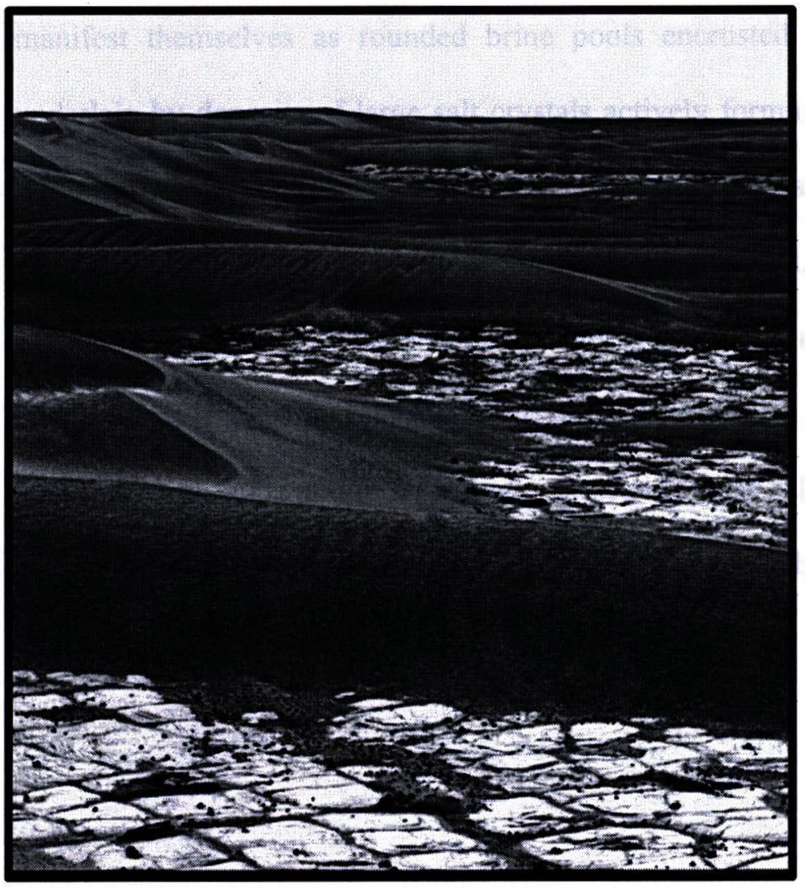

Figure 3.3 – Meridiani Planum as viewed from the Opportunity Rover. Note the fine-grained sand dunes rolling across the underlying desiccated sulfate-deposits, and the presence of numerous hematite nodules. (Image courtesy NASA).

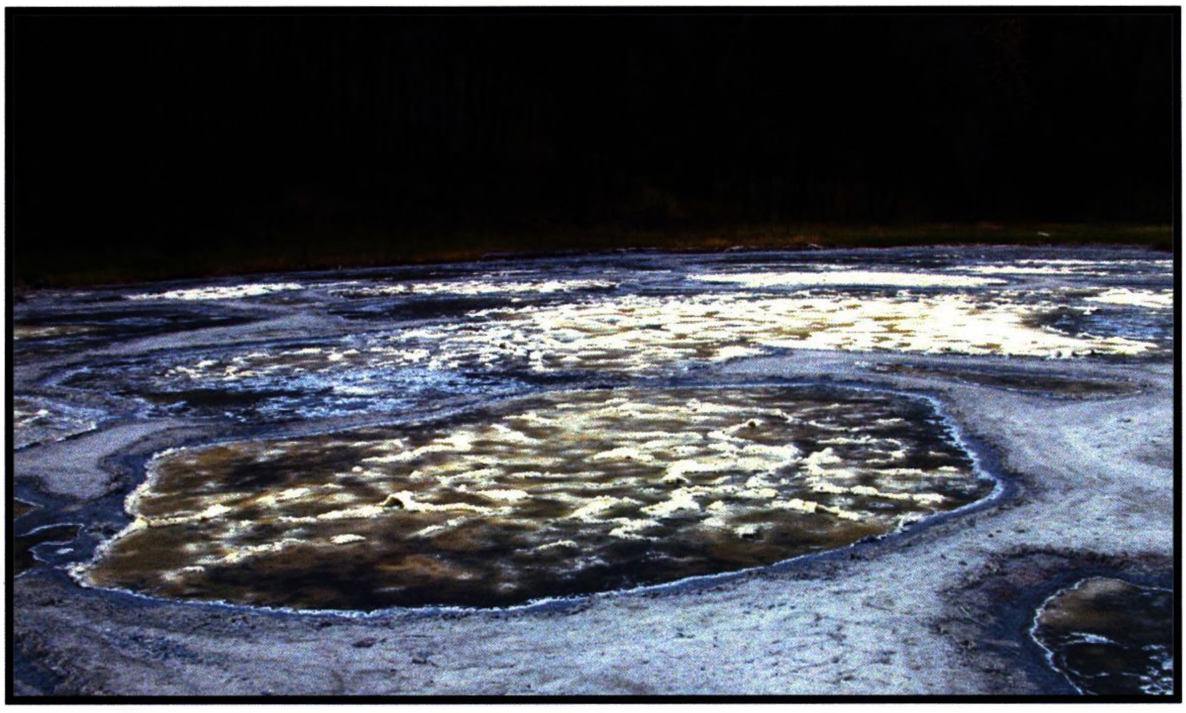

Figure 3.4 – Basque No. 2 brine pools as seen in August of 2006. Note the salt crusts beginning to cover the pools as they dry out, and the slight red-coloration near the pool edge due to the presence of brine shrimp. The central pool is ~ 2.5 m x 1 m wide, and about 2 cm deep.

---

manifest themselves as rounded brine pools encrusted with dried sulfate salts, and underlain by deposits of large salt crystals actively forming within pockets of brine. As these salt crystals grow, they commonly trap both organics and organisms in the process, and result in the overall preservation of organic material. If similar brine-rich systems exist on Mars, then it is conceivable that any organism, or organic material present, could also become trapped and preserved by salt crystal growth. If the site is not disturbed by subsequent geologic and/or hydrologic possesses, these salt crystals should remain intact indefinitely, making them prime sites of astrobiological, geological and hydrological interest.

Heterogeneity of the Basque Lakes Environment

The classification of the Basque Lakes as a hypersaline environment (Goudge 1924; Cummings 1940; Nesbitt 1990; Renaut 1990) dominated by the presence of magnesium sulfate brines possessing a circumneutral pH (Nesbitt 1990) is incomplete, as the lakes exhibit seasonal variability in water level, salinity, pH, temperature, and biota. During the thaw each spring, the lakes receive overland flow and meltwater from snow and ice. It is during this time that the lakes reach their highest levels and possess their most dilute brines. During our trip to the site in June of 2007, we observed a substantial increase in water level at Basque Lake No. 1 with brine reaching a depth of ~ 1.5 m at the center, compared to the ~ 15- 30 cm depths observed in Basque No. 2 and No. 4. Sampling of the brine water at the edge of the lake, and the center (via raft), revealed there was very little physical or compositional difference laterally, however, as we paddled towards the center of the lake we observed a density-based mixing effect caused by our paddling, suggesting that the brine is, in fact, vertically stratified. This vertical stratification seemed to allow magnesium sulfate salts to remain undissolved at the bottom of the lake despite the overlying dilute brines, and interestingly, salt was only observed to remain in the rounded pool areas, which are thought to be the sites of groundwater influx (Goudge 1924; Cummings 1940; Nesbitt 1990; Renaut 1990). This would seem to indicate that in the early spring there is little influx of diluted ground water through these pools (or the salt would presumably dissolve), or that the brines are sufficiently concentrated at the lake bottom to buffer this effect. Importantly, it also indicates that despite the presence of dilute brine waters in the immediate vicinity some salt crystals do not dissolve, facilitating their role as organic preservation vessels.

The spring biota of the lakes is dominated by brine shrimp, a halophilic eukaryote that becomes numerous enough to give the brine a distinctly reddish-hue. Centimeter scale brown colonies composed primarily of diatoms were also observed and sampled as they floated near the surface, and comparably sized, sparsely distributed, dark-green, colonies of single celled cyanobacteria (revealed by light microscopy) were observed on the muddy ridges between pools. DIC microscopy of the brines and sediments demonstrated that the brine itself contained very few planktonic organisms, while the sediments possessed substantially more organisms by comparison, however, none of the samples taken in the spring were found to have populations of halophiles consistent with the millimeter scale (thickness) microbial mats observed to cover the brine pools during the summer months (Figure 3.5). This is likely due to predation by the brine shrimp as their diet consists primarily of *Dunaliella*, diatoms and other microorganisms (Cuellar 1990).

During the summer of 2006, the Basque lakes were observed to have dried out almost completely, containing only small amounts of brine in the brine pools themselves, while the remainder of the 'lake' area consisted of muddy ridges coated in a white salt crust (Figure 3.6). Conversely, in August of 2007, Basque Lake No. 1 still contained over a meter of brine at the center and was covered in an extremely thick (~1-5 cm) floating mat composed of green filamentous algae (Figure 3.7). The surface of the mat possessed trapped bubbles of gas, presumably oxygen, and was sporadically covered in mm scale white salt crystals. The underside of the mat was colonized by pink-colored Archaea, and possessed meter scale tendrils that anchored it to the bottom of the lake. In the near-shore

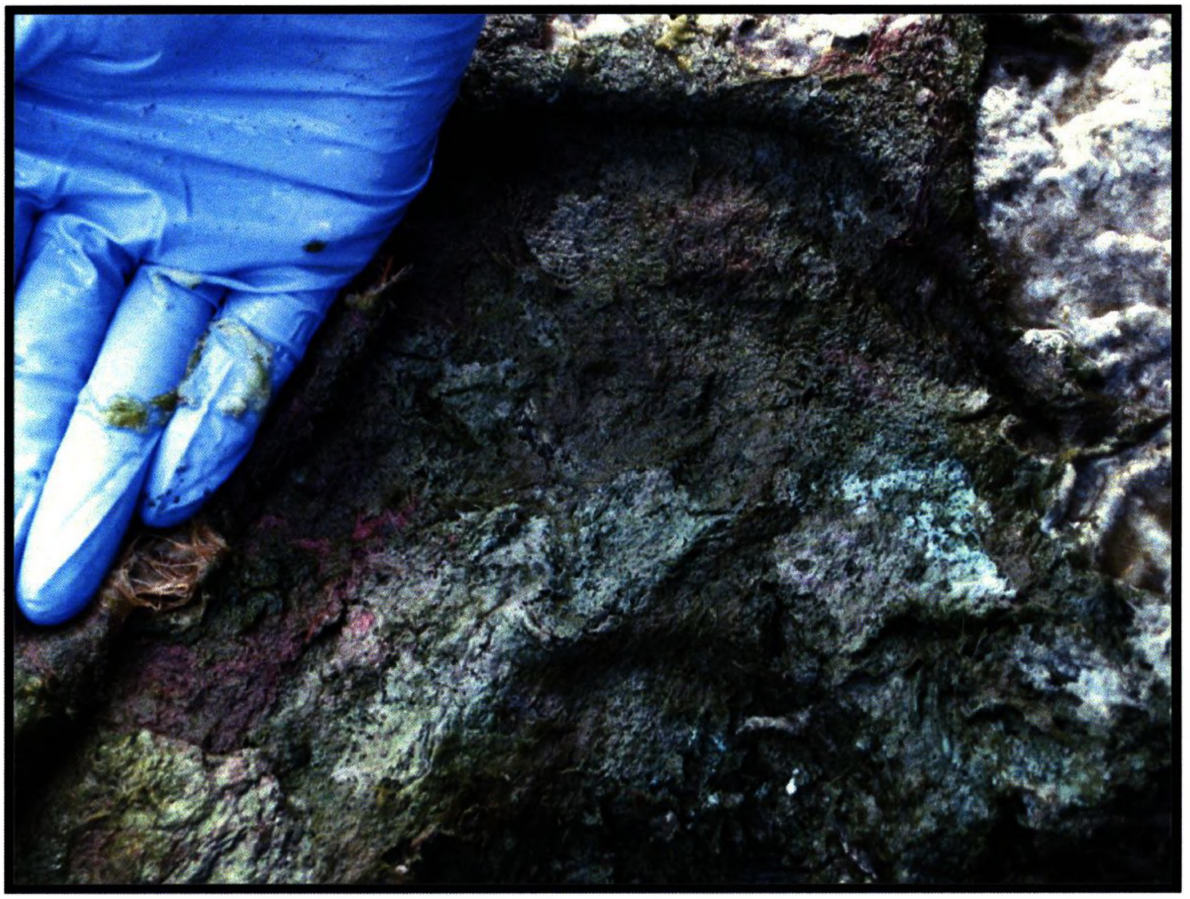

Figure 3.5 – A multilayered mottled green, red and white microbial mat found along the shore of Basque Lake No. 2W in August 2007. The mat was 4-6 layers thick, ~ 5-8 mm each, and retained a green and red coloration all the way to the bottom.

---

environment several areas of pitch-black organic sediments were discovered that were coated in deep red-colored mats of Archaea, some of which also possessed dark purple areas that may have been colonies of red sulphur bacteria. Long time residents of the area were questioned regarding the frequency of extremely wet conditions at Basque No. 1, and we were informed that these conditions have not occurred in at least 25 years, and no one had ever seen this much water present in the middle of the summer, or observed a lake-wide algal bloom. These observations would seem to indicate that although the Basque Lakes environment is dominated by extremely dry conditions, it periodically

Figure 3.6 – Mud ridges, commonly coated in salt, separate numerous irregularly shaped brine pools at Basque Lake No. 1 in August of 2006.

experiences flood-like seasons where availability of water, and more dilute brine conditions allow for tremendous biomass production over the span of a few months.

The timing of our fieldwork was fortuitous as it allowed us to observe this dramatic influx of surface water over the course of a single year, giving us an unexpected insight into the physical and biological variability of the site. First, the bloom of biological activity that resulted from increased water activity demonstrated the positive growth response of the biosphere (i.e., microbial mats, biofilms, planktonic organisms, etc.) to the removal of osmotic stress. Second, the growth of eukaryotes out of prokaryote-dominated mats demonstrated a strong population shift when selective pressures were

Figure 3.7 – Basque Lake No. 1 as observed from the roadside in August of 2007. The entire lakeshore was coated in a thick algal mat that continued out all the way to the middle of the lake. The mat was extremely cohesive and required us to chop through it with paddles, inset image. This image is of the same lake sampled 12 months previous when it was a dry salt flat.

removed, highlighting the enhanced competitiveness of the bacteria when conditions are more extreme (i.e., hypersaline). Third, even under high water conditions, some of the pre-existing salt crystals were preserved from previous seasons. This preservation of salt crystals may allow a layering effect of high and low biomass salts to occur, as subsequent dry years bury and trap crystals rich in organic material, between layers of salt that are never fully dissolved again during a wet season.

Over the course of the fall and winter, the brine slowly cools and the surface of the Basque lakes freezes to form a continuous ice cover. This causes a corresponding

concentration of ionic species in the remaining brine, allowing some liquid to remain below the ice or in the subsurface at all times, as was observed in February of 2008. The decrease in temperature, and increase in brine concentration caused by the freeze-out of water would presumably result in salt crystals forming in the brine, and raining out on to the lake bottom. This rainout may act as a dissolution buffer and stratification agent that allows larger salt crystals or crystal aggregates located at the groundwater outflow points to remain intact through the following spring thaw. As in all ice-covered ecosystems, biological activity can be maintained through winter, although the low light conditions (due to the ice cover) presumably would create a selective pressure favoring low light photosynthesizers, such as cyanobacteria, and various anaerobic organisms.

Spatial Relationship of Preserved Salts and Organic Material in the Basque Lakes

Once water loss through evaporation outstrips water input through overland, or groundwater flow, a gradual increase in brine concentration will occur. As the brine concentration increases, various halophilic organisms will experience optimum growth conditions, and then pass into a stressed state in which growth and reproduction are more metabolically challenging. As evaporation continues to the point of evaporite formation, accumulated biomass has the potential to become trapped in the newly forming salt crystals. However, the individual mm scale crystals that formed at the air-water interface possessed the least biomass of all samples we analyzed. This implies that evaporation alone is not necessarily conducive to the preservation of halophilic microorganisms and/or their associated organic molecules (Table 3.1).

Table 3.1

Biomass Content of Salt Samples Obtained from Different Settings in the Basque Lakes

	Sample Origin	Sample Name	Biomass Content $mg_{biomass}/g_{salt}$	
Samples Containing High Biomass	Basque No. 1	Crystals found at depth below a central brine pool.	0.52	Average Biomass Content 1.71 $mg_{biomass}/g_{salt}$
	Basque No. 1	Large subsurface crystals from below a brine pool.	1.55	
	Basque No. 2	Crystals found at the top of a brine covered pool core.	0.74	
	Basque No. 2	Crystals found in the middle of a brine covered pool core.	0.94	
	Basque No. 2	Large crystals from the bottom of a brine covered pool core.	1.09	
	Basque No. 2	Crystals from the middle of a central brine pool core.	1.67	
	Basque No. 2	Crystals from the bottom of a central brine pool core.	2.36	
	Basque No. 2	Large translucent crystals from below a brine pool.	3.12	
	Basque No. 4	Large crystals from under a central brine pool.	0.30	
	Basque No. 4	Crystals from the mud below a brine pool.	1.78	
	Basque No. 4	Subsurface pool sediments and crystals.	2.20	
	Basque No. 4	Large muddy crystals from below a central brine pool.	4.21	
Samples Containing Moderate Biomass	Basque No. 1	Pool bottom crystals, mud and brine.	0.17	Average Biomass Content 0.46 $mg_{biomass}/g_{salt}$
	Basque No. 1	Less solid crystals found at depth below a central brine pool.	0.30	
	Basque No. 2	Crystals from the hard salt layer below green 'slushie' crystals.	0.15	
	Basque No. 2	Crystals from the top of a brine pool core.	0.17	
	Basque No. 2	Hard salt layer from the bottom of a central brine pool.	0.19	
	Basque No. 2	Salt crystals containing small green pieces of biomat.	0.23	
	Basque No. 2	Crystals from a central brine pools bottom crystal layer.	0.27	
	Basque No. 2	Central pool crystals found below the surface salt layer.	0.34	
	Basque No. 2	Crystals taken from a brine pools solid bottom crystal later.	0.52	
	Basque No. 2	Green crystal 'slushie' from a drying brine pool.	0.54	
	Basque No. 2	Central brine pool crystals from below the upper salt layer.	0.67	
	Basque No. 2	Green brine with crystals and chironomids.	0.67	
	Basque No. 2	Pool bottom hard salt layer.	1.00	
	Basque No. 2	Green brine and salt crystals.	1.49	
	Basque No. 2W	Pool bottom salt plug.	0.13	
	Basque No. 2W	Yellowish looking pool bottom salt plug.	0.17	
	Basque No. 2W	Pool bottom salt plug containing yellow and brown particles.	0.18	
	Basque No. 3	Central pool crystals from below the top salt layer.	0.46	
	Basque No. 3	Bottom hard crystal layer of pool.	0.59	
	Basque No. 4	Thick pool salt layer.	0.10	
	Basque No. 4	Hard salt layer from pool at the southern side of the lake.	0.73	
	Basque No. 4	Salt crystals from a surface biofilm.	1.06	
Samples Containing Low Biomass	Basque No. 1	Small faintly green surface salt crystals.	0.19	Average Biomass Content 0.16 $mg_{biomass}/g_{salt}$
	Basque No. 1	Small faintly green crystals from a brine pools salt crust.	0.31	
	Basque No. 2	Yellowish salt and brine from a central brine pool.	0.09	
	Basque No. 2	Surface pool crystals and brine.	0.13	
	Basque No. 2	White salt bubble on brine pool surface.	0.13	
	Basque No. 2	Pool surface crystal samples.	0.21	
	Basque No. 2W	Clean white salt from a pool salt plug.	0.08	
	Basque No. 4	Thick pool surface salt layer.	0.08	
	Basque No. 4	Thin crystal film on brine pool surface.	0.25	

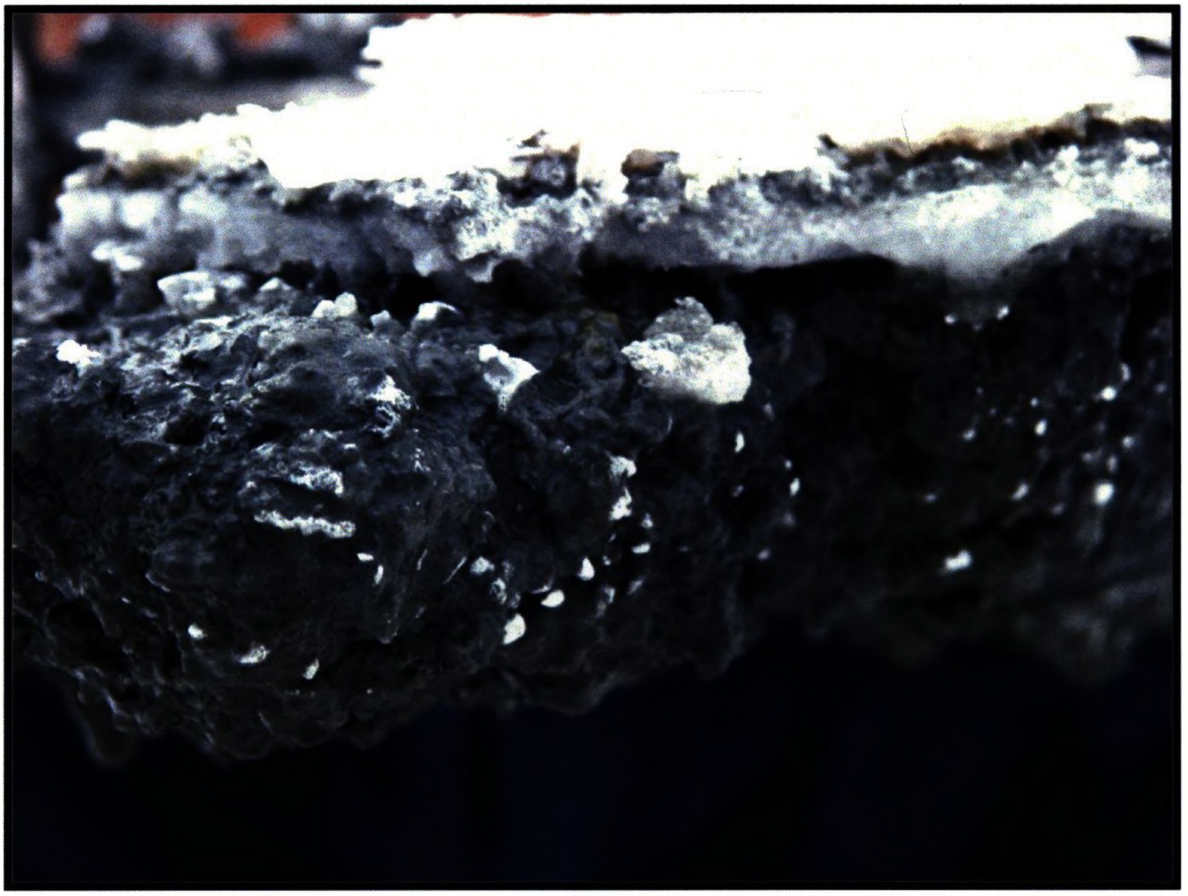

Figure 3.9 – A large salt crystal 'iceberg' found growing beneath the surface of a brine pool. The solid surface salt 'cap' feature suggests that continued crystal growth must be occurring downward into the underlying mud and brine.

Light microscopy of natural microbial mats and enrichment samples revealed the presence of salts forming within microbial colonies, suggesting that the crystallization process may in fact be initiated before the brine reaches saturation if a crystal nucleates within the microenvironment of a microbial mat (Figure 3.8), where hydration layers result in a local decrease in water activity. This process seems to be relatively efficient at trapping organic material, as samples derived from and near microbial mats were found to contain more preserved organic material than that of the surface salts. The large clear salt crystals obtained from the hard bottom layers of brine pools were also found to contain a moderate amount of trapped organics, likely resulting from the evaporative precipitation

and settling out of salt crystals from the brine on to extant surface colonies and biofilms (Table 3.1).

Biomass assay values for the comparatively larger (0.5 - 2 cm) salt crystals obtained from the black mud's located immediately below brine pools (Figure 3.9) had the highest preservation potential as all samples analyzed were found to possess a high biomass content (Table 3.1). This result is surprising as one would have expected biomass contents to be highest in microbial mats or surface deposits, that experience high rates of evaporation, rather than the underlying sediments. Even more interestingly is, not only is biomass being preserved in the subsurface, both active crystal growth and recrystallization are occurring despite the crystals being surrounded by liquid brine. Based on this data, it would seem that the best place to look for preserved organic matter is not in fact on the surface of evaporite deposits, but rather in the sediments underlying them. In terms of astrobiological exploration, this suggests that the location and sampling of near-subsurface deposits of layered evaporites should be focused in regions known to have, or have had, prolonged periods of evaporite formation punctuated by local or regional groundwater flow throughout its history.

Biomass data from dried Basque Lake brines indicated that although the surface brine in which new crystals are actively forming possess a high dissolved organic content, the crystals themselves seem to exclude it, trapping only a small amount of dissolved organics within fluid inclusions. Intuitively this could be the result of cellular degradation and decomposition occurring in the brine, as the samples were collected from brine pools during the hottest time of the year, presumably when cell death and decay would have

been at a maximum, and the growth of heterotrophic organisms at a minimum. This observation is consistent with small crystals observed with confocal microscopy (Chapter 2), which were found to contain relatively few cells trapped within fluid inclusions (Figure 3.10), and lacked void spaces filled with organics altogether. Crystals derived from the bottom of brine pools, and out of microbial mats were found to contain moderate amounts of organic material, and were observed to possess fluid inclusions containing only cells or a mix of cells and associated organics, and occasionally void spaces filled with both organics and cells. This would suggest that during the drying process organic material and cells are concentrated at the bottom of brine pools, where they are later trapped by crystal growth which leads to the formation of the "hard crystal layers" commonly observed at the bottom of Basque Lake brine pools.

Subsurface Evaporite Formation, a Unique Preservational Setting

The subsurface environment of brine pools is markedly different than that of the pool surface, as it is not exposed directly to the atmosphere. This seems to result in two different types of crystals forming and being preserved below the surface. At the pool edges where there is the least water input, and the strongest drying effect, a massive deposit of small (0.2 - 0.5 cm) crystals develops which appears to be very similar to the small crystals formed at the surface, and likely results from the burial of surface crystals over time. Alternatively, near the inner region of the pool a complex mix of crystal dissolution and crystal growth appears to occur, which results in a 'sponge-like' matrix supported by large crystals interspersed with cavities containing black sediments and brine. The intergrown nature of the large crystals in this zone suggests that some crystals may have been dissolved by groundwater influx, while remaining crystals are altered by

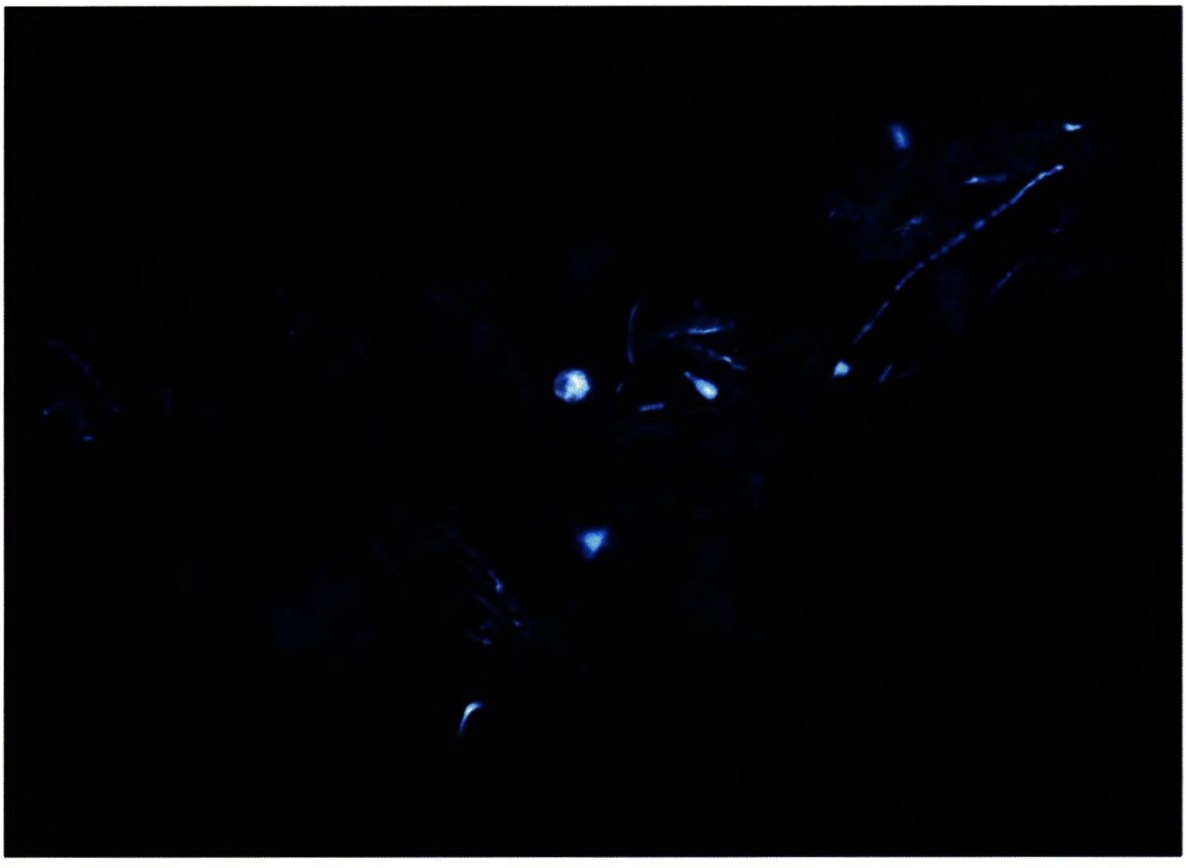

Figure 3.10 – Confocal microscopy image of cells and organic matter trapped in a large fluid inclusion from a Basque Lake No. 1 salt crystal. Notice the distinctly bright cells are often embedded in diffusely glowing organic material while others 'float' in the trapped brine water.

re-crystallization and continued growth after burial. During the growth phase these subsurface salt crystals seem to push sediments and organic material away from them as the crystal grows, resulting in remarkably clear crystals overall. However, when two or more growing crystals meet, organic material and sediments can become trapped between them and incorporated into the new larger crystal as it grows.

Observable Condition of Organic Material within Sulfate Salts

Salt crystals imaged using confocal microscopy highlighted that the majority of crystals contain irregularly shaped void spaces commonly filled with sediment and/or organic material. Visual inspection of the material using Brightfield microscopy was difficult, as

most often it appeared only to be a blurry amorphous mass, occasionally containing small translucent sediment grains. However, when observed using confocal microscopy these regions were resolved into complex zones filled with autofluorescent extracellular polymers, dark sediments, and a variety of fluorescent cells (Figure 3.11), the most common of which were cocci. Since the extracellular polymers glowed faintly when exposed to the laser, it would imply that they must contain some sort of fluorescent molecule, likely derived from lysed cells, although it is unclear if this material was initially present and was trapped along with the cells, or if it represents cells that have undergone lysis since entrapment occurred. These types of void spaces were only observed in large intergrown crystals sampled from the hard bottom layers of pools and the subsurface, and have not been observed in any of the smaller single crystals (< 10 mm) sampled.

The second type of preservation, small (5 - 10 x 5 - 20 μm) fluid inclusions, is typically observed as euhedral to subhedral hexagonal-voids elongated along one axis, usually containing easily visible cells. Confocal images of these regions revealed that they generally contain only a few single cells or planar microcolonies, and are rarely deep enough to contain more than two stacked cells ~ 2 μm depth. It was also not unusual to find inclusions that appeared empty when observed with both confocal and light microscopy. Larger cells such as *Dunaliella* were commonly observed to have lysed since entrapment, however decay does not appear to occur rapidly, or at all in some inclusions, as intact pieces of *Dunaliella* cell walls, flagella, and vacuoles were observed in two separate small (5-10 μm) fluid inclusions.

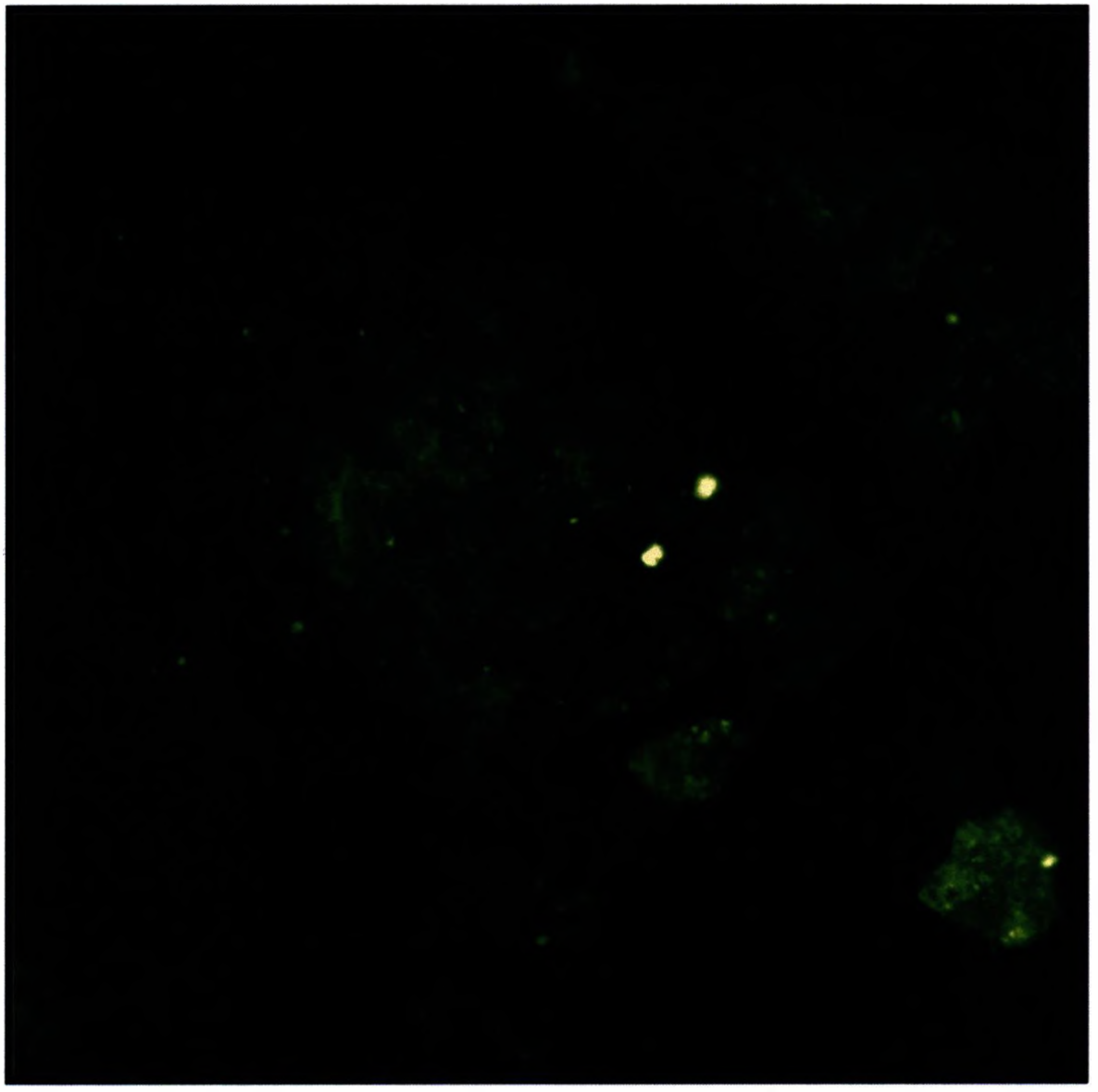

Figure 3.11 – Confocal microscopy image of several planar void space regions between intergrown Basque No. 2 crystals. Notice the abundance of both extracellular material and cells contained within the void spaces suggesting that crystal growth occurred near a microbial colony, trapping both organic material and cells inside the cavities as the salt crystal slowly grew and encompassed the colony. Scale bar is 10 μm.

In this study, all natural crystals observed with confocal microscopy possessed at least a few fluid inclusions containing trapped cells, although the majority of them contained numerous fluid inclusions and/or void spaces filled with a combination of cells and organic material. This data matches that from the biomass assay, which consistently found organic material in all of our samples, and would seem to suggest that not only is

preservation of organic material within sulfate salts possible, it is also quite common. Additionally, in the case of fluid inclusions, entrapment also seems to possess preservative properties that allow both whole and lysed cells to remain unaltered. This has direct implications for astrobiology as it suggests that organisms trapped within primary salt crystals have not only their organic biosignatures preserved, but their viability as well, as suggested by Vreeland et al., (2000). To determine if the cells trapped within our salt samples were still viable three salt crystal samples were treated with our surface dissolution technique (Chapter 2) and placed into separate test tubes each containing 18 mL of filter sterilized BBM (Brine Based Media). After several days all three samples had developed a milky-white turbidity indicating the positive growth of heterotrophs, and confirming the presence of viable organisms within the salt crystals.

Once trapped, any organism capable of remaining viable within a salt crystal may gain protection from harsh environmental conditions by entering a type of protected dormancy or stasis. The ability to survive within salt crystals would be a tremendous evolutionary advantage for any halophilic organism, as it would give them the opportunity to protect themselves from damaging ambient conditions during times of environmental instability. If true, it would intuitively suggest that these same organisms might be able to survive harsh Martian conditions, i.e., low water, high salt, and high UV exposure, by entering a dormant state, reawakening later to continue growth once more favorable environmental conditions return and they are released from their crystalline cocoons.

Analysis Techniques, a Combined Approach to Astrobiological Sampling

Each of the four techniques used in this study possessed strengths and weaknesses with regards to the detection of organic material within a sulfate matrix. When considering the future design and instrumentation of new robotic missions tasked with the search for life on other planetary bodies, there is a distinct advantage to including some instruments and techniques over others. For remote sensing objectives from orbit, or characterization of surface targets that are out of range of direct sampling, or are in areas inaccessible by land based rovers, reflectance IR offers a rapid, surface sensitive, and non-destructive means to characterize materials and identify areas that contain enrichments of organic matter. This technique however cannot differentiate between non-biologically produced lipids or amino acids in solution, and those contained in an organism's cell wall, cytoplasm or proteins.

In order to determine if a biosignature is actually from an organism and not a dissolved or disseminated organic molecule, the fastest, easiest, and by far most informative way is by visual identification using some form of light microscopy. The power of light microscopy techniques lies in their ability to magnify small samples allowing us to rapidly identify any complex structures that may be indicative of life. As discussed in Chapter 2 the two visual techniques employed in this study, DIC and confocal microscopy, were instrumental in determining that the reflectance IR biosignatures from our salt crystals did in fact originate from cells and the extracellular organics and polymers associated with them. The importance of this visual confirmation can be demonstrated by simply comparing the biosignatures produced by the natural salts, to those produced by the crystallized, filtered field brines. In both cases reflectance IR detected organic molecule

biosignatures, however, visual inspection of the artificially created crystals demonstrated that they did not in fact contain any cells.

The disadvantage of light microscopy techniques is that they require some degree of sample preparation to produce useable images. Sample material must be collected and placed onto a transparent mount, and in the case of confocal microscopy, fluorescent tags must be added to allow visualization of organisms that do not contain autofluorescent compounds. In addition, light microscopy is not well suited to identifying organisms which are attached to, or found within, sample materials, and cannot produce clear images of samples more then a few microns thick, due to the glare associated with other objects lit in the sample. This is not an issue with confocal microscopy as it has been designed to produce clear images from thick samples, however, the matrix/medium must be transparent at both incident and excitation wavelengths or no image will be produced.

By considering each technique's strengths and weaknesses a sampling strategy/procedure can be developed to search for life on Mars and/or the Jovian satellites. Reflectance IR is the first logical technique to use as it allows a rapid analysis of large areas, enabling close inspection of sites containing enrichments of organic material. Once a general region has been selected, IR can then be used on a local scale to determine exactly where organic molecules are most plentiful, and if they contain molecular bonds such as one would expect to find in living systems. Once a specific site has been selected, a carbon assay can be performed on selected samples to determine quantitative values of organic carbon contained within sampled material, and to determine if other assays, such as those for carbohydrates or protein, may be useful in identifying the type of organics present.

Samples that are found to contain molecules of interest can then be imaged with a relatively fast and simple technique such as light microscopy to determine if there are any complex structures (cells) present that are indicative of life. Finally, if a sample is found that appears to contain cells, a high resolution imaging technique that can be coupled with chemical analysis, such as SEM (Scanning Electron Microscopy) or Micro-IR, can be employed to determine the exact location and composition of the organic feature, as well as its detailed morphology and plausibility as a living cell, or fossilized organism.

OVERALL CONCLUSIONS

The Basque Lake area of British Columbia, Canada, is an excellent terrestrial analogue site for Martian magnesium sulfate deposits, as these lakes are groundwater-fed, closed-basin systems, which possess both Mg-sulfate rich brines and abundant magnesium sulfate minerals. The lakes are inhabited by a variety of halophilic organisms from all three kingdoms of life, Archaea, Bacteria, and Eukarya, which grow in both the surface and the near-subsurface environments. Salt samples obtained from the Basque Lakes were found to contain biomass, ranging from 0.078 to 4.21 $mg_{biomass}/g_{salt}$ and confocal/light microscopy highlighted the presence of halophilic organisms trapped within natural salt crystals. It was determined that both halophilic organisms and their associated organics are primarily preserved within void spaces between intergrown crystals, or in isolated fluid inclusions, and that some of the trapped organisms remained viable. Laboratory enrichments derived from Basque samples were used to assess the types of organisms present, and were analyzed with reflectance IR to highlight the biosignatures produced by a consortia of halophilic organisms and their constituent organics. Reflectance IR of natural salts demonstrated that detection of organic material within a sulfate matrix is possible using established biosignatures, the most sensitive of which were the 1550 ± 20 cm^{-1}, C-N, N-H, -COOH absorptions and the 1040 ± 10 cm^{-1} C-OH, C-N, PO_4^{3-} bond features. Due to its rapid non-destructive nature, and ability to detect small amounts of organic material within a dominant sulfate matrix, reflectance IR is a valuable tool for astrobiological objectives. When combined, reflectance IR, biochemical assays, and confocal/light microscopy are a powerful suit of techniques well suited for the characterization and interpretation of planetary materials.

FINAL THOUGHTS

The incredible successes in the last five years of Mars exploration have shed a tremendous amount of light on some of the Red planet's most captivating mysteries, while providing a wealth of information that continues to propel Mars exploration today. As we continue to learn more about the past and present climate of our celestial neighbor, we count the days until mankind at last sets foot on this enigmatic world. As questions regarding Martian life, past, present and future continue to burn bright in the public imagination, we dream of one day setting foot on Mars and finding immediate proof of our planetary relatives existence. In all likelihood, fossils or biochemical remnants of a past Martian biosphere will be what we discover first, if there are any to discover at all. Although it will be difficult, if not impossible, to conclude that Mars has never harbored life, as one would presumably have to inspect every outcrop, and plumb every depth of the planet to be sure, this project has shed some light on the type of places to look first. The ubiquitous occurrence of biomass in all our study's samples, suggests that if there were ever halophilic organisms on Mars, it's fairly likely that they have been preserved at some point during the formation of Mars various salt deposits. Once trapped however, it's unclear how long organic material will survive within a salt crystal if exposed to Mars current cryospheric conditions. The next logical step in detecting Martian halophiles, it would seem, is to determine what protection, if any, entrapment in salt crystals provides, and if any organism is in fact capable of surviving the ravages of the Martian climate once entombed. By addressing these questions, we may ascertain both the likelihood of finding near-surface Martian organisms, as well as shed some light on a process that may have allowed ancient terrestrial halophiles to survive past climatic variation on our world as well.

REFERENCES

Ansan, V., and Mangold, N., 2006. New observations of Warrego Valles, Mars: Evidence for precipitation and surface runoff. *Planetary and Space Science* 54, 219-242.

Baker, V. R., Strom, R. G., Gulick, V. C., Kargel, J. S., Komatsu, G., Kale, V. S., 1991. Ancient oceans, ice sheets and the hydrological cycle on Mars. *Nature* 352, 589-594.

Baker, V. R., 2001. Water and the Martian landscape. *Nature* 412, 228-236.

Chavdarian, G. V., Sumner, D. Y., 2006. Cracks and fins in sulfate sand: Evidence for recent mineral-atmospheric water cycling in Meridiani Planum outcrops? *Geology* 34, 229-232.

Christensen, P. R., 2003. Formation of recent Martian gullies through melting of extensive water-rich snow deposits. *Nature* 466, 45-48.

Cuellar, O., 1990. Ecology of brine shrimp from Great Salt Lake, Utah, U.S.A. (Branchiopoda, Anostraca). *Crustaceana* 59, 25-34.

Cummings, J. M., 1940. Saline and hydromagnesite deposits of British Columbia. *British Columbia Department of Mines: Bulletin No. 4.*

Dohm, J. M., Anderson, R. C., Barlow, N. G., Miyamoto, H., Davies, A. G., Taylor, G. J., Baker, V. R., Boynton, W. V., Keller, J., Kerry, K., Janes, D., Fairen, A. G., Schulze-Makuch, D., Glamoclija, M., Marinangeli, L., Ori, G. G., Strom, R. G., Williams, J.-P., Ferris, J. C., Rodriguez, J. A. P., de Pablo, M. A., Karunatillake, S., 2008. Recent geological and hydrological activity on Mars: The Tharsis/Elysium corridor. *Planetary and Space Science* 56, 985-1013.

Fairen, A. G., Dohm, J. M., Baker, V. R., de Pablo, M. A., Ruiz, J., Ferris, J. C., Anderson, R. C., 2003. Episodic flood inundations of the northern plains of Mars. *Icarus* 165, 53-67.

Fairen, A. G., Dohm, J. M., Uceda, E. R., Rodriguez, A. P., Baker, V. R., Fernandez-Remolar, D., Schulze-Makuch, D., Amils, R., 2005. Prime candidate sites for astrobiological exploration through the hydrogeological history of Mars. *Planetary and Space Science* 53, 1355-1375.

Goudge, M. F., 1924. Magnesium sulfate in British Columbia. *Canada Department of Mines, Investigations of Mineral Resources and the Mining Industry* 62-101.

Harrison, K. P. and Chapman, M. G., 2008. Evidence for ponding and catastrophic floods in central Valles Marineris, Mars. *Icarus* 198, 351-364.

Hartmann, W. K., Malin, M., McEwen, A., Carr, M., Soderblom, L., Thomas, P., Danielson, E., James, P., Veverka, J., 1999. Evidence for recent volcanism on Mars from crater counts. *Nature* 397, 586-589.

Heldmann, J. L., and Mellon, M. T., 2004. Observations of Martian gullies and constraints on potential formation mechanisms. *Icarus* 168, 285-304.

Heldmann, J. L., Carlsson, E., Johansson, H., Mellon, M. T., Toon, O. B., 2007. Observations of Martian gullies and constraints on potential formation mechanisms II. The northern hemisphere. *Icarus* 188, 324-344.

Jakosky, B. M. and Phillips, R. J., 2001. Mars' volatile and climate history. *Nature* 412, 237-244.

Marquez, A., angel de Pablo, M., Oyarzun, R., Viedma, C., 2005. Evidence of gully formation by regional groundwater flow in the Gorgonum-Newton region (Mars). *Icarus* 179, 398-414.

McLennan, S. M., Bell, J. F., Calvin, W. M., Christensen, P. R., Clark, B. C., Souza, P. A., Farmer, J., Farrand, W. H., Fike, D. A., Gellert, R., Ghosh, A., Glotch, T. D., Grotzinger, J. P., Hahn, B., Herkenhoff, K. E., Hurowitz, J. A., Johnson, J. R., Johnson, S. S., Jolliff, B., Klingelhofer, G., Knoll, A. H., Learner, Z., Malin, M. C., McSween, H. Y., Pocock, J., Ruff, S. W., Soderblom, L., A., Squyers, S. W. Tosca, N. J., Watters, W. A., Wyatt, M. B., Yen, A., 2005. Provenance and diagenesis of the evaporite-bearing Burns Formation, Meridiani Planum, Mars. *Earth and Planetary Science Letters* 240, 95-121.

Nesbitt, H. W., 1990. Groundwater evolution, authigenic carbonates and sulfates, of Basque Lake No. 2 basin, Canada. *Fluid Mineral Interactions: A Tribute to H. P. Eugster, The Geochemical Society, Special Publication No. 2,* 355-369.

Reiss, D., Hiesinger, H., and Gwinner, K., 2008. Regional differences in gully occurrence on Mars: A comparison between the Hale and Bond craters. *Workshop on Martian Gullies: Theories and Tests* 8027.

Renaut, R. W., 1993. Morphology, distribution and preservation potential of microbial mats in the hydromagnesite-magnesite playas of the Cariboo Plateau, British Columbia, Canada. *Hydrobiologia* 267, 75-98.

Schon, S. C., Fassett, C. I., Head, J. W., 2008. Meander loops and point bar sequences: Evidence of a stable delta plain environment in Jezero crater. *Lunar and Planetary Science* XXXIX, 1354.

Squyres, S. W., Knoll, A. H., Arvidson, R. E., Clark, B. C., Grotzinger, J. P., Jolliff, B. L., McLennan, S. M., Tosca, N., Bell Ill, J. F., Calvin, W. M., Farrand, W. H., Glotch, T. D., Golombek, M. P., Herkenhoff, K. E., Johnson, J. R., Klingelhofer, G., McSween, H. Y., Yen, A. S., 2006. The Opportunity rover's Athena science investigation at Meridiani Planum, Mars. *Nature* 306, 1698-1703.

Tanaka, K. L., Skinner, J. A., Hare, T. M., Joyal, T., Wenker, A., 2003. Resurfacing history of the northern plains of Mars cased on geologic mapping of Mars Global Surveyor data. *Journal of Geophysical Research* 108, 24-1-32.

Vreeland, R.H., Rosenzwelg, W. D., Powers, D. W., 2000. Isolation of a 250 Million-year-old halotolerant bacterium from a primary salt crystal. *Nature* 407, 897-900.

Wood, L. J., 2006. Quantitative geomorphology of the Mars Eberswalde delta. *GSA Bulletin* 118, 557-566.

APPENDIX

APPENDIX A

GENERAL METHODS THEORY

LOWRY PROTEIN ASSAY

The Lowry protein assay is an analytical method that allows one to make a quantitative measurement of a sample's protein content, based on the reaction between the Folin Phenol Reagent (phospho-molybdic-phosphotungstic) and reduced, copper-bound, protein species. In the presence of a highly alkaline solution (≥ pH 10) containing dissolved copper ions, the copper will complex with protein available in solution. This reaction is not catalytic, but it does proceed rapidly, generally reaching the reaction equilibrium after 5 – 10 min. Upon addition of the Folin solution, the reagent rapidly binds with protein molecules, reaching its peak reaction rate within a few seconds at a pH of 10. The bound reagent is then slowly reduced by the copper-treated protein, and changes color from yellow to blue. Any delay in mixing of the sample at the time the Folin reagent is added will reduce the final sample color. Sample protein content is then determined by photospectrometer where the color intensity (absorbance value) of blue light at 650 nm is compared to that of a known calibration curve (Lowry et al. 1951).

Since all living cells contain protein in approximately the same proportion, it should then be possible to use this method to determine the biomass (cellular) content of a sample, assuming it predominantly consists of, or was derived from, cells. By replacing the pure protein standard used in the assays calibration curve with yeast extract (a lysate of yeast cells containing all cellular components) the protein content of a sample then becomes a proxy for the total biomass content of a sample. In this way not just the protein content,

but also the biomass content/cellular component of a natural sample can be determined, allowing for a rapid and relatively accurate estimation of natural microbial populations.

CONFOCAL MICROSCOPY

Confocal Microscopy is an imaging technique used to produce high-resolution images of biological material, through the use of fluorescent pigments that can absorb and re-emit certain wavelengths of light. Typically this involves pretreatment of the sample with fluorescent probes designed to attach to cellular components of interest, however, any natural pigments the sample may posses will absorb and fluoresce as well. The primary advantage of confocal microscopy over traditional Widefield microscopy is that confocal microscopy can eliminate the out-of-focus-glare generally associated with thick (>2 μm), or high magnification images. This clarity is achieved in two ways, first; by illuminating the sample with a focused beam of light, usually a laser, rather than illuminating the entire sample at once as in Widefield microscopes (Figure A1 A), and secondly by using a pinhole that allows only in-focus light to reach the detector (Figure A1 B). The images produced by this method are referred to as optical sections, and represent a single 'slice' taken through the sample. Since a large amount of the light being re-emitted by the sample is prevented from reaching the detector, conventional image recording methods, such as film, do not work, as the image they produce is extremely dim. To overcome this problem a photomultiplier-detector is used to enhance the light signal received from each point on the sample, and a computer builds up the corresponding virtual image.

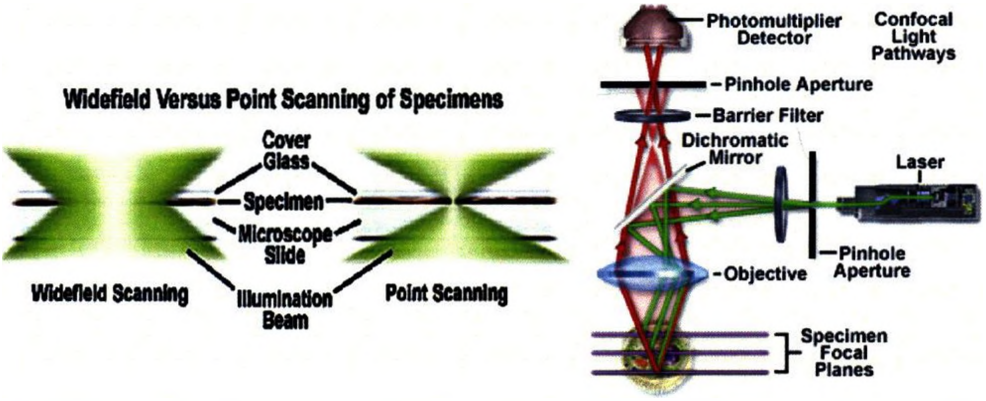

Figure A1 – (A) Sample illumination with a Widefield scanning microscope (left), and a Point scanning Confocal Microscope [right]. (B) Typical confocal microscope light-path; Light emitted from the source travels through the objective lens and is focused on to the sample; then re-emitted light travels upward toward objective again, through the pinhole, and into the photomultiplier-detector.

Newer confocal systems equipped with more than one laser light source also have the option of using multiple wavelengths of light simultaneously to illuminate the sample, producing greatly improved 'multi-channel images' of samples containing more than one fluorescent pigment. An additional benefit of confocal microscopy is its ability to image live and/or moving samples, producing relatively quick and easy time-lapse images. In addition, confocal microscopy has also enabled the automated collection/creation of three-dimensional sample images, by taking multiple images captured at a set distance interval and combining them together to produce a manipulatable 3D image.

DIFFUSE REFLECTANCE INFRARED

FOURIER TRANSFORM SPECTROSCOPY

Diffuse Reflectance Infrared Fourier Transform Spectroscopy (DRIFTS) is an analysis technique that applies both the measured intensity and wavelength of infrared light reflected, or transmitted then reflected, from a sample, to determine its structural and chemical properties. Infrared light of varying wavelengths is capable of exciting

molecular vibrations into higher energy states. For a molecule to be infrared active molecular bonds or functional groups must have a net dipole energy change during exposure to the IR source, and this variation must be detectable as a change in the molecules reflected spectrum.

To produce a molecular spectrum, a single beam of infrared radiation is emitted by the FTIR (Fourier Transform Infrared) device, the beam is then split into two parallel beams by a 'beam splitter', one of which is focused on an internal mirror, while the other is focused on the sample. The infrared beam returning from the sample is reflected by a mirror moving at a constant speed and recombined with the original beam to produce constructive and destructive interference, as a result of their different path lengths. The product of this scan is a plot of voltage vs. mirror position called an interferogram. The interferogram is then mathematically Fourier transformed by a computer into a plot of absorbance vs. wavenumber, which contains diagnostic reflectance features typical of the sample.

The data produced by FTIR analysis is accurate and reliable, making it a good method for identifying unknown samples and their chemical constituents. This identification process is achieved by pattern-matching the sample spectra produced with those of known molecular standards. In addition to identification of inorganic components FTIR is also capable of detecting and identifying organic molecules that are either pure samples or constituents within an abiotic matrix. This versatility makes FTIR a valuable tool for quickly locating, characterizing, and identifying remote and/or in-situ sample materials.

APPENDIX B

SALT CRYSTALLIZATION IN Na-SULFATE ENRICHMENT CULTURES

During field trips to the Basque Lakes in August of 2006, June of 2007 and August of 2007, time was taken to collect samples from several other hypersaline lakes in the area. In addition to samples collected from other Mg-sulfate lakes (e.g. Clinton Lake), we also collected a number of samples from both Last Chance Lake and Saltwort Pond, two hypersaline lakes dominated by Na-sulfate chemistry. In a similar manner to samples collected from the Basque Lakes, both Last Chance and Saltwort Pond sample material was resuscitated in the laboratory, and cultured to examine the halophilic organisms that inhabit these lakes. Suitable brine based media (BBM) was created using the same protocol as the magnesium sulfate BBM, however, as these are sodium sulfate systems the final brine composition was approximately 2.0 mol/L Na_2SO_4 rather than $MgSO_4$.

Most aerobic primary enrichments grew normally, producing cultures dominated by either green or red photosynthetic microorganisms; however, several of these cultures were later observed to precipitate large salt crystals in the bottom of their test tubes (Figure B1). After the initial precipitation event, cultures exhibiting this phenomenon were typically observed to undergo several additional episodes of crystallization over the course of several weeks, each of which was usually bounded by a dark 'band' of trapped pigmented organisms (Figure B2). The enrichment samples that eventually produced salt crystals were kept in the same area of the lab as all other enrichment cultures (thus they should have experienced the same physical conditions; i.e. temperature, humidity and illumination), however, only ~ 1 in 20 cultures were observed to precipitate salts. The majority (10 out of 12 salt producing cultures), were dominated by single-celled green

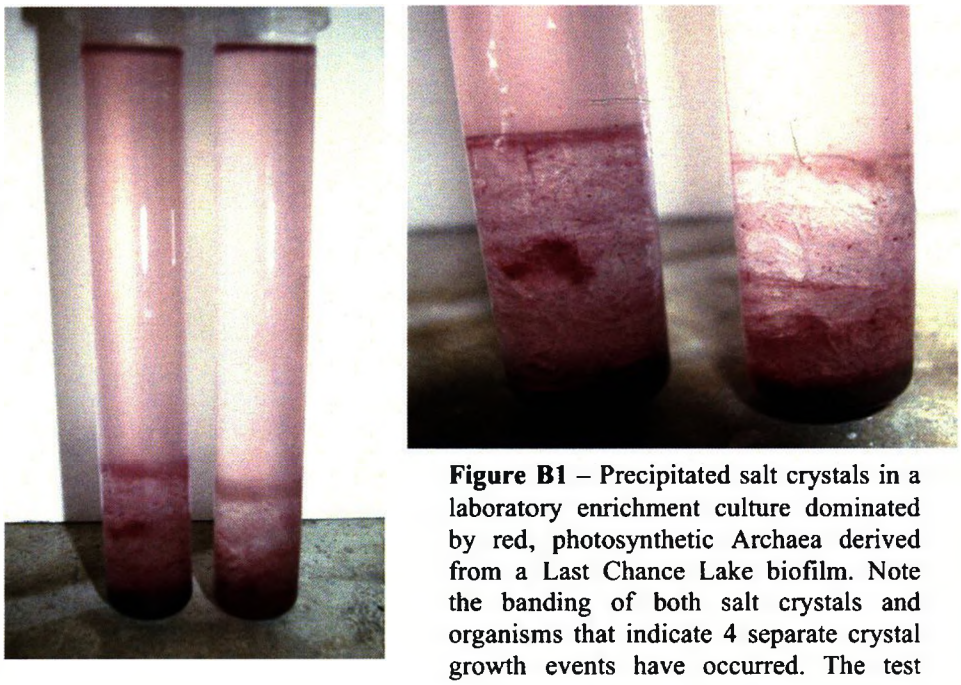

Figure B1 – Precipitated salt crystals in a laboratory enrichment culture dominated by red, photosynthetic Archaea derived from a Last Chance Lake biofilm. Note the banding of both salt crystals and organisms that indicate 4 separate crystal growth events have occurred. The test

---

autotrophic species, while the two remaining cultures were dominated by red single-celled Archaea. Attempts to re-culture these samples directly (using either a liquid inoculum, or by dissolving the precipitated salt crystals in new media), failed to reproduce the salt crystallization phenomenon in a consistent manner. Of the samples re-cultured to date, only 4 have been successful in reproducing salt crystal precipitation events, all of which are dominated by single-celled green photoautotrophic species. These observations suggest that there is some organism (possibly the autotrophs themselves), or consortia of organisms, that are related to the salt crystal formation, and that these species may be very slow growing, or require specific growth conditions to survive.

The salt crystals produced to date have been identified as mirabilite ($Na_2SO_4 \cdot 10H_2O$) by XRD analysis and density tests, and control tubes kept with the cultures have not been observed to precipitate any salt until they have undergone substantially more evaporation (Figure B3, B4) than their biological counterparts. This implies that the biosphere is

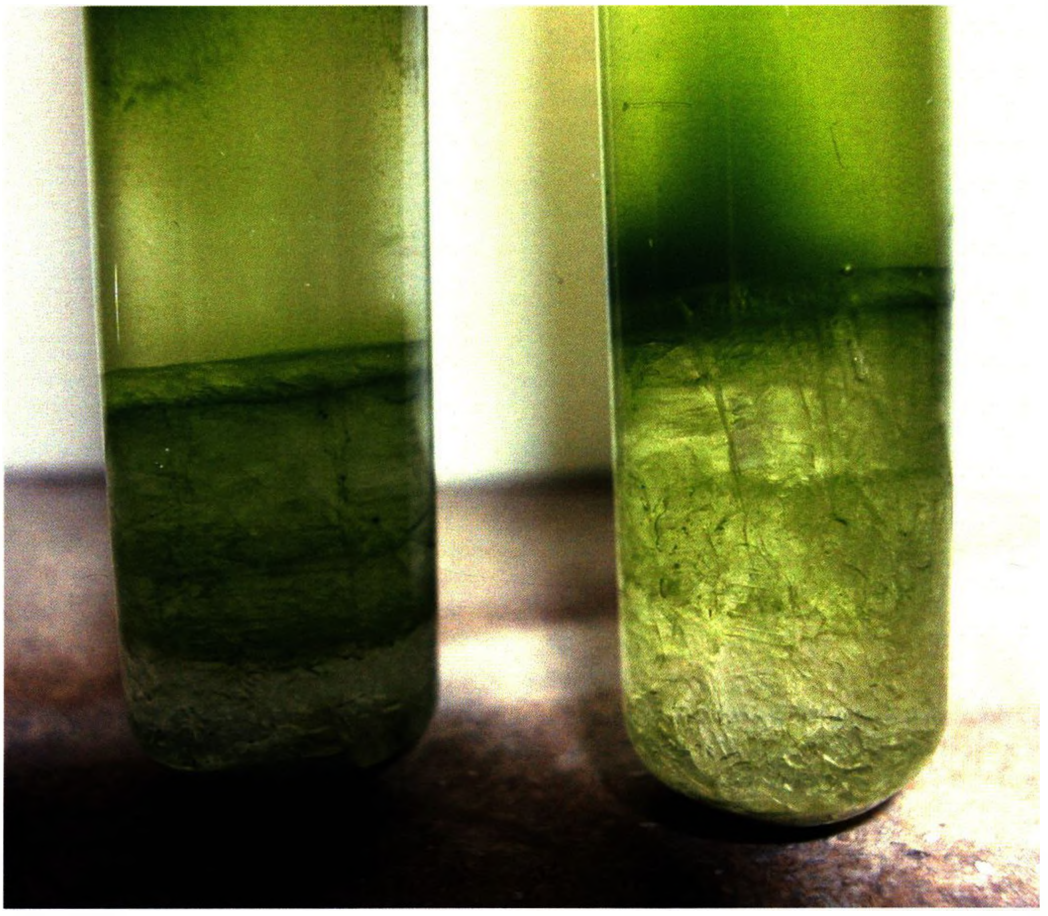

Figure B2 – Characteristic growth banding of green autotrophic species between subsequently precipitated salt crystals in a laboratory enrichment sample from Last Chance Lake. Test tubes are 13 mm wide.

---

having some effect on the production of salt in these brines. Interestingly, Last Chance brine that has been filter sterilized and supplemented with nutrients was also observed to produce salts in 8 out of 9 samples cultured. Alone, the fact that the enrichment cultures produced mirabilite does not speak immediately to biology activity; however, the lack of early-forming salt in brine controls indicates that halophilic organisms are influential during salt crystal formation in otherwise stable brines.

The biologically mediated precipitation of salt from Na-sulfate brines has not been studied to date, nor is there any mention of it in the literature regarding either halophilic organisms, or sodium sulfate dominated systems. Thus it is possible that this is the first

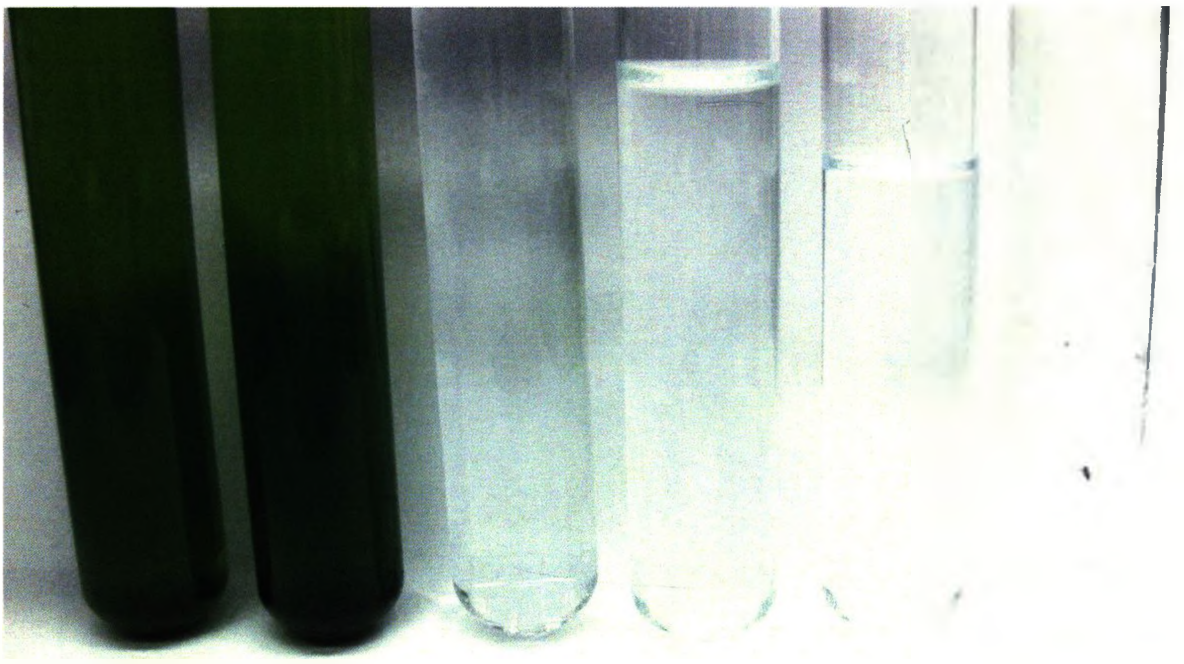

Figure B3 – Two Last Chance laboratory enrichment samples dominated by green autotrophs, both of which exhibit one precipitated salt layer at the bottom of the tube (far left). For comparison, a series of sterile media laboratory evaporation experiments (middle to right). Note that only the very last tube (far right) has precipitated any salt abiotically. Test tubes are 13 mm wide each.

---

time this phenomenon has been observed in-vitro. Here I propose that these observations are in fact evidence of biologically induced salt crystal formation, likely as a result of water activity variation and brine saturation/supersaturation, do to biomass production and the subsequent formation of salt crystals within microcolonies of halophilic organisms. The mechanism is as follows.

Sodium sulfate brines that have been inoculated with halophilic organisms experience a slow decline in water activity due to evaporative concentration, the use of water to produce biomass through photosynthesis, and to hydration layers surrounding extant microorganisms. If microbial population growth is not limited by the availability (or lack) of required nutrients, then the upper population limit will eventually be determined by the availability of water. Under hypersaline conditions water molecules are 'bound' to

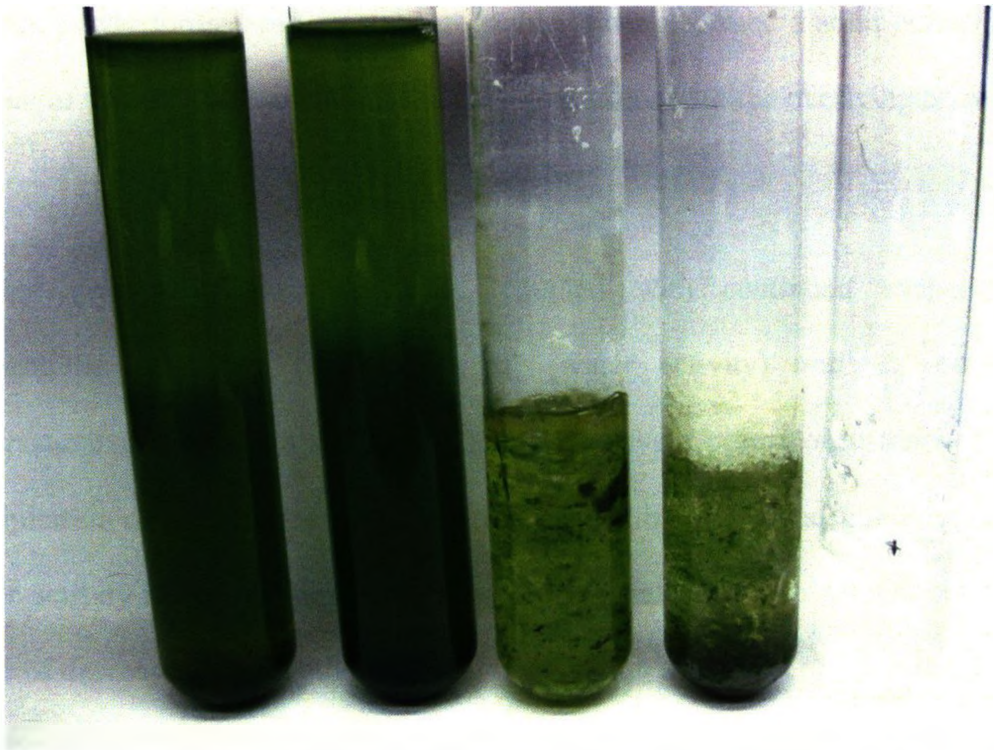

Figure B4 – Evolution of precipitated salt from Last Chance Lake enrichment cultures over time. Two separate enrichment cultures exhibiting one crystallization event (left and far left), one culture that has been left until all remaining brine evaporated (middle), one culture that has been left to continue desiccating after all the brine had evaporated (second from right), and the brine media control containing a small number of abiotically precipitated salt crystals (far right). The test tubes are all 13 mm wide.

---

dissolved ionic species, effectively making them unavailable for further use in chemical reactions, however, some of this bound water can be 'freed' if salt were to precipitate out of solution. Once a microbial population has reached a maximum for the environment, the brine will continue to be concentrated at the brine-air interface via evaporation. The combination of high biomass production, and locally decreased water activity (caused by the presence of biofilms/microcolonies, or by a sudden change in the physical environment, i.e. a drop in temperature), creates a state in which salt crystals can form within microbial colonies suspended in the brine. Once this state has been reached, any nucleating salt crystals forming within a microcolony would begin to grow rapidly, resulting in the eventual loss of buoyancy and the precipitation of salt out of solution. This process will continue until the water activity of the system is back in equilibrium,

and the newly formed salt crystals are stable, having formed a solid crystal mass at the bottom of the tube, with a minimal surface area exposed to the overlying brine.

Further growth of microorganisms, coupled with continued evaporation, again concentrates the brine (and lowers it's water activity) until it reaches another supersaturated state and a salt crystal nucleation event occurs once more. The resulting precipitation of salt crystals out of solution lowers the brine concentration (and raises the water activity of the solution), and allows microbial growth to resume once again. The cycle of decreased water activity, and corresponding saturation of the brine, will continue as long as viable microorganisms have nutrients available for growth and reproduction, and as long as a nucleation event occurs to allow salt precipitation (and resultant brine dilution) to occur. Our current inability to reliably reproduce this experiment indicates that we still have an incomplete knowledge of the factors affecting the stability of Na-sulfates in the presence of concentrated brines and halophilic organisms. However, since the presence of biology appears to be the determining factor allowing this process to occur, I currently hypothesize that the media conditions may not optimal for whatever organism, or group of organisms, are responsible for this phenomenon. Despite the fact that we are as of yet unable to fully explain these observations, they still suggest that halophilic organisms in Na-sulfate systems may play a key role during the precipitation of salt from solution. It also appears that this role often leads to the entrapment of halophilic organisms within salt crystals, simultaneously suggesting a preservation mechanism for halophilic organisms in natural Na-sulfate rich hypersaline environments.

APPENDIX C

MINERALOGICAL IDENTIFICATION OF DRIED BASQUE LAKE FIELD SALTS AND ENTRAINED SEDIMENTS USING X-RAY DIFFRACTION

To determine if there are any biosignatures present in the natural salt samples collected from the Basque Lakes, it was necessary to establish the mineralogical composition of both the host salt crystal, and any other entrained mineral phases. The protocol used for reflectance IR analysis required us to first crush, then dry our natural salt samples in an oven at 70°C for 24h to reduce the water content of the sample. This allowed us to collect data that is suitable for biosignature detection, and mineral identification, and as a result we chose to analyze crushed/dried samples of salt with the XRD as well, to ensure the samples were as similar as possible.

To facilitate the rapid determination of both soluble and insoluble phases present within our samples, two large (1-2 cm) salt crystals were selected from the Basque Lakes; one crystal was selected that appeared brown due to brown and beige-colored sediments trapped within the crystal (Figure C1), and one that appeared black do to the entrapment of black-colored sediments within the crystal (Figure C2). Both crystals were individually crushed with a mortar and pestle, dried in an over at 70°C for 24h, and powdered for whole sample X-Ray Diffraction (XRD) analysis. Each sample was mounted separately on to a glass slide, then placed horizontally into the X-Ray diffractor. An oscillating scanning mode was used (moving the sample in both the X and Y planes) to maximize the amount of sample being exposed to the X-Ray beam, and each frame was collected for 30 minutes (Figure C3 and C4). The diffraction patterns obtained were subsequently integrated and converted into plots of peak position vs. intensity, and further analyzed

with the software program Eva for visual comparison to known mineral diffraction patterns (Figure C5 A and B).

After each sample scan was completed the powdered salt samples were placed separately onto 45 μm filters, and washed with deionized water to remove soluble salt components, leaving only the entrained, insoluble, mineral grains behind. These samples were then dried by vacuum, ground into a fine powder with a mortar and pestle, and mounted as above into the X-ray diffractor (Figure C6 and C7). Separate scans were completed for each salt sample using the same parameters as before, and the diffraction patters (Figure C8 and C9) were converted into plots of peak position vs. intensity for identification of the non-soluble brown (Figure C10) and black (Figure C11) sample components. The mineral species identified by XRD can be found in Table C1 below.

Table C1: Mineralogy of Dried Crystal Samples From Basque Lake No. 2 and No. 4

Sample Name	**B4 Salt with Brown Sediments**	**Sample Name**	**B2 Salt with Black Sediments**
Description	*A 2 cm transparent crystal containing distinct regions of brown-colored sediments, obtained from the mud below a Basque No. pool.*	*Description*	*A 2 cm transparent crystal containing distinct regions of brown-colored sediments, obtained from the mud below a Basque No. pool.*
Soluble Minerals	**Chemical Formula**	**Soluble Minerals**	**Chemical Formula**
Blodite	$Na_2Mg(SO_4)_2 \cdot 4H_2O$	Blodite	$Na_2Mg(SO_4)_2 \cdot 4H_2O$
Gypsum	$CaSO_4 \cdot 2H_2O$	Eitelite	$Na_2Mg(CO_3)_2$
Hexahydrite	$MgSO_4 \cdot 6H_2O$	Gypsum	$CaSO_4 \cdot 2H_2O$
Kieserite	$MgSO_4 \cdot H_2O$	Hexahydrite	$MgSO_4 \cdot 6H_2O$
Loweite	$Na_{12}Mg_7(SO_4)_{13} \cdot 15H_2O$	Krausite	$KFe(SO_4)_2 \cdot H_2O$
Mendozite	$NaAl(SO_4)_2 \cdot 11H_2O$	Loweite	$Na_{12}Mg_7(SO_4)_{13} \cdot 15H_2O$
Romerite	$Fe_3(SO_4)_4 \cdot 14H_2O$	Starkeyite	$MgSO_4 \cdot 4H_2O$
Starkeyite	$MgSO_4 \cdot 4H_2O$		
Insoluble Minerals	**Chemical Formula**	**Insoluble Minerals**	**Chemical Formula**
Anorthite	$(Ca,Na)(Al,Si)_2Si_2O_8$	Clinochlore	$Mg_{4.88}Fe_{0.22}Al_{1.88}Si_{2.96}O_{10}(OH)_8$
Clinochlore	$Mg_{4.88}Fe_{0.22}Al_{1.88}Si_{2.96}O_{10}(OH)_8$	Hematite	Fe_2O_3
Heulandite	$CaAl_2Si_7O_{18} \cdot 6H_2O$	Hydromagnesite	$Mg_5(CO_3)_4(OH)_2 \cdot 4H_2O$
Hydromagnesite	$Mg_5(CO_3)_4(OH)_2 \cdot 4H_2O$	Kanemite	$NaHSi_2O_4(OH)_2 \cdot 2H_2O$
Kanemite	$NaHSi_2O_4(OH)_2 \cdot 2H_2O$	Laumontite	$Ca_{0.89}(Al_2Si_4O_{12})(H_2O)_{1.88}$
Kaolinite	$Al_2(Si_2O_5)(OH)_4$	Magnesite	$MgCO_3$ and $(Mg,Fe)CO_3$
Magnesite	$MgCO_3$ and $(Mg,Fe)CO_3$	Rasvumite	KFe_2S_3
Muscovite	$KAl_3Si_3O_{10}(OH)_2$	Quartz	SiO_2
Quartz	SiO_2	Troilite	FeS

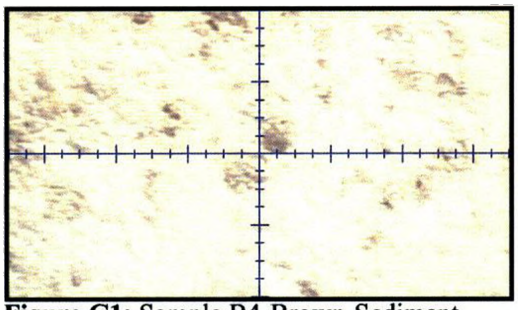

Figure C1: Sample B4-Brown-Sediment powder mounted for XRD.

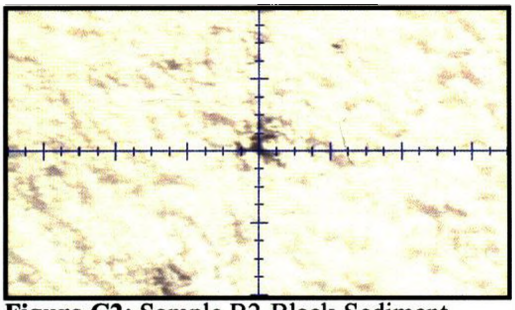

Figure C2: Sample B2-Black-Sediment powder mounted for XRD.

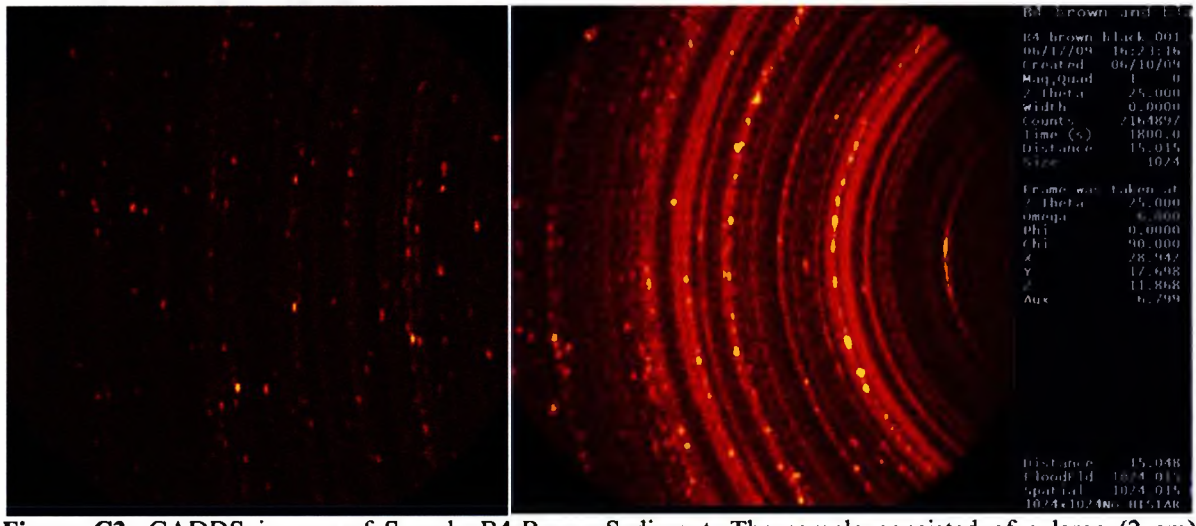

Figure C3: GADDS images of Sample B4-Brown-Sediment. The sample consisted of a large (2 cm) transparent salt crystal containing brown-colored sediments, obtained from the mud below a Basque Lake No. 4 brine pool. Note the presence of both rings and dots on the GADDS images indicating the sample was composed of both single crystals and polycrystalline powders.

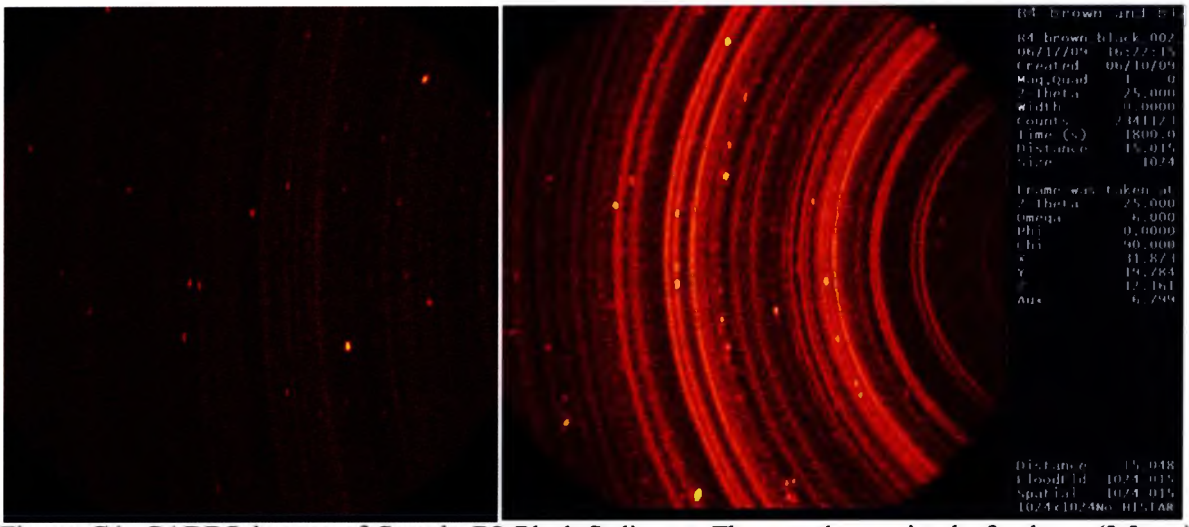

Figure C4: GADDS images of Sample B2-Black-Sediment. The sample consisted of a large (2.5 cm) transparent salt crystal containing black-colored sediments, obtained from the black mud below a Basque Lake No. 2 brine pool. Note the presence of both rings and dots on the GADDS images indicating the sample was composed of both single crystals and polycrystalline powders.

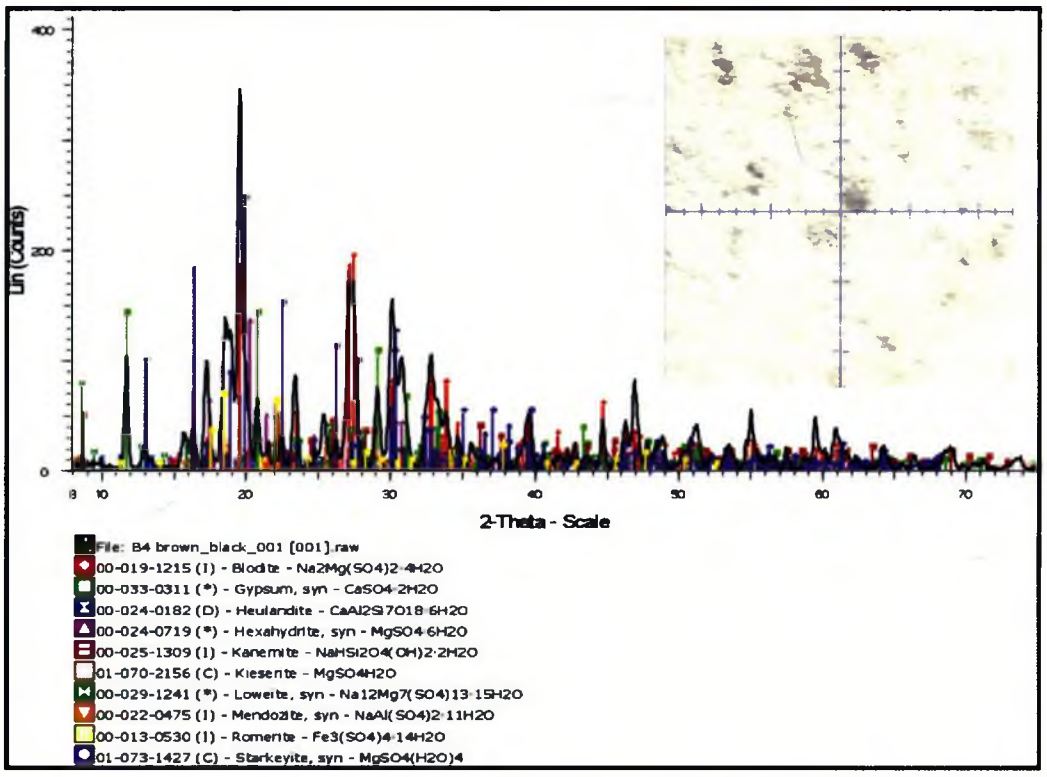

Figure C5 (A): Eva diffraction pattern for Sample B4-Brown-Sediment. The sample pattern is dominated by a variety of soluble mineral phases, with a minor amount of various insoluble mineral grains.

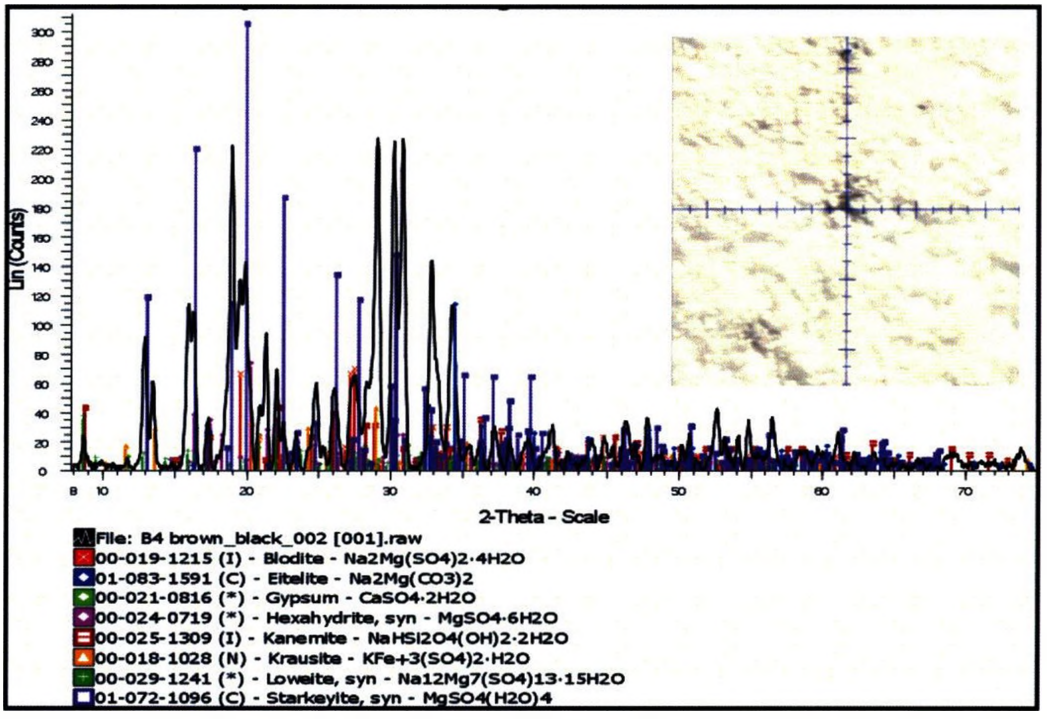

Figure C5 (B): Eva diffraction pattern for Sample B4-Black-Sediment. The sample pattern is dominated by a variety of soluble mineral phases but also contains a very minor percentage of insoluble mineral grains.

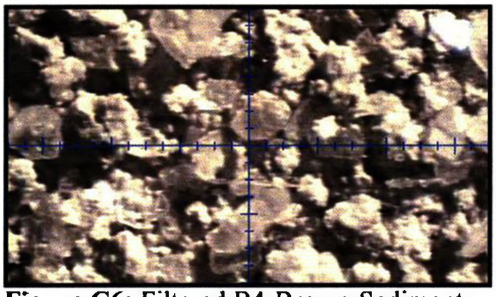

Figure C6: Filtered B4-Brown-Sediment powder mounted for XRD.

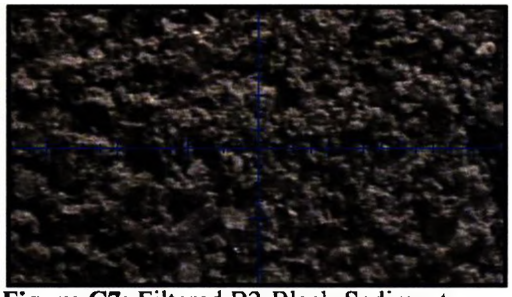

Figure C7: Filtered B2-Black-Sediment powder mounted for XRD.

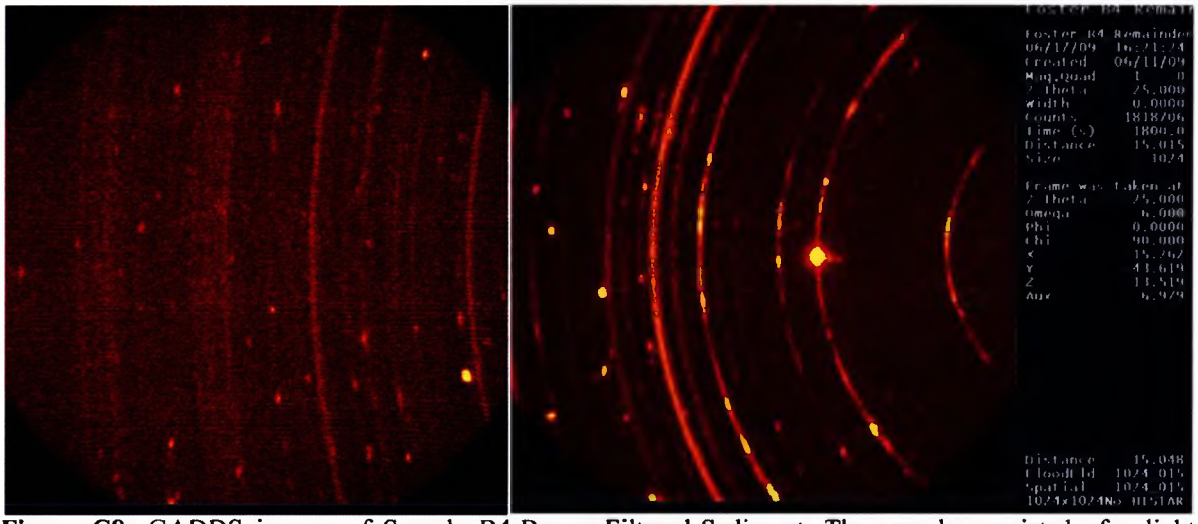

Figure C8: GADDS images of Sample B4-Brown-Filtered-Sediment. The sample consisted of a light beige-brown-colored powder, obtained by dissolving/removing the soluble salt from a Basque Lake No. 4 crystal. The presence of both rings and dots on the GADDS images indicates that the sample is composed of both single crystals and polycrystalline powders, however single crystals appear to be more abundant.

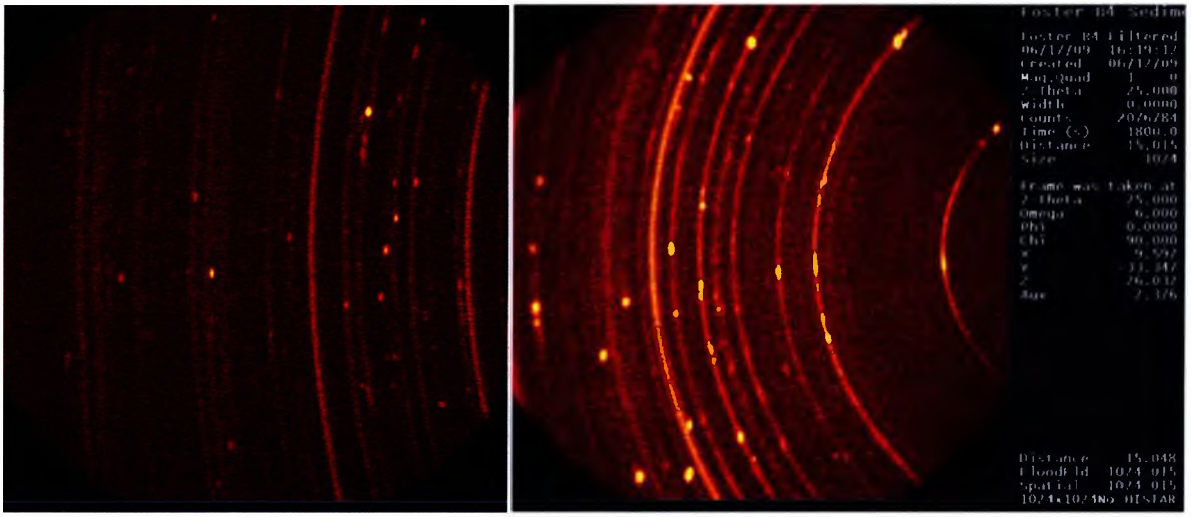

Figure C9: GADDS images of Sample B2-Black-Filtered-Sediment. The sample consisted of a black-dark-brown-colored powder, obtained by dissolving/removing the soluble salts from a Basque Lake No. 2 pool crystal. The presence of both rings and dots on the GADDS images indicates that the sample was composed of both single crystals and polycrystalline powders, however single crystals appear to be more abundant.

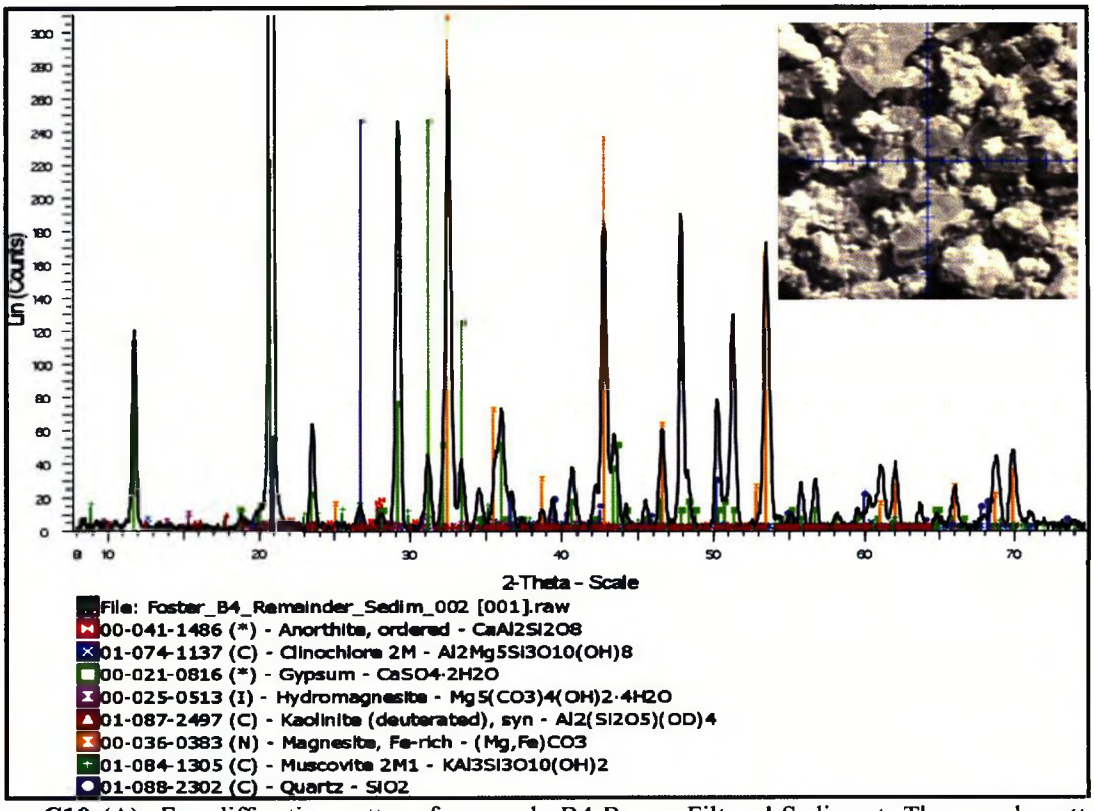

Figure C10 (A): Eva diffraction pattern for sample B4-Brown-Filtered-Sediment. The sample pattern is dominated by gypsum and insoluble mineral phases, most prominently silicates.

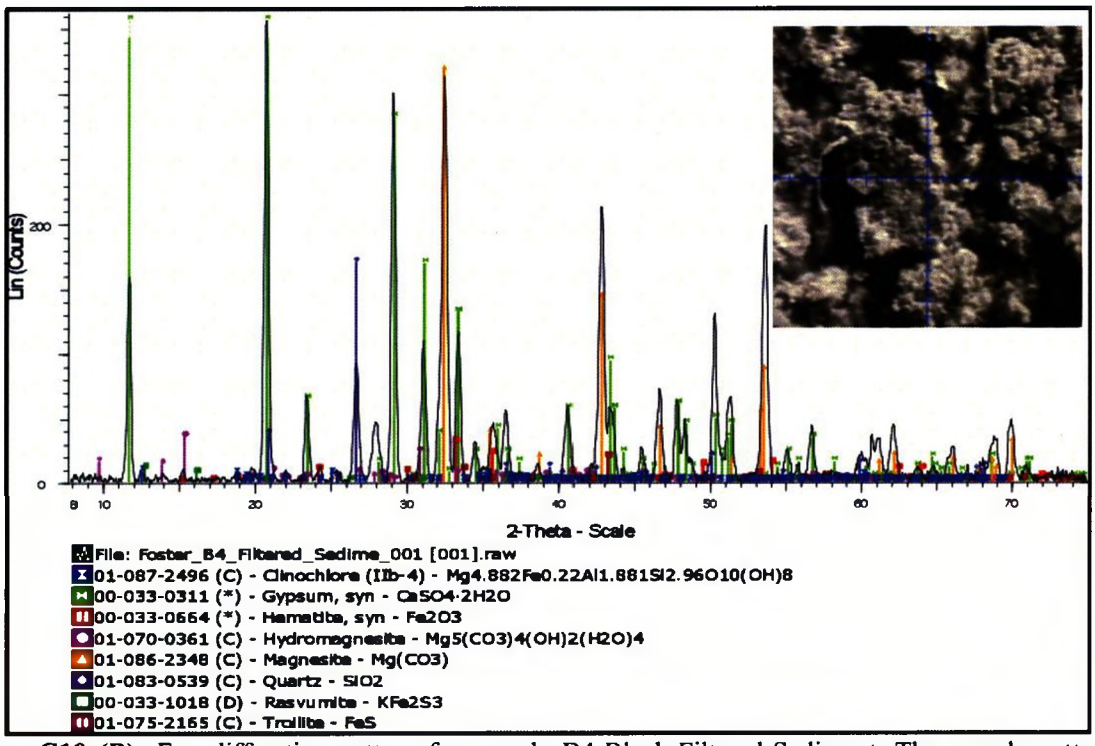

Figure C10 (B): Eva diffraction pattern for sample B4-Black-Filtered-Sediment. The sample pattern is dominated by gypsum and insoluble mineral phases such as silicates and sulfides.